2007

Interactions of mtFabH with its Substrates and Inhibitors Reveal Novel Mechanistic Insights

Sarbjot Singh Sachdeva
Virginia Commonwealth University

INTERACTIONS OF mtFabH WITH ITS SUBSTRATES AND INHIBITORS

REVEAL NOVEL MECHANISTIC INSIGHTS

A dissertation submitted in partial fulfillment of the requirements for the degree of Doctor of Philosphy at Virginia Commonwealth University

by

SARBJOT SINGH SACHDEVA
Bachelor in Pharmacy, Hamdard University, New Delhi, India, 2001

Director: Kevin A. Reynolds
Professor, Department of Medicinal Chemistry (former)
Professor and Chairman, Department of Chemistry, Portland State University

Virginia Commonwealth University
Richmond, Virginia
November 2007

This Dissertation is dedicated to my parents,
Mr. Kuldip Singh Sachdeva and Mrs. Rajinder Kaur Sachdeva,
for their unconditional love and support.

Acknowledgement

I wish to express my sincere gratitude first to Dr. Kevin Reynolds, my advisor, for his continuous support and encouragement throughout this arduous process. Without him, this endeavor would not have been possible.

My heartfelt thanks go to the team of crystallographers comprised of Dr. Tonie H. Wright, Dr. J. Neel Scarsdale and Dr. Faik Musayev, who made the structural part of this work possible and accessible to me. I would also like also to acknowledge my appreciation for Dr. Wright, Dr. Scarsdale, Dr. Umesh Desai and Dr. Glen Kellogg for serving as my graduate committee members and for their assistance with this process.

I wish to thank my colleagues in Dr. Reynold's laboratory for their assistance with my experiments, and for their frequent stimulation of my interest and curiosity. A special thanks to OHSU proteomics lab's Ms Debra McMillen for her assistance with my mass spectrometric work.

I am also grateful to the staff at the VCU Department of Medicinal Chemistry and School of Pharmacy for making the logistics of this process as smooth as possible.

Finally, last but definitely not the least, I would like to express my utmost love and gratitude to my wife, Jasmine, and especially to my parents and my sister for their unconditional love and support during these years.

Table of Contents

Page

List of Tables

List of Figures

List of figures used in appendix 1.

List of abbreviations

AccABCD	Acetyl CoA carboxylase
ACP	Acyl carrier protein
ACPM	*Mycobacterium tuberculosis* ACP
AIDS	Acquired immunodeficiency syndrome
CQ	Chloroquine
CoA	Coenzyme A
CPM	Counts per minute
Da	Daltons
DHFA	Dihydro-folate reductase
DMSO	Dimethyl sulfoxide
DNA	Deoxyribonucleic acid
DOTS	Directly Observed Treatment - Short course
DTT	Dithiothreitol
ecACP	*Escherichia coli* ACP
ecFabH	*Escherichia coli* β-ketoacyl-ACP synthase
E. faecalis	*Enterococcus faecalis*
ESI-MS	Electrospray Ionization - mass spectrometry
ETH	Ethionamide
FAS	Fatty acid synthase
FabH	β-ketoacyl-ACP synthase
FabA/Z	β-hydroxyacyl-ACP dehydrase
FabB	β-ketoacyl-ACP synthase I
FabD	Malonyl-CoA:ACP transacylase
FabF	β-ketoacyl-ACP synthase II
FabG	β-ketoacyl-ACP reductase
FabH	β-ketoacyl-ACP synthase III
FabI/K	Enoyl ACP reductase
H. influenzae	*Haemophilus influenzae*
IC_{50}	50% inhibitory concentration
INH	Isoniazid

InhA	*M. tuberculosis* enoyl ACP reductase
ISO	Isoxyl, thiocarlide
KAS I	Ketoacyl synthase I
KAS II	Ketoacyl synthase II
KAS III	Ketoacyl synthase III
KatG	*M. tuberculosis* catalase-peroxidase
kDa	Kilodaltons
Kb	Kilobases
MabA	*M. tuberculosis* β-ketoacyl-ACP reductase
mAGP	Mycolyl-Arabino-Galactan-Peptidoglycan complex
MALDI MS	Matrix assisted laser desorption ionization - mass spectrometry
MALDI-TOF	Matrix Assisted Laser Desorption Ionization –Time of Flight
MDR-TB	Multi drug resistant tuberculosis
MeOH	Methanol
MIC	Minimum inhibitory concentration
mtFabH	*Mycobacterium tuberculosis* β-ketoacyl-ACP synthase
OD	Optical density
PCR	Polymerase chain reaction
PEG	Polyethylene glycol
pfFAbH	*Plasmodium falciparum* β-ketoacyl-ACP synthase
PZA	Pyrazinamide
QSAR	Quantitative structure-activity relationship
RPM	Rotation per minute
S. aureus	*Staphylococcus aureus*
SAR	Structure activity relationship
SDS-PAGE	Sodium dodecyl sulfate polyacrylamide gel electrophoresis
SPA	Scintillation proximity assay
TB	Tuberculosis
TCA	Trichloro-acetic acid
TFA	Trifloro-acetic acid
THF	Tetrahydrofuran
TLM	Thiolactoycin

Abstract

Interactions of mtFabH with its substrates and inhibitors reveal novel mechanistic insights

By Sarbjot Singh Sachdeva, Ph.D.

A dissertation submitted in partial fulfillment of the requirements for the degree of Doctor of Philosophy
at Virginia Commonwealth University.

Virginia Commonwealth University, 2007

Major Director: Kevin A. Reynolds
Professor, Department of Medicinal Chemistry (former)
Professor and Chairman, Department of Chemistry, Portland State University (current)

Tuberculosis emerged from its grave to be one of the deadliest diseases of the present time after recently developing a synergy with AIDS. A fatty acid condensing enzyme-mtFabH has been proposed to connect the key processes involved in biosynthesis of mycolic acids, an important component of mycobacterial cell wall. It condenses long acyl Coenzymes A (CoA; up to C_{20}CoA) with malonyl Acyl Carrier Protein (ACP) to form the elongated β-ketoacyl-ACP which further undergoes rounds of elongation to form mero-mycolate branch of mature mycolic acids. Owing to its proposed central position in mycolic acid synthesis, mtFabH has attracted considerable attention as a good anti-mycobacterial target.

In this study, we utilized important biochemical tools such as site directed mutagenesis, mass spectrometry and X-ray crystallography to address some of the key unanswered questions regarding the intricate workings of mtFabH. We solved the first co-crystal structure of substrate C_{12}CoA with mtFabH and further analyzed the substrate specificity of this acylation step. This structure depicts the mode of acyl-CoA binding in mtFabH channels; and its comparison with the parallel *E.Coli*-acetyl CoA structure provides important similarities and differences in substrate binding in these two FabH enzymes. It also posed an important question about the trajectory of long acyl chain CoA into the deep and "seemingly closed" substrate binding pocket of mtFabH. By utilizing disulfide-based inhibitors, we showed that large conformational changes are necessary to facilitate ligand trafficking in mtFabH while the high catalytic turnover rate of the enzyme is maintained. We also proposed the most likely location of the involved loop.

A much faster and less cumbersome assay for mtFabH was also developed and it was utilized to characterize a series of inhibitors. This assay utilizes the commercially available radioactive malonyl-CoA in lieu of malonyl-ACP, the physiological substrate, and thus can serve as ACP independent assay for mtFabH.

These studies further our understanding of the biochemistry of mtFabH, which along with the faster assay could be helpful in designing potent mtFabH inhibitors as anti-tubercular agents in the future.

1. Introduction

1.1 Tuberculosis: a global burden

Tuberculosis is one of the deadliest diseases of the present time: one third of the world's total population - approximately two billion people - is currently infected with it, and it causes more deaths than any other single infectious disease.[1] According to the World Health Organization (WHO), about eight million people develop active TB every year and close to two million die from it.[2] It is estimated that by the end of year 2020, nearly one billion new infections will be reported; of those, about 200 million people will have active TB and about 70 million will die from it, if new and improved treatments are not introduced.[3,4]

TB is caused by mycobacteria of 'tuberculosis complex' primarily *Mycobacterium tuberculosis*, but also *Mycobacterium bovis* and *Mycobacterium africanum*. This highly contagious disease is transmitted through the air by inhalation of infective droplet nuclei spread by sneezing, coughing, talking or spitting, and it infects lungs, brain, spinal cord, bones, and joints and various other organs. The rod shaped, acid-fast TB bacillus invades the lungs through the air canal from where it may spread to various other parts of the body through the blood stream, if left untreated. Development of anti-tubercular drugs such as isoniazid, rifampicin, ethambutol and pyrazinamide led to the near-eradication of TB two decades ago but recent emergence of HIV/AIDS and its

synergy with TB has caused the resurgence of TB on a much larger scale than ever, especially in developing countries (Figure 1). In 1993, the gravity of the problem led WHO to declare TB as a global emergency in an attempt to heighten political and public awareness. TB is the leading killer among HIV-infected persons, because they have weakened immune systems, with quarter million TB deaths being HIV-related.

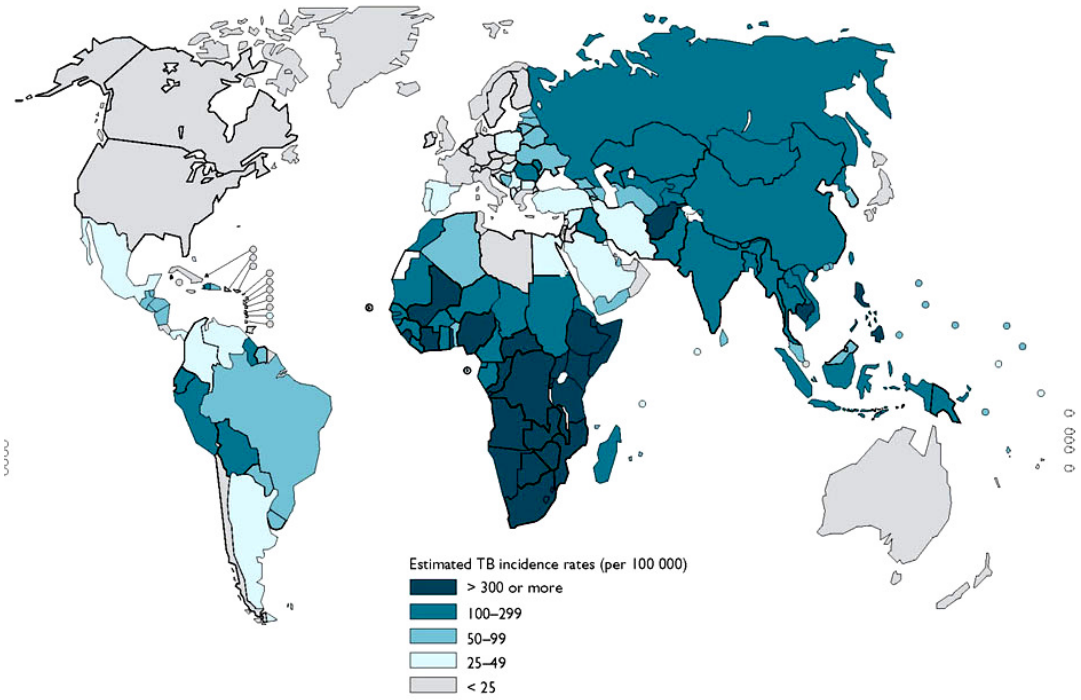

Figure 1: The estimated incidence rates of tuberculosis in different parts of the world in the year 2003. The data is reported by World Health Organization (WHO) and numbers are given per 100,000.

A further complicating factor that has resulted in the rise of TB is emergence of new strains of *M. tuberculosis* which are resistant to one or more current anti-tubercular drugs (**M**ulti **D**rug **R**esistant **TB** or **MDR-TB**).[5,6] According to a recent survey by WHO

and its partners, MDR-TB is present in all of the 109 countries surveyed.[1] Multiple reasons have been associated with the development of this resistance by the TB bacillus, including patient's non-compliance with treatment, prescription of incorrect treatment, unreliable drug supply, or inconsistent or incomplete treatment.[7] The current revised TB treatment recommended by World Health Organization (WHO) is a 6-8 month 'short' therapy with a frontline anti-tubercular drug cocktail consisting of isoniazid, rifampicin, ethambutol, pyrazinamide and streptomycin specifically implemented by the DOTS program (Directly Observed Treatment, Short course).[1] Extensive research is underway in many federal, academic and industrial laboratories to explore new targets and drugs to fight this growing global problem.

1.2 Mycobacteria: the Fort Knox of bacteria

The exceptional pathogenicity and virulence of TB bacteria are largely associated with its formidable cell wall,[8-10] a very unique structural feature of the Cornyebacterium-Mycobacterium-Nocardium (CMN) branch of Actinomycetes order, to which *M. tuberculosis* belongs. This unusual and highly hydrophobic mycobacterial cell wall is composed of three main structural components: arabinogalactan, peptidoglycan and the hallmark of mycobacteria, mycolic acid (Figure 2). These three components are covalently linked (thus often referred to as mycolyl-Arabino-Galactan-Peptidoglycan complex or mAGP) and provide the basic framework of the mycobacterial cell wall.[11] Mycolic acids, in particular, are of special interest because of their unique chemical structure and their highly lipophilic nature, which primarily regulates the permeability of

the mycobacterial cell wall.[12,13] The importance of mycolic acid is evidenced by the fact that it comprises 60 % of the weight of the cell wall.[14]

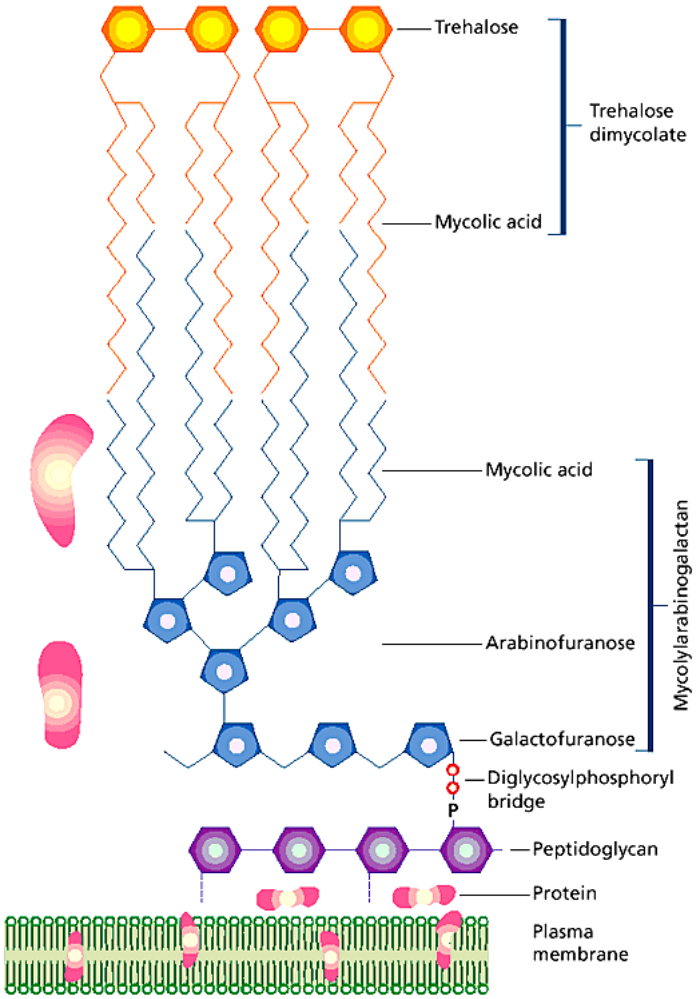

Figure 2: Schematic representation of the mycobacterial cell wall. A layer of peptidoglycan encapsulates the plasma membrane and is covalently linked to mycolyl-arabinogalactan by an unusual disaccharide phosphate bond. The mycolic acid chains are shown perpendicular to the plasma membrane and the exposed portion is seen interacting with trehalose dimycolate, the extractable lipids of mycobacterial cell wall.

Mycolic acids are high molecular weight α- alkyl β- hydroxy fatty acid (C_{50}-C_{90}) that are found either covalently attached to the mycobacterial cell wall in the form of

mAGP or non-covalently as in trehalose dimycolates, the so-called extractable lipids. They form a thick, robust lipid layer on the mycobacterial cell wall and perform a myriad

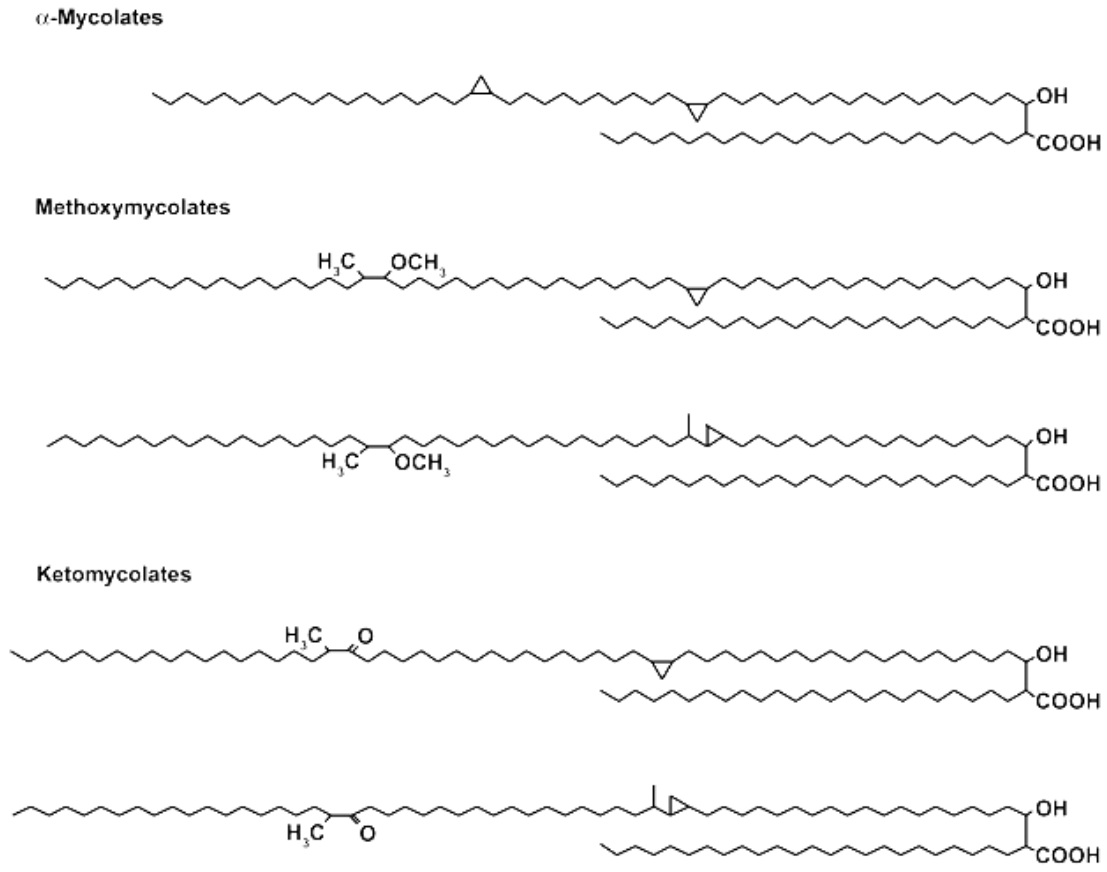

Figure 3: Various types of mycolic acids found in *M. tuberculosis*. α-Mycolates are the most abundant mycolic acid type (~57%) in *M. tuberculosis* and its mero chain contains two *cis*-cyclopropanes. Methoxymycolates, the second most abundant class of mycolic acid in *M. tuberculosis* (~32%), contain an a-methyl methyl-ether moiety in the distal position and a *cis*-cyclopropane or an α-methyl *trans*-cyclopropane in the proximal position. Ketomycolates, which are less abundant (~11%), contain an a-methyl ketone moiety in the distal position and proximal functionalities as in the methoxy series. (Adopted from ref. 27)

of gate keeper functions such as protecting the bacteria from the toxic external environments of the host immune system[8,15,16] and commonly used antibiotics.[17] The

alkyl chains of mycolic acids are species-specific with the α-alkyl branch ranging from 22-26 carbons and the long meromycolic acid ranging from 50-63 carbons. *M. tuberculosis* contains the longest alkyl branches in its genera with an α -branch up to 26 carbons and meromycolic acid arms up to 63 carbons. The meromycolic arm of mycolic acids is further functionalized by a combination of unsaturation, cyclopropanation and oxygenation (Figure 3). These are proposed to impart and regulate various important cell wall properties of mycobacterium, such as fluidity and anchoring to the host cell surface molecules, thereby defining its role in survival and pathogenesis.[13,18,19] These unique properties, conferred only by mycolic acids, make TB bacilli one of the toughest disease opponents ever faced by mankind.

1.3 Mycolic Acid and Fatty Acid Biosynthesis

The backbone of mycolic acids, the shorter alpha branch and the longer meromycolate alkyl chains, are synthesized by the ubiquitous and well-characterized Fatty Acid Synthases (FAS). Fatty acid biosynthesis, an essential process in all organisms, is catalyzed by two distinct systems, Type I in mammals and fungi[20] and Type II in plants and bacteria[21] (Figure 4). The Type I FAS system is characterized by one (in mammals) or two (in fungi and *Corynebacterium ammoniagenes*) polypeptide chains containing multiple domains, which catalyze all of the different steps of the FAS cycle. These polypeptides include the Acyl Carrier Protein (ACP), which ferries the growing acyl chain from one domain to another. In the Type II system, each FAS reaction is carried out by a discrete enzyme encoded by an individual gene.

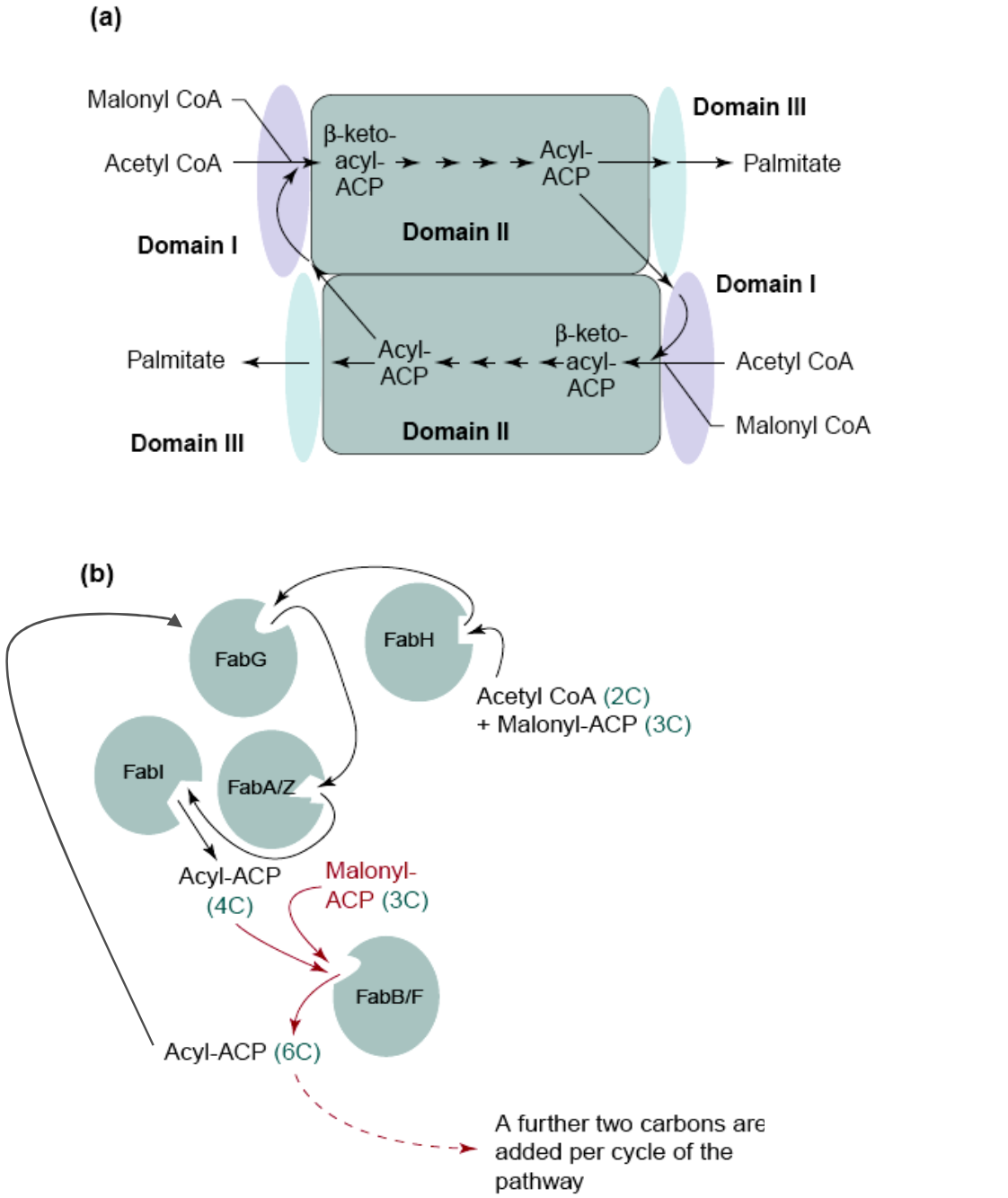

Figure 4: The organization of fatty acid biosynthesis in Type I (a) and Type II FAS (b): (a) In mammals, a single multifunctional polypeptide complex (existing as a dimer) performs fatty acid biosynthesis and the growing acyl chain remains bound until chain elongation is complete. (b) In bacteria, each of the FAS II reaction is performed by discrete proteins and the pathway intermediates are ferried from one specific protein to the next as thioester derivatives of acyl carrier protein (ACP). The figure in bracket (e.g. 2C) denotes the length of the carbon chain. (Adopted from ref. 23)

The intermediates in a Type II FAS are carried from one enzyme to another by a discrete acyl carrier protein (ACP). The various reactions carried out by the Type I and Type II FAS system are essentially the same in spite of their organizational differences.[22,23] In general, transfer of the acyl moiety from acyl coenzyme A (CoA) to the active site cysteine of ketosynthase III (FabH), followed by condensation with malonyl-ACP to form the β-ketoacyl-ACP product, is the reaction that initiates the FAS process. The analogous ketosynthases, FabB and FabF, which take up acyl ACP in place of acyl-CoAs as substrate, catalyze subsequent condensation reactions. Malonyl-ACP is derived from the transfer of a malonyl group from malonyl-CoA to ACP catalyzed by the enzyme malonyl-CoA: ACP transferase or FabD. After each condensation step, the growing β-ketoacyl product is converted into acyl-ACP by the sequential enzymatic action of β-ketoacyl-ACP reductase (FabG), β-hydroxyacyl ACP dehydrase (FabA or FabZ), and an NADH-dependent enoyl ACP reductase (FabI) (Figure 5).

Mycobacteria are distinct from other bacteria because they possess both Type I and Type II fatty acid biosynthesis systems.[24,25] The type I FAS of mycobacteria is responsible for the *de novo* production of the α- branch of the mycolic acid as well as the meromycolate "primer" acyl chain that is further elongated by the type II FAS system. A key regulatory enzyme termed mtFabH or ketoacyl-synthase III (KAS III) forms the pivotal link between the last cycle of FAS I and the first cycle of FAS II systems in *M. tuberculosis*.[26,27] mtFabH preferentially catalyzes the condensation of C_{16}/C_{24} acyl-CoA (released from FAS I) and malonyl-ACP to form the corresponding β-ketoacyl-ACP product, which is further taken up by the Type II FAS system of mycobacterium and

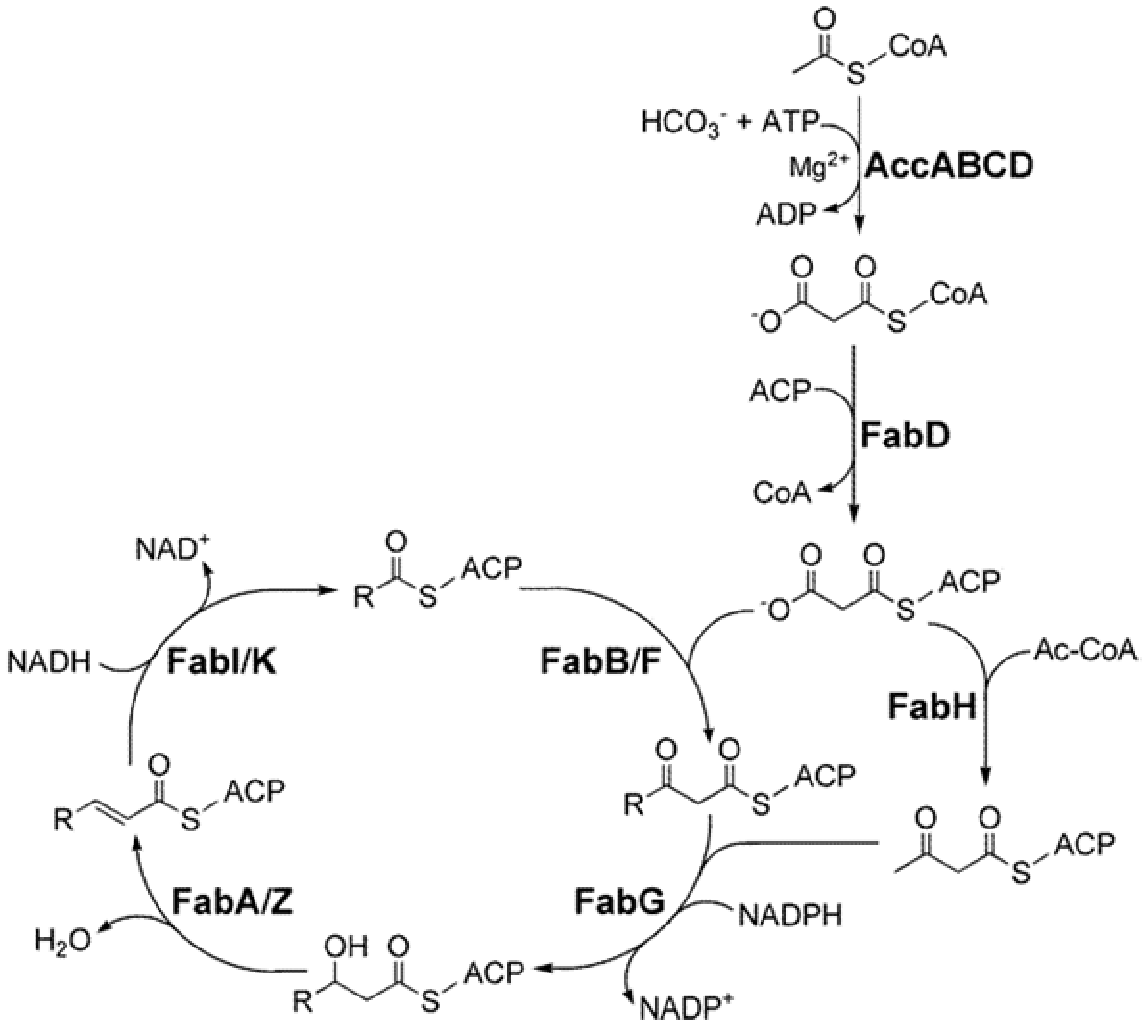

Figure 5: The bacterial type II FAS pathway depicting the general reactions of fatty acid biosynthesis. The organization of Type I and Type II FAS is different as shown in figure 4 but the nature of reactions carried out by both systems are essentially the same. First, Acetyl-CoA (Ac-CoA) is carboxylated by heterotetrameric AccABCD to form malonyl-CoA which is then tranferred to ACP by enzyme FabD. Fatty Acid Biosynthesis is catalyzed by iterated cycles of condensation (FabH, FabB, FabF), reduction (FabG), dehydration (FabA or FabZ) and reduction (FabI or FabK) steps as shown above. (Adopted with modifications from ref.22)

elongated to C_{24}-C_{63} carbon meromycolates. Finally, these meromycolates are condensed with the shorter (C_{23}-C_{26}) alpha alkyl chain from FAS I to form mature mycolic acids (Figure 6).[28]

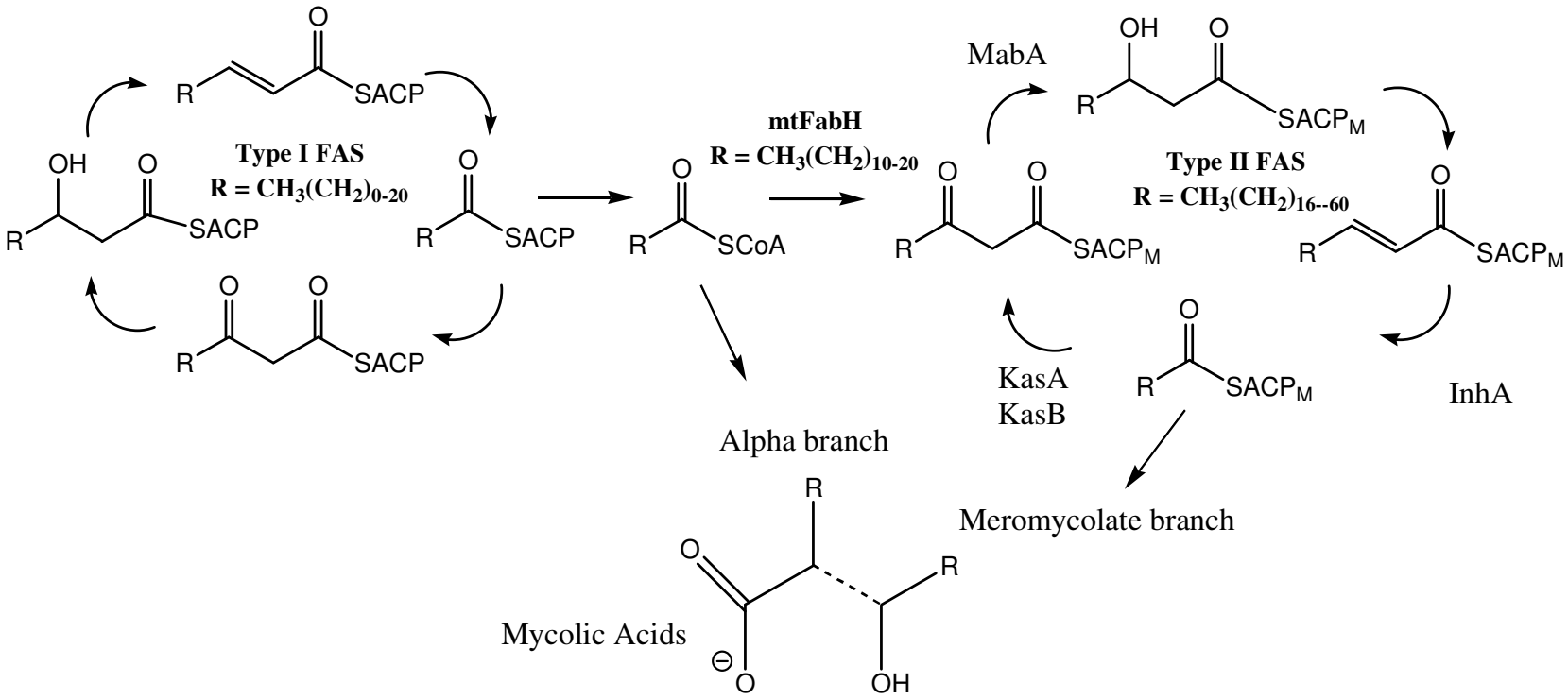

Figure 6: Importance of mtFabH in fatty acid elongation and mycolic acid biosynthesis in *M. tuberculosis*. The fatty acids produced by the type I synthase are removed from the complex by an unidentified transacylase yielding long-chain acyl-CoAs. These acyl-CoAs are used either for alpha branch of mature mycolic acids or by mtFabH, which initiates a round of elongation by the type II Synthase that eventually produces the meromycolate branch of mycolic acids. The shorter alpha branch from FAS I and the longer meromycolate from FAS II condense to form mature mycolic acids, which are incorporated into the cell wall.

1.4 Mycolate biosynthesis: the target of current anti-tubercular drugs

Mycolic acid, due to its incredible chemical structure and crucial role in mycobacterial virulence and impenetrability, has always been a very important target in anti-mycobacterial drug design. Many of the currently used and highly effective anti-tubercular drugs inhibit fatty acid biosynthesis involved in synthesis of alkyl chains of mature mycolates, thus validating the suitability of mycolate and fatty acid biosyntheses as excellent drug targets.[29] Important anti-tubercular drugs, which act by inhibiting one or more components of FAS in TB bacteria, are shown in Figure 7 and clinically relevant drugs are discussed in detail below.

1.4.1 Isoniazid (INH)

Isoniazid (INH or isonicotinic acid hydrazide) was first discovered as an anti-tubercular drug in 1952 and since then it has been used clinically as a frontline drug of choice for treatment of tuberculosis. Both *M. tuberculosis* and *M. bovis* were found susceptible to INH with a MIC range of 0.02 –0.2 µg/ml. INH acts as a bactericidal agent by causing bacterial lysis within twenty four hours of its treatment. Although the drug had been known to block mycolic acid biosynthesis,[30-33] the precise enzymatic target and thus the mechanism of action of INH remained elusive for over forty years. In 1994, for the first time, Banerjee et al[34] traced the target of INH to be a product of the structural gene *inhA*, which was later found to code for an NADH-dependent FAS II enoyl-ACP

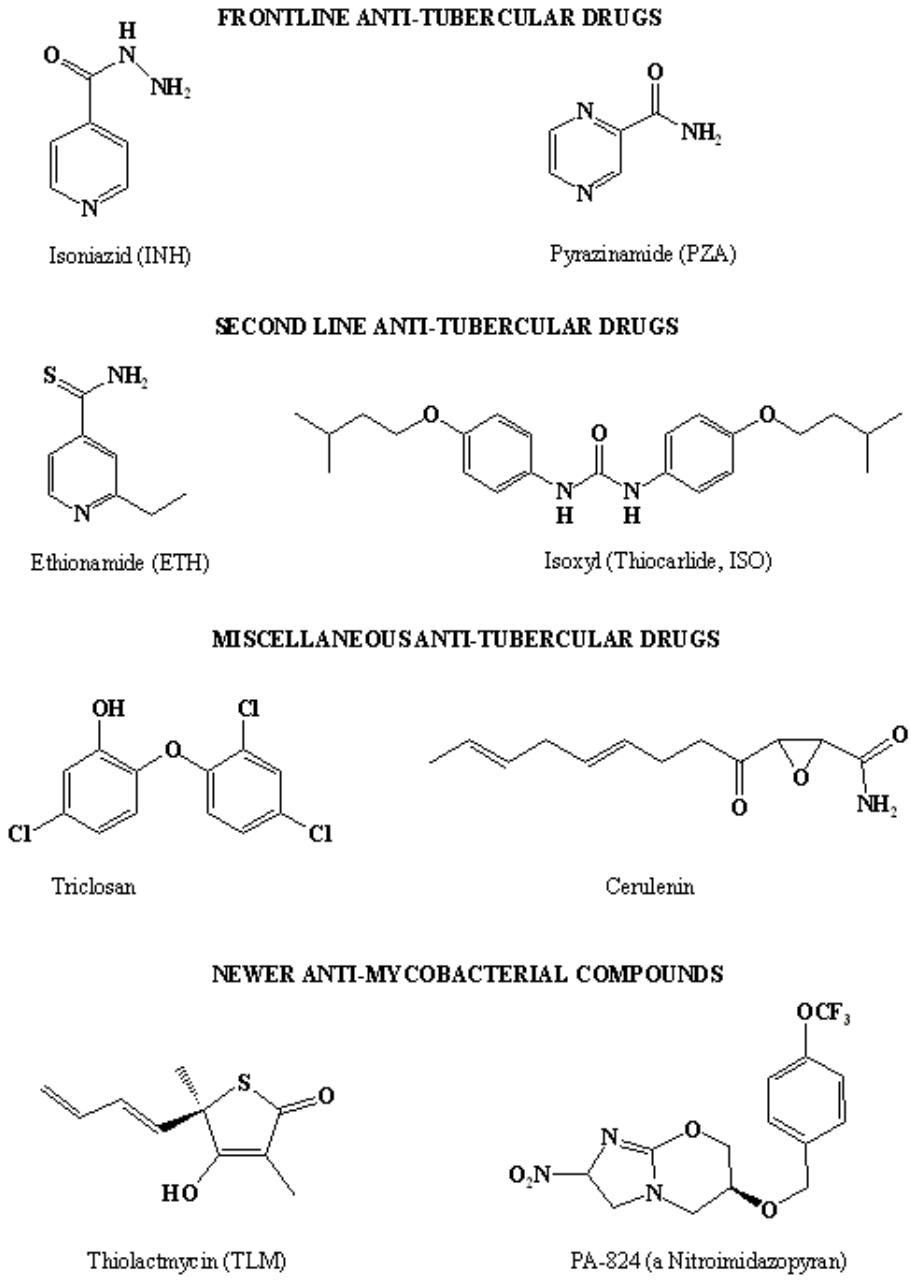

Figure 7: Structures of various anti-mycobacterial agents: Anti-tubercular agents, which inhibit one or more components of mycolic acid biosynthetic pathway.

reductase in *M . tuberculosis* termed InhA (equivalent to FabI of *E. coli*). However, with the finding that another fatty acid enzyme – the condensation enzyme KasA (an *E. coli* ketoacyl-synthase I equivalent) of type II FAS in *M. tuberculosis* – is also bound to a INH-ACPM complex and therefore a potential target of INH,[35] it is currently debated whether INH may have more than one target in *M. tuberculosis*. Moreover, a non-FAS enzyme, dihydrofolate reductase (DHFR) of nucleic acid biosynthesis, has also recently been proven to be inactivated by INH and is thus also claimed to be a physiological target of INH.[36] Probably the success of INH all these years was, in fact, due to its inhibition of more than one enzyme, which has made it difficult for bacteria to develop resistance against it.

1.4.1.1 Isoniazid: mechanism of action and resistance development

INH is shown to be a prodrug in *M. tuberculosis*: it requires activation by an oxidizing enzyme, KatG peroxidase, to be converted into its active intermediate as shown in Figure 8. It is proposed that INH is first oxidized by KatG peroxidase to produce the highly reactive intermediate 1 or 2 (isonicotinic acid anion or a free radical), which then reacts respectively with either NAD^+ or $NAD^{\cdot}$ (in the absence of KatG) to form the INH-NAD adduct. This final electrophilic adduct is shown to bind and inhibit InhA at a nanomolar range[37] and is also most likely the species involved in inhibition of KasA. The idea that the activated adduct formed between INH and NAD^+ could possibly attack any of the cellular NADH dependent enzymes has, at least theoretically, fostered the belief

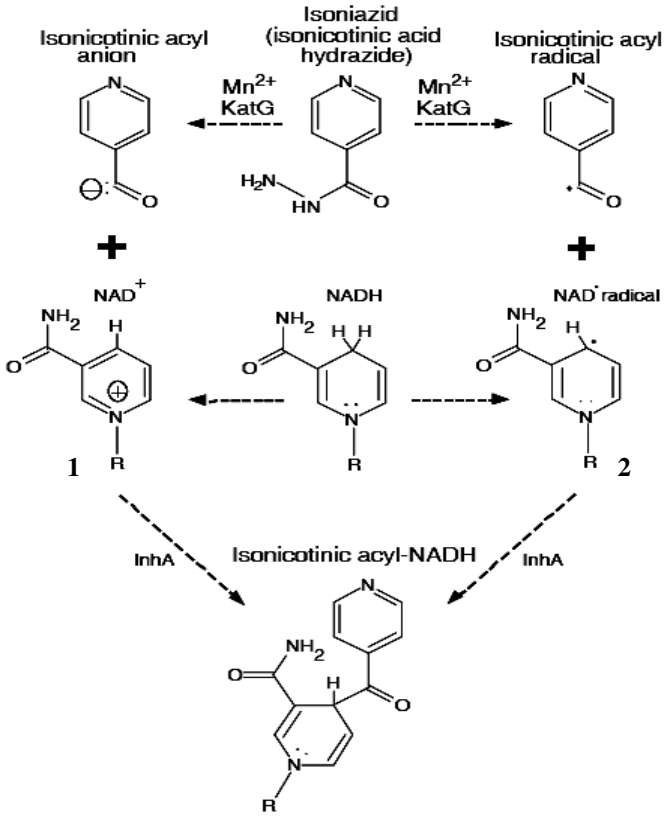

Figure 8: Proposed pathway for formation of the isonicotinic acyl-NADH inhibitor of InhA. Two possible scenarios are shown, in which an activated form of isoniazid (isonicotinic acyl anion or radical) covalently attaches to a form of NADH (NAD1 or NAD. radical) within the active site of InhA, while retaining a tetrahedral carbon at position four of the nicotinamide ring. (Adopted from ref. 37)

that more than one NADH-dependent enzyme could be a target for INH. Although INH resistance has been shown to correlate to mutation or deletion in the *KatG* gene in at least 50% of clinically resistant *M. tuberculosis* strains,[38] analysis of all available resistant strains suggests potential involvement of at least four other genes, including *KasA and inhA*.[6] The number of total enzymes involved in INH inhibition and the extent of inhibition is currently debatable, but all evidence so far inarguably maintains that InhA is the major target of INH.

1.4.2 Pyrazinamide (PZA)

Pyrazinamide (PZA) was discovered in 1952 in an attempt to find more potent analogs of nicotinamide, a compound found to have weak anti-tubercular activity. But unlike isoniazid, pyrazinamide was not used extensively in treatment of TB until the mid-1980s. The later finding that PZA exerts strong synergistic and accelerating effects on other anti-tubercular drugs has resulted in its current recommendation in every combination therapy for the treatment of the disease. The MIC of PZA varies from 8-60 µg/ml depending on the assay method and media employed.[39] It is found to be active against *M. tuberculosis*, but not against *M. bovis* and other rapidly-growing mycobacterial species.

1.4.2.1 Pyrazinamide: Mechanism of action and resistance development

Like INH, pyrazinamide is also a pro-drug that requires amide hydrolysis by mycobacterial pyrazinamidase (a nicotinamidase) to convert to pyrazinoic acid, its active form.[40] This mechanism of activation is evidenced by the fact that pyrazinoic acid and its various analogs were found to have at least equivalent or better activity against clinically resistant strains of *M. tuberculosis* and naturally resistant strains of *M. bovis*, which lacks pyrazinamidase activity.[41,42] After activation, PZA is found to exert its anti-tubercular effect by inhibiting the Type I FAS multifunctional enzyme in *M. tuberculosis* with no effect on Type II enzymes. PZA inhibits [C^{14}] acetate incorporation into C_{16}-C_{24}/C_{26} fatty acid whereas [C^{14}] palmitate incorporation into mycolic acid is unaffected, strongly suggesting that type I FAS is indeed the target; interestingly, however, PZA does not block mycolic acid synthesis, which raises important doubts about its mode of action. Resistance against PZA is shown to be related to loss of pyrazinamidase activity in *M. tuberculosis*.

1.4.3 Miscellaneous inhibitors

Apart from the WHO-recommended frontline anti-tubercular drugs INH and PZA, several second-line drugs including ethionamide, thioacetazone, and thiocarlide (isoxyl) have been shown to exert anti-tubercular activity via the proposed inhibition of one or more components of mycolic acid biosynthesis (see Figure 7). Also well known antibacterials like triclosan and cerulenin are also proven to exert their inhibitory effect

by acting on one or more enzymes of fatty acid biosynthesis in bacteria. Thus, there is ample evidence available that mycolic acid biosynthesis is an excellent drug target.

A relatively newer addition to the anti-tubercular drug list is the compound PA-824 which also shows significant activity against the clinically resistant TB strains.[43,44] PA-824, a 3-substituted nitroimidazopyran, was initially discovered for cancer treatment and has been shown to possess highly specific activity towards *M. tuberculosis* complex by possibly inhibiting mycolic acid biosynthesis and protein synthesis. It is now widely touted as the next potential TB drug, as it has shown great promise in pre-clinical trials. PA-284 is also proposed to be a pro-drug based on the available data, but its exact nature of inhibition and physiological target are still unclear.[45]

Thiolactomycin (TLM), a unique thiolactone antibiotic produced as a secondary metabolite of the soil fungi *Nocardia* sp., has been shown to have potent anti-microbial activity against several pathogens[46-48] including the saprophytic strain *Mycobacterium smegmatis* mc^{2155} and the virulent strain *M. tuberculosis Erdman*.[49] It blocks the Type II fatty acid synthase system in *M. tuberculosis* by inhibiting two key FAS condensing enzymes, ketoacyl synthase I (KasA) and III, both in-vitro and in-vivo; this ultimately leads to blockage of mycolic acid biosynthesis and cell death.[49,50] These findings have encouraged the synthesis of a series of TLM analogs, many of which were found to be more potent than their parent compound TLM.[51-54]

1.5 mtFabH as an emerging anti-tubercular target

Over the last decade, the resurgence of TB has created the necessity to find novel anti-tubercular targets and drugs. Key anti-tubercular drugs including frontline drugs like isoniazid (INH) and pyrazinamide (PZA) have been found to exert inhibitory action by blocking the synthesis of fatty acid, which corroborates the validity of FAS enzymes as

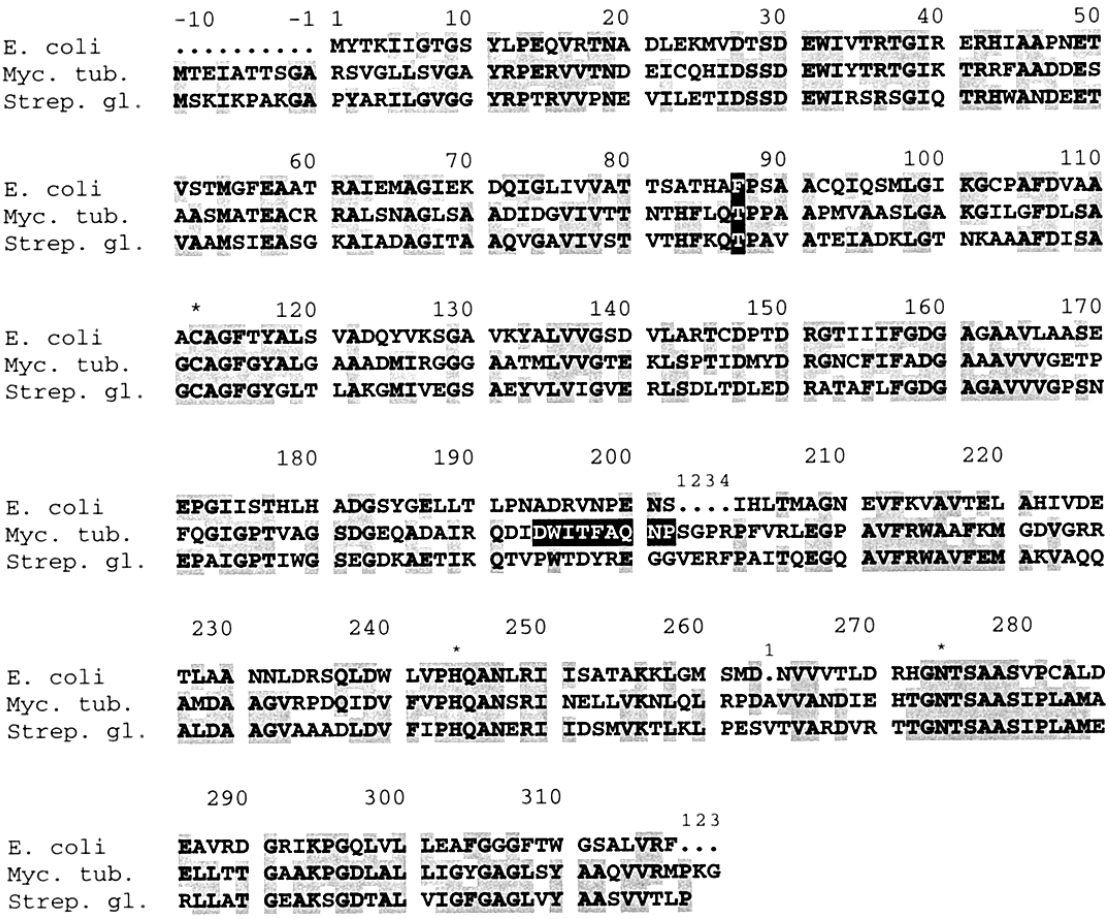

Figure 9: Sequence alignment of FabH from *E. coli*, *S. glaucescens*, and *M. tuberculosis*. Positions of inserts in the latter two sequences are based on comparison of tertiary structures, not on sequence similarity, and are numbered with extensions to the residue number just preceding the insert. *Boxed* residues are a-helix present in mtFabH and missing in ecFabH and the putative specificity determinant at residue 87 (see figure 11 for detail). *Asterisks* denote active-site residues. (Adopted from ref.27)

targets for the development of novel anti-tubercular drugs. What makes mtFabH unique from other FAS enzymes is its capacity to link the two indispensable FAS systems; the enzyme thus plays a key role in mycolic acid biosynthesis in *M. tuberculosis*. Moreover, the absence of a human homologue of FabH has helped it garner significant interest as an anti-tubercular target and considerable effort is being directed at understanding its detailed mechanism by researchers around the globe.

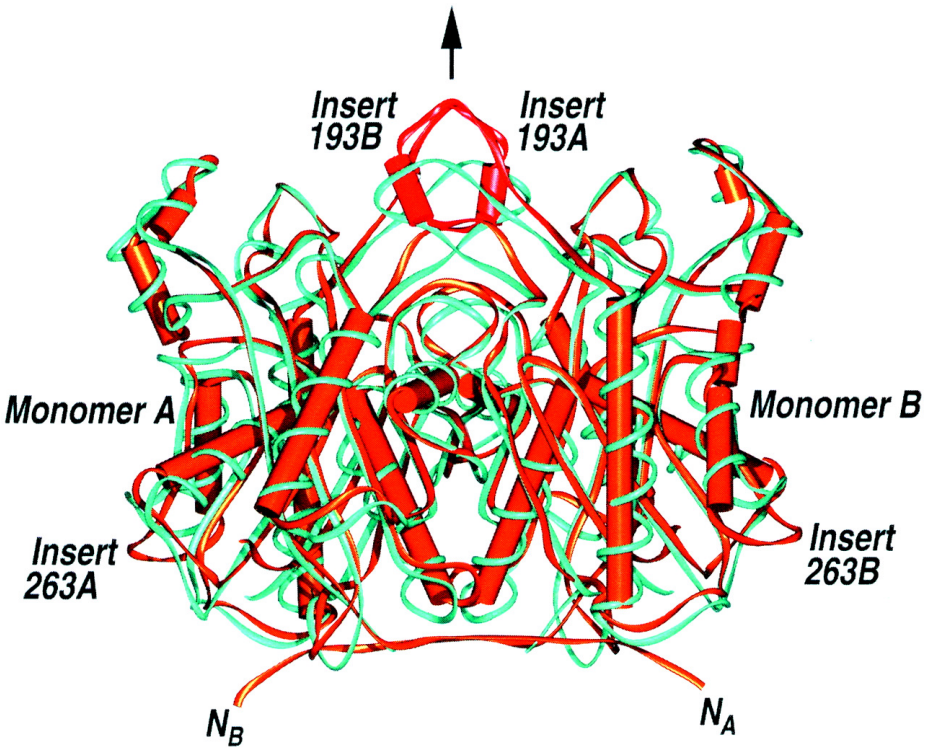

Figure 10: Comparison of backbone folds for ecFabH (*blue*) and mtFabH (*bronze*) dimers. The insert at position 202 in mtFabH relative to ecFabH and the contiguous α-helix (*cylinder*) immediately preceding this insertion in mtFabH are colored *red*. The *arrow* indicates the non-crystallographic 2-fold axis defining the functional mtFabH dimer. (Adopted from ref. 27)

mtFabH is one of three condensing enzymes found in the type II FAS system of *M. tuberculosis*.

This approximately 70 kD homodimer is encoded by the open reading frame Rv0533c (*fabH* ~ 1005 bp) of *M. tuberculosis* (H37Rv) chromosomal DNA and found to have high sequence similarity to its *E. coli* (ecFabH) and *S. glaucescens* (sgFabH) homologues (Figure 9). [26,55,56]The closely related FabH enzymes, mtFabH and ecFabH, are seen to have the same core structure (figure 10) with the same characteristic buried Cys-His-Asn catalytic triad and the coenzyme-A/ACP binding channel; but unlike ecFabH, mtFabH takes up longer acyl-CoAs (C_6 – C_{20}) (Table 1), which is consistent

Acyl-CoA		mtFabH (with ecACP)	mtFabH (with ACPM)	ecFabH
			Enzymatic activity (pmoles/min/ug)	(* 10^3)
Acetyl CoA	(2:0)	n.d.	n.d.	50.5 +/- 4.5
Butyryl CoA	(4:0)	n.d.	n.d.	5.30 +/- 0.20
Isovaleryl CoA	(5:0)	n.d.	n.d.	3.80 +/- 0.02
Hexanoyl CoA	(6:0)	0.39 +/- 0.07	1.74 +/- 0.07	3.40 +/- 0.60
Octanoyl CoA	(8:0)	5.98 +/- 0.19	5.49 +/- 0.93	n.d.
Decanoyl CoA	(10:0)	6.34 +/- 0.49	6.16 +/- 0.24	n.d.
Lauroyl-CoA	(12:0)	8.01 +/- 1.07	7.24 +/- 0.18	3.30 +/- 0.20
Myristoyl CoA	(14:0)	2.24 +/- 0.10	9.46 +/- 0.41	n.d.
Palmitoyl CoA	(16:0)	1.33 +/- 0.10	9.27 +/- 0.56	n.d.
Stearoyl CoA	(18:0)	0.60 +/- 0.10	10.39 +/- 0.51	n.d.
Arachidoyl CoA	(20:0)	0.06 +/- 0.02	9.02 +/- 0.0.27	n.d.

Table 1: Substrate specificity of mtFabH (with homologous and heterologous ACP) and ecFabH towards various acyl-CoAs. For mtFabH specificity, the β -hydroxyacyl-ACP (either ec-ACP or mtACP) product formed is reduced with sodium $NaBH_4$ and extracted with toluene and counted with liquid scintillation counter. For ecFabH specificity, enzyme activity was determined using 50 mM acyl-CoA, 7 mM malonyl- ACP, 100 mM NADPH, 1.5 mg *S. pneumoniae* FabG and 5 ng of *E. coli* FabH. The FabH-FabG spectrophotometric-coupled assay was used to determine the substrate specificity of *E. coli* FabH for various acyl-CoA primers. In the coupled assay malonyl-ACP and acyl-CoA are condensed by E. coli FabH to yield β-ketoacyl-ACP, which is a substrate of *S. pneumoniae* FabG. FabG catalyzes the reduction of β-ketoacyl-ACP to β -hydroxyacyl-ACP and the concomitant oxidation of NADPH to $NADP^+$, a coupled reaction which was be monitored spectrophotometrically at 340 nm. (n.d.- Not determined)

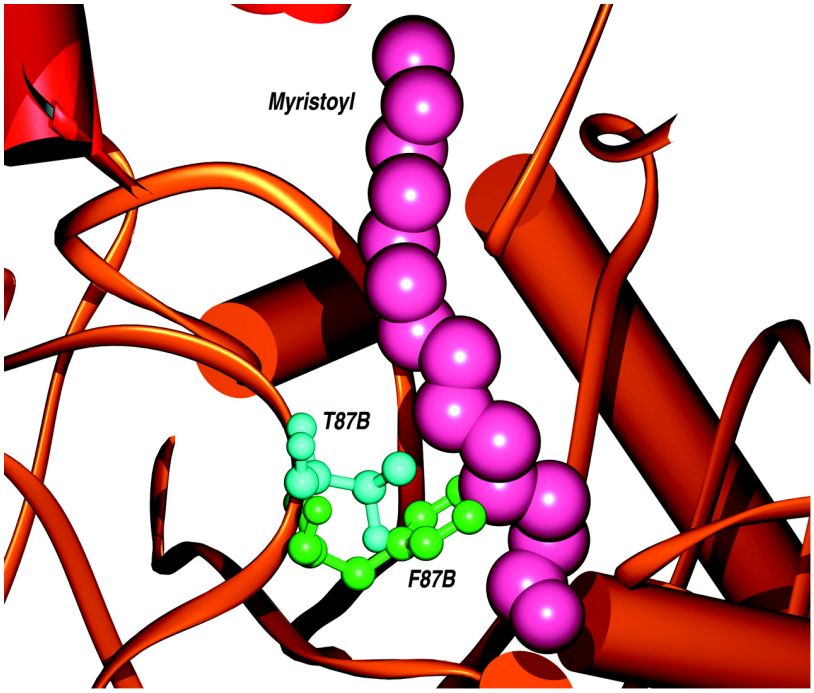

Figure 11: Modeled position of the myristoyl group in binding channel 2 showing the position of residue 87B, which is a threonine in mtFabH (*blue*) and a phenylalanine in ecFabH (*green*). Residue 87 is proposed to contribute to fatty acid chain length specificity for these two enzymes. (Adopted from ref. 27)

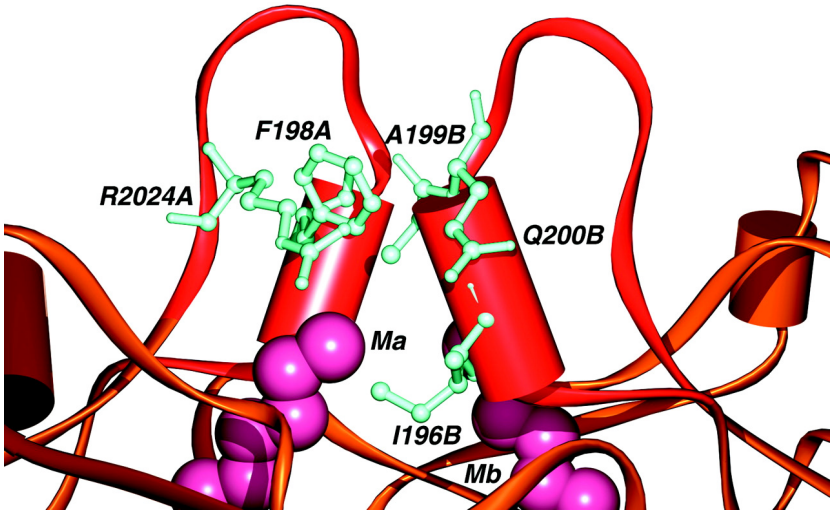

Figure 12: Magnified view of the distal end of the myristoyl-binding site in mtFabH at the junction of the inserts of each monomer. The insert and preceding α-helix are shown in *red*, and the modeled myristoyl group (*Ma* and *Mb* in each subunit) is shown in *lavender*. Note the space in the FabH binding site for two more carbons on the end of myristoyl. (Adopted from ref. 27)

with its role of extending the type I FAS acyl-CoA products. The preference for a longer acyl chain in mtFabH is proposed to arise from the presence of permissive Thr^{87B} (compared to Phe^{87B} *in E. coli*) which opens up the putative acyl channel in mtFabH to accommodate the longer acyl group (Figure 12). In the homologous sgFabH, the presence of identical Thr^{87B} (Figure 9) and the relaxed substrate specificity relative to ecFabH fully support this hypothesis.[55] The acyl chain length specificity for mtFabH was proposed to be limited to a maximum of C_{16}CoA due to the positioning of a steric cap produced by the alpha helix at positions 194-202 on the acyl channel (see Figures 9 and 13). This maximal chain length effect was later seen to be the result of the heterologous ACP (ecACP) used in the study, as the utilization of homologous ACPM resulted in efficient condensation of physiologically relevant substrates (up to C_{20}-CoA) (Figure 11).[57]

1.5.1 Mechanism of the mtFabH reaction

mtFabH is proposed to utilize C_{16} - C_{20} acyl-CoAs produced by the Type I FAS system and condenses them with malonyl-ACPM by a multi-step 'ping-pong' mechanism to form the corresponding two-carbon-longer β-ketoacyl-ACP product (Figure 14). The first step is the formation of an acyl-mtFabH intermediate by the attack of Cys112 thiolate of mtFabH on the carbonyl carbon of the first substrate acyl-CoA (transacylation). In the subsequent step, CoA is released and the second substrate malonyl-ACP binds in the same pocket and decarboxylates to produce a carbanion. This carbanion then attacks the electrophilic acyl carbonyl of acyl-mtFabH to form the final β-ketoacyl-ACP product (condensation) which is released to recycle the free mtFabH. This

long-chain β-ketoacyl-CoA product is then processed by the Type II FAS in *M. tuberculosis* to form the mature meromycolate chains.

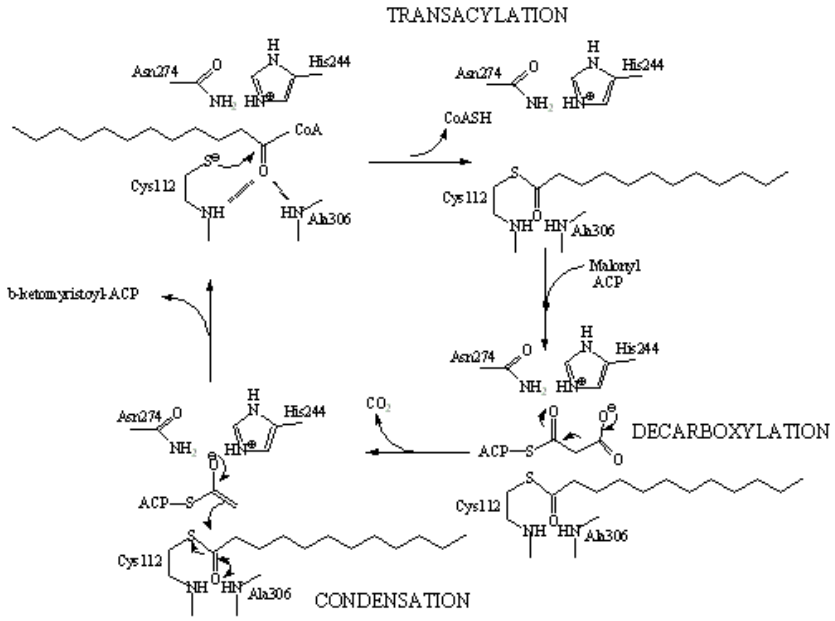

Figure 13: Mechanism for the mtFabH catalyzed initiation of fatty acid biosynthesis. The acyl-CoA depicted here is lauroyl CoA (12:0) which is elongated by 2 carbons provided by malonyl moiety attached to ACPM.

1.6 Thesis objectives

The discovery of mtFabH and its proposed pivotal role in *M. tuberculosis* functioning has instigated significant interest in this enzyme, and the recent unraveling of the mtFabH structure has provided important preliminary structure-function insights into this enzyme. Some very crucial and relevant questions, however, still remain unanswered. Also, the lack of an easier and more efficient assay format to test potential inhibitors for this enzyme constitutes a serious roadblock to development of a specific inhibitor. Thus, we directed our efforts towards investigating different mechanistic aspects of the enzyme using various ligands; the long-term goal and future prospects were to discover novel, potent, and selective inhibitors of mtFabH. The specific aims in these regards were as follows:

1. **Development of an easier and relatively faster assay format to aid in discovery of potential inhibitors of mtFabH**. The previous mtFabH assays require cumbersome washing steps, expensive scintillation proximity beads or the tedious preparation of biotinylated acyl carrier proteins. These factors are an impediment to the faster screening of potential inhibitors and thus a more efficient assay format should expedite their discovery. Here, we describe a much faster and less cumbersome mtFabH assay that directly utilizes commercially available substrate malonyl-CoA (in place of Malonyl-ACP) and thus overcomes the above mentioned disadvantages associated with previous methods.

2. **Evaluation of the acyl binding pocket of *mtFabH*:** The unique acyl binding pocket of mtFabH has been speculated but not proven to be responsible for its different substrate specificity compared to homologous ecFabH. Thus, we co-crystallized the Michaelis Complex between mtFabH and the first substrate acyl-CoA to evaluate its binding mode in the putative channels and to further compare it with the available ecFabH-acetyl-CoA co-crystal structure. This structural comparison should aid in design and development of effective inhibitors for these enzymes.
3. **Probing the reactivity and substrate specificity of both monomers of the mtFabH:** The slower acylation rate relative to overall rate of condensation reaction for mtFabH reported by Besra et al. poses a question-mark on proposed functional equivalency between the two subunits of mtFabH. Also it further points towards a more involved (complex) role of cognate ACPM in the overall reaction. Here, we have utilized a mixture of C_6-C_{20} CoAs and decyl-CoA disulfide to investigate the reactivity and substrate specificity of individual monomers of the mtFabH dimer. The results indicate a role of ACPM in priming and/or offloading of 3-ketoacyl ACPM product.
4. **Separate entrance and exit portals for ligand traffic in mtFabH**: The unique substrate specificity of mtFabH and other downstream *M. tuberculosis* FAS II enzymes such as InhA and MabA for longer acyl-CoAs and ACPs poses an interesting question of large ligand trafficking in these enzymes. We utilized a series of disulfide-based inhibitors and a mtFabH mutant (whose pantotheinate binding channel is blocked by A246F mutation) to investigate the entry/exit of large ligands

to/from the deep and seemingly restricted mtFabH binding sites. We utilized mass spectrometry and x-ray crystallographic studies to provide the experimental support for an alternate route/conformation for ligand trafficking in mtFabH. This is a first for the FabH class of enzymes, especially for mtFabH, and could be a key to understanding the molecular interactions preceding the formation of the first mtFabH-ligand complex and also following the product formation.

5. **Analysis of potential new mtFabH inhibitors**: A series of FabH inhibitors have been identified for *E. Coli* and *Plasmodium Falciparum* FabH by techniques such as in-silico screening and chemical database searches. These inhibitors were evaluated for their activity against mtFabH and attempts were made to analyze the basis of inhibition against FabH class of enzymes.

2. Development of M*ycobacterium tuberculosis* β-Ketoacyl-Acyl Carrier Protein Synthase III (mtFabH) assay

2.1 Summary

The enzyme β-ketoacyl-ACP synthase (KAS III or FabH) is the key enzyme that initiates fatty acid biosynthesis in a type II dissociated FAS. It catalyzes the condensation of acyl-CoA and malonyl-ACP to form a β-ketoacyl-ACP product that is further processed to form mature fatty acids that are involved in various essential cellular processes like phospholipid biosynthesis, cell wall formation, etc. Herein described is a new assay for the *Mycobacterium tuberculosis* FabH (mtFabH) enzyme involved in a key initiation step in the synthesis of mycolic acids, which are an integral component of the cell wall. The assay eliminates the need for the cumbersome washing steps, specialty scintillation proximity assay beads, and the preparation of acyl carrier proteins, required in other assay formats. This discontinuous assay involves the reduction of radiolabled long chain β-ketoacyl-CoA product to its di-hydroxy derivative, which partitions into a non-polar phase for quantitation, while the reduced radiolabeled substrate derivative remains in the aqueous phase.

2.2 Introduction

The most commonly used and established method to assay FabH involves the use of radioactive acyl-CoA and malonyl-ACP to form a radioactive β-ketoacyl-ACP product. This radioactive protein (ACP) product can be precipitated with acid, washed and counted, while the radioactive substrate stays in the aqueous phase. The accuracy of the assay requires extensive time–consuming washing steps. Nonetheless, this general approach has been used to assay FabH from various pathogenic microorganisms such as *E. coli, E. faecalis, H. influenzae, S. pyogenes* and *S. aureus*.[58,59] Unfortunately, this method can't be used to assay mtFabH because the long chain acyl-CoA substrates utilized by mtFabH have poor water solubility and are not readily resolved from the β-ketoacyl-ACP product by the acid precipitation and extensive washing steps. Other assay formats such as a Scintillation Proximity Assay (SPA)[27] and a filter disk assay[26] have been described and can successfully be used for mtFabH. However, these assays involve either tedious preparation of a biotinylated malonyl-ACP substrate (SPA) or numerous washing steps (filter disk assay). The assay described here is a faster and more cost efficient for mtFabH, and eliminates the requirement of prior preparation of ACP substrates. Each individual step of the assay format is described in detail with special notes explaining the key steps. Furthermore, the advantages and disadvantages of this new assay method are discussed.

2.3 Experimental procedure:

2.3.1 Materials:

The following reagents and conditions were used in the assay. The stock and working concentrations are indicated where required.

1. Lauroyl-CoA or other long chain acyl-CoA (Sigma) – the stock solution of 100mM or 10 mM were made in aqueous hydrochloric acid, pH 3.5, then diluted to 100uM working concentrations, aliquoted into appropriate working volumes and stored at – 80 ^{o}C.

   Note: As acyl-CoA substrates are known to be unstable at neutral and higher pH, the solutions were made in acidic pH (aqueous hydrochloric acid solutions at pH 3.5) and stored in aliquots at –80 ^{o}C in working volumes (avoiding the need to repeatedly thaw and refreeze the solutions and the associated increased degradation).

2. Radioactive [2-^{14}C] Malonyl-CoA (American Radiolabeled Chemicals Inc.)(Stock concentration 1.8 mM; specific activity, 55mCi/mmol) diluted approximately 7.2 times in aqueous hydrochloric acid solution (pH 3.5); the resulting 250 µM solution was aliquoted into appropriate working volumes and stored at – 80 ^{o}C.

   Note: The purity of the commercially available radioactive malonyl-CoA is a very important factor in this particular assay. Radioactive malonyl-CoA is prepared by the reaction of monothiophenylmalonate [malonyl-2-^{14}C] and coenzyme A and the [2-^{14}C] malonyl-CoA product is purified by column chromatography. The radioactive

reactant is relatively non-polar, and if present in the [2-^{14}C] malonyl-CoA sample, can lead to a high background during the assay and a substantially reduced signal to noise ratio. The manufacturer's technical data sheet states that under these conditions the rate of decomposition is approximately 2% over the first six months.

3. The over-expression of mtFabH enzyme in *E coli* and its purification has been described previously.[27]
4. Sodium borohydride, toluene and tetrahydrofuran (THF) were from Fisher Scientific.
5. Double distilled (DD) water (Sigma) for preparing buffers and reagents.

   Note: Divalent cations like Mg^{2+}, Mn^{2+} catalyze the decomposition of sodium borohydride ($NaBH_4$) preventing effective reduction of the β-ketoacyl-CoA product. Thus distilled water free of divalent ions was used in both the working assay and the preparation of the reducing reagent solution.[60]
6. Potassium chloride powder, dibasic potassium phosphate powder (required for making reducing reagent) was ordered from Sigma.
7. Screw cap microcentrifuge tubes (VWR).

   Note: Sodium borohydride produces significant effervescence when mixed with aqueous solutions. There is thus a potential for loss of the radioactive material from the vial at this point. A screw cap micro centrifuge tube should be used and tightened carefully before shaking the sample.
8. EcoScint A scintillation cocktail (National Diagnostics).
9. High-Density Polyethylene (HDPE) Liquid Scintillation Vials (Wheaton Science).

2.3.2. Method:

The reaction was carried out in 20 µl total volume. This low volume using a minimum of the commercial radioactive malonyl-CoA sample with an unchanged specific activity balanced a high signal to noise ratio with a low cost. A larger volume assay would either require additional radioactive malonyl-CoA (increased cost) or addition of unlabeled malonyl-CoA (decreasing the specific activity and signal to noise ratio). The concentrations of various components in a typical assay are shown in table 2. These volumes permitted determination of an IC_{50} value for a mtFabH inhibitor, but can be modified to perform routine enzymatic studies by replacement with an additional 2 µl of buffer.

Component	Stock Conc.	Volume used	Final conc./ amount
Lauroyl-CoA	100 µM	2.5 µl	12.5 µM
Malonyl-CoA	250 µM	1 µl	12.5 µM
Inhibitor	10 X	2 µl	1 X
mtFabH		2 µl	0.2 µg
Sodium phos., pH 7.0	100 mM	12.5 µl	72 mM
Total volume		20 µl	

Table 2: List of various components of a typical mtFabH assay.

Steps:

1. The desired number of lauroyl-CoA, malonyl-CoA and mtFabH aliquots were thawed and kept at 4 ^{0}C.
2. In a screw cap microcentrifuge tube, 2.5 µl of 100 µM lauroyl-CoA solution (final concentration 12.5 µM lauroyl-CoA), 1 µl of the 250 µM [2-^{14}C] malonyl-CoA

solution (approx. 31,000 counts, final concentration 12.5 µM) and 2 µl of 10X inhibitor concentration (for inhibitor IC_{50} studies) were added. Then 0.1M sodium phosphate buffer, pH 7.0 was added to make up the volume to 18 µl.

Note: The solvents used to deliver inhibitors have a predictable inhibitory effect on the activity of mtFabH. The effect of various concentrations of dimethylsulfoxide (DMSO) and methanol (MeOH) is shown in figure 14. These figures indicate that the concentrations of solvent should ideally be at or below 1 % in the final assay volume.

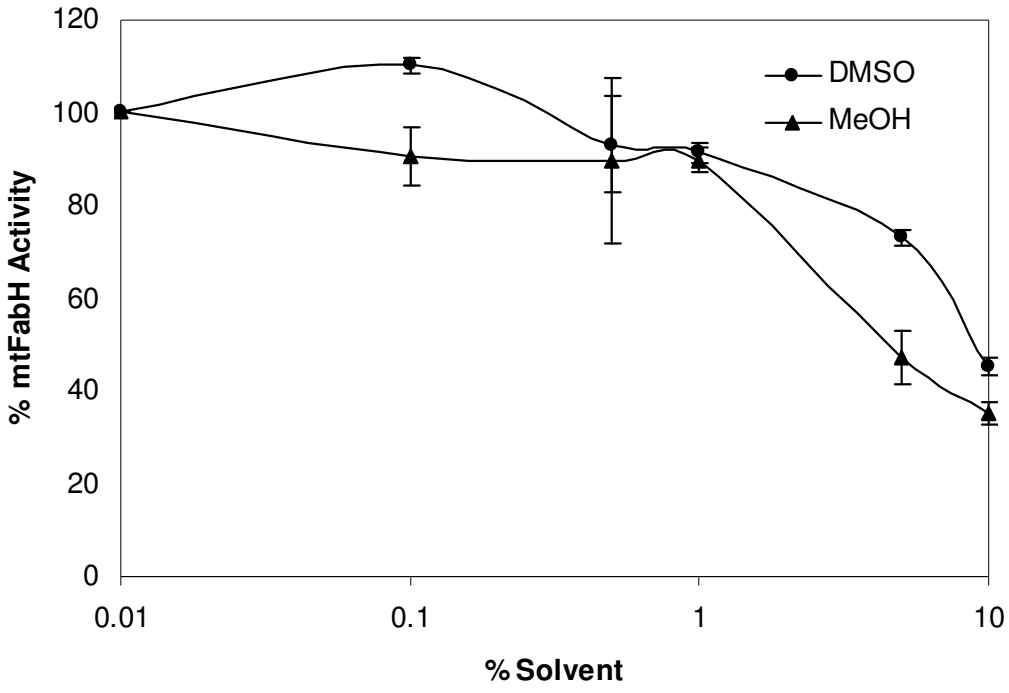

Figure 14: Effect of solvent concentrations (DMSO and methanol) on mtFabH activity.

3. The reaction was initiated by addition of 2 µl of mtFabH (0.2 – 0.4 µg) solution in 0.1 M sodium phosphate buffer, pH 7.0. Cap the microcentrifuge tube and kept at 37 ^{0}C for a designated time (typically 30-90 minutes). Under these assay conditions a linear reaction rate was observed for over a 2-hour assay period. (Figure 15).

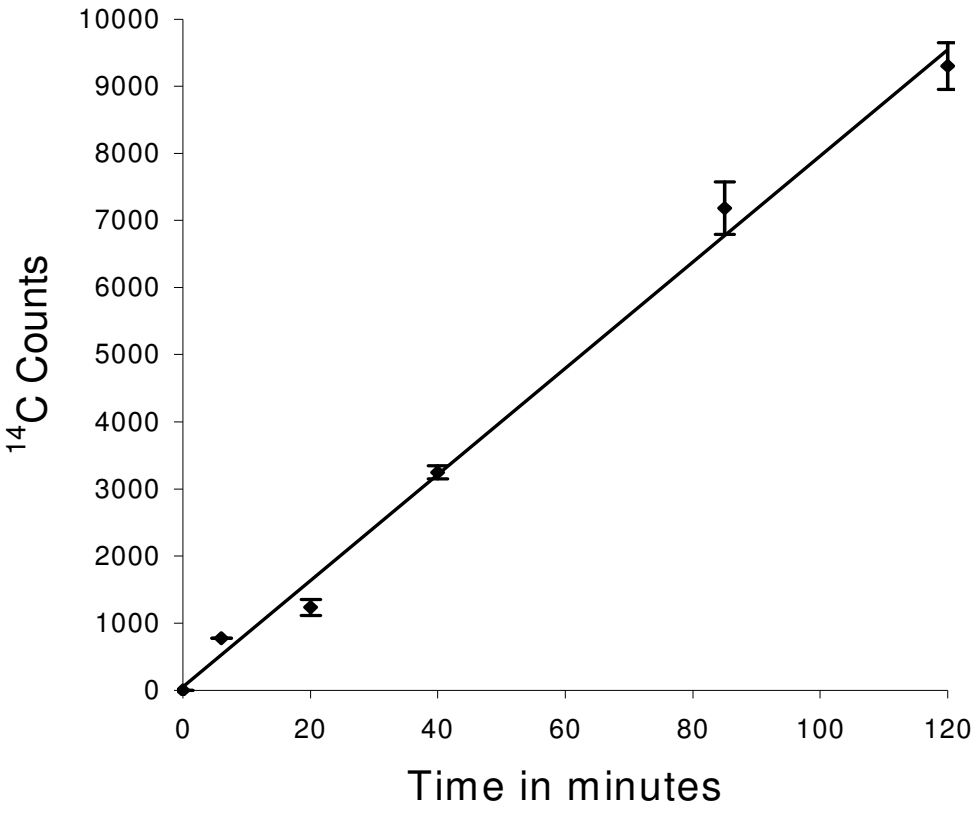

Figure 15: Linearity of mtFabH activity with time. Enzyme is incubated with substrates at 37 ^{o}C for the specified time and product formation quantitiated as described above.

4. The reducing reagent was generated by adding 5 mg of $NaBH_4$ to 1 ml of a 70% 100 mM K_2HPO_4, 100mM KCl, 30% THF solution. This solution was prepared fresh, and kept on ice until used.

Note: The reducing solution consisted of 100 mM K_2HPO_4, 100mM KCl, 30% THF with sodium borohydride as the reducing agent. THF decreases the time required to quantitatively reduce the acyl thioesters (from 2 h to 10 min).[60] The buffer can be stored at room temperature and $NaBH_4$ should be added just before use. This reduction solution can be used for up to 2 hr if kept on ice, but potentially can lead to a loss of consistency in the assay results.

5. A 0.5 ml of this reducing solution was added to the assay mixture; the vials were capped and shaken vigorously. Incubate the mixture at 37 ^{0}C degree for 15 minutes.

   Note: Reduction of long chain acyl-CoA is quantitative within 10 min. If inconsistent results are obtained the reduction reaction can be carried out for a longer time.

6. Then 500 µl toluene was added to the mixture, the solution was mixed vigorously and then allowed to separate at room temperature.
7. 320 µl of the upper phase (toluene) solvent was removed and combined with approximately 3 ml of a toluene or xylene based scintillation liquid
8. The radioactivity of the toluene extract was determined with a Scintillation Counter and the actual radioactivity in non-aqueous phase was calculated by doubling the observed radioactivity.

   Note: The volume of toluene solution increases to about 640 µl due to partitioning of THF into toluene.

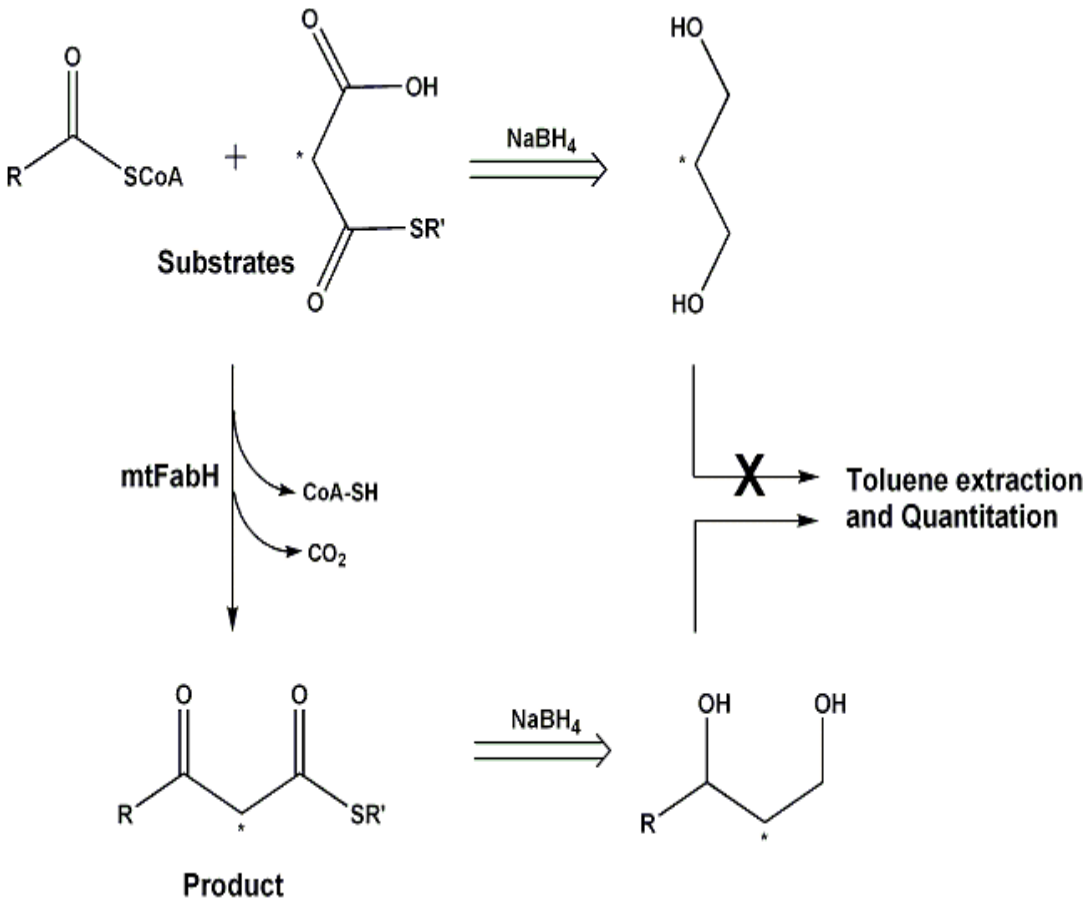

Figure 16: Schematic of mtFabH assay. The principle of separation of radioactive substrate and product is described in section 1.2. Radioactive center is shown by asterisk *. R' can be either CoA or ACP.

2.4 Results and Discussion:

The commonly used assays for FabH enzymes (TCA precipitation and other assay formats) are very time consuming and tedious to perform. The radioactive long chain acyl substrate processed by mtFabH is very difficult to separate from the radioactive product by the conventional washing step used in these assays. Recently, Brown et al[57] have developed an alternative assay method for mtFabH based on an assay used originally by Garwin et al [61] for related FabF/FabB enzymes. This assay (Figure 16) involves the reduction of the assay mixture after reaction completion to produce radioactive substrate and product derivatives, which differ from each other in polarity. This difference permits simple separation of the two and quantitation of the radioactive product. The assay uses FabD to produce radioactive 2-^{14}C malonyl-ACP in-situ from holo-ACP and malonyl-CoA. The mtFabH catalyzes a decarboxylative condensation of this malonyl-ACP with the long chain acyl-CoA substrate ranging from hexanoyl CoA to arachidonyl CoA (C_6 – C_{20}), (see Table 3) to form a long chain β-ketoacyl-ACP. Reduction of this product by $NaBH_4$ gives the corresponding radioactive long chain alkyl-1, 3-diol product with a ^{14}C label at C2. This product derivative can be partitioned into non-aqueous phase whereas the radioactive propane-1, 3-diol obtained by reduction of the radioactive malonyl thioesters stays in an aqueous phase. We have further simplified this by using malonyl-CoA directly as a substrate, instead of malonyl-ACP (see figure 16).

	mtFabH Specific Activity (nMoles/min/mg)		
Acyl-CoA primer chain length	ec-Malonyl-ACP (*)	mt-Malonyl-ACP (*)	Malonyl-CoA (#)
C6	0.39+/-0.07	1.74+/- 0.28	0.38+/- 0.064
C8	5.98+/- 0.19	5.49+/-0.93	0.69+/- 0.18
C10	6.34+/- 0.49	6.16+/- 0.24	0.758+/- 0.095
C12	8.01+/- 1.07	7.24+/- 0.18	1.77+/-0.041
C14	2.24+/-0.10	9.46+/- 0.41	0.3528+/- 0.0269
C16	1.33+/- 0.10	9.27+/- 0.56	0.128+/- 0.086
C18	0.60+/- 0.10	10.39+/- 0.51	0.036+/- 0.0009
C20	0.06+/- 0.02	9.02+/- 0.27	0.155+/- 0.0133

Table 3: Effect of ACP on acyl group specificity of mtFabH. Total condensation activity of mtFabH is determined using ec-malonyl-ACP, mt-malonyl-ACP or malonyl-CoA and a range of different acyl-CoA substrates. (* - Data adopted from reference 57, # - data for the assay described herein).

A slower reaction rate for mtFabH is observed when malonyl-CoA was used in place of a malonyl-ACP substrate (Table 3). Dodecanoyl CoA is the preferred substrate for assays using either malonyl-CoA or ec malonyl-ACP (generated from the *Escherichia coli* ACP). With this acyl-CoA substrate the reaction rate is found to be about 4-fold slower with malonyl-CoA than with ec-malonyl-ACP or malonyl-ACPM (generated from the *M. tuberculosis* ACP). Catalysis with longer chain acyl-CoA substrates by the mtFabH is markedly reduced using either ec-malonyl-ACP or malonyl-CoA, but not malonyl-ACPM. One advantage of this modified assay is that all the substrates are commercially available. There is no need to obtain a purified ACP, or convert it to either the corresponding malonyl-ACP or biotinylated-malonyl-ACP, leading to significant savings in both time and cost. The direct utilization of radioactive malonyl-CoA in the

assay also maximizes the use of this substrate for the assay, avoiding the inevitable losses associated with conversion to malonyl-ACP. The assay also uses lower concentrations of malonyl-CoA (12.5 µM versus the 50 µM) typically used in other formats, both decreasing the amount of material and potentially increasing the range of the assay to include both poor and good competitive inhibitors. A final advantage of this new assay format is an excellent 60:1 signal to noise ratio (the scintillation proximity assay[27] is approximately 10:1).

2.5 Conclusion:

In conclusion, the assay described herein is a much faster and less cumbersome way to screen the potential inhibitors of mtFabH enzyme. Furthermore, the assay doesn't use ACP and thus can serve as an "ACP independent assay" for mtFabH enzyme. This particular aspect can be utilized to investigate the role of various types of ACP substrates for example- cognate vs non-cognate ACP. This assay is used to evaluate a series of novel mtFabH inhibitors in later chapter (6) of this dissertation.

3. Crystal structure of a substrate complex of M*ycobacterium tuberculosis* β-Ketoacyl-Acyl Carrier Synthase III (mtFabH) with Lauroyl-Coenzyme A

3.1 Summary

β-ketoacyl-acyl carrier protein synthase III (FabH) catalyzes a two step reaction that initiates the pathway of fatty acid biosynthesis in plants and bacteria. In *Mycobacterium tuberculosis*, FabH catalyzes extension of lauroyl, myristoyl and palmitoyl groups from which cell wall mycolic acids of the bacterium are formed. The first step of the reaction is an acyl group transfer from acyl-coenzyme A to the active-site cysteine of the enzyme; the second step is acyl chain extension by two carbon atoms through Claisen condensation with malonyl-acyl carrier protein. The crystal structure of a type II dissociated *M. tuberculosis* FabH, which catalyzes extension of lauroyl, myristoyl and palmitoyl groups, has been determined before. In this study, we describe the first long-chain Michaelis substrate complex of a FabH, that of lauroyl-coenzyme A with a catalytically disabled Cys→Ala mutant of *M. tuberculosis* FabH. An elongated channel extending from the mutated active-site cysteine defines the acyl group binding locus that confers unique acyl substrate specificity on *M. tuberculosis* FabH. CoA lies in a second

channel, bound primarily through interactions of its nucleotide group at the enzyme surface. The apparent weak association of CoA in this complex may play a role in the binding and dissociation of long chain acyl-CoA substrates and products and poses questions pertinent to the mechanism of this enzyme.

3.2 Introduction

The crystal structure of the homodimeric type II mtFabH was found to be very similar in conformation to the other determined FabH structures,[62,63] which adopt the thiolase fold. The thiolase fold defines a growing family of enzymes that includes yeast peroxisomal 3-ketoacyl-CoA thiolase,[64] β-ketoacyl-acyl carrier protein synthases I (FabB)[65] and II (FabF),[66,67] two plant type III polyketide synthases[68,69] and one FabH homologue from a type II bacterial polyketide synthase gene cluster.[70] In contrast to the *Escherichia coli* FabH structures, the mtFabH structure has a long channel extending from its active-site Cys112, which has been tentatively identified as a long-chain acyl group binding channel. This channel could accommodate an acyl chain of 12–16 carbon atoms, consistent with the specificity of mtFabH observed in solution reactions.[26,27] A second channel, also extending from the active-site cysteine, corresponds to the CoA binding channel identified in the *E. coli* FabH crystal structures. However, in the unliganded mtFabH crystal structure, this second channel was occupied by electron density that could be accurately modeled as a lauric acid, whose presence we ascribed to adventitious binding during expression and purification of the recombinant mtFabH.

To test our identification of these putative substrate binding channels and to determine the binding mode of the physiologically relevant longer chain acyl-CoA to mtFabH, we have determined the crystal structure of a substrate complex of lauroyl-CoA with a catalytically inactive C112A mutant of this FabH. This complex represents the presumed Michaelis complex of the reaction, which precedes acylation of the active-site Cys112 and release of the CoA cofactor. Replacement of the active-site Cys112 of FabH by alanine removes the enzyme acyl acceptor residue, thereby preventing the initial transacylation and capturing the Michaelis complex.

3.3 Experimental Procedures

3.3.1 Materials

All general chemical supplies not listed below were ordered from standard companies and were reagent grade or better. The source of specific supplies were as follows: BL21DE codon plus cells and pET-15b plasmid for cloning were bought from Novagen, Quikchange™ XL site-directed mutagenesis kit was from Stratagene, HiTrap ™ Chelating and Desalting columns used for protein procedures were from GE Biosciences (formerly Amersham Biosciences), 50 kDa cutoff Microcon and Centricon filters used were from Fisher scientific, crystal screen kits 1 and 2 and other crystallization supplies were from Hampton research, primers were ordered from Integrated DNA Technology and the QiaPrep Miniprep™ kit for DNA extraction was from Qiagen.

3.3.2 Construction of mtFabH mutants

The C112S and C112A mutations were made on the open reading frame Rv0533c (mtFabH), which was cloned into the expression vector pET-15b as described.[27] Mutants were made according to the protocol provided for the Stratagene Quickchange XL site-directed mutagenesis kit and primers designed to substitute serine and alanine for Cys112. Primers used for introducing point mutations were, for the C112S mutant: forward 5′-GAT CTT TCG GCG GGG AGC GCC GGA TTC GGA TAT G-3′, reverse 5′ -CAT ATC CGA ATC CGG CGC TCC CCG CCG AAA GAT C-3′, and for the C112A mutant: forward 5′-GAT CTT TCG GCG GGG GCC GCC GGA TTC GGA TAT G-3′ and reverse 5′-CAT ATC CGA ATC CGG CGG CCC CCG CCG AAA GAT C-3′. Mutations were confirmed by sequence analysis of the constructs. Plasmid was purified using the QIAprep miniprep kit following the protocol available with the kit.

3.3.3 Enzyme expression and purification

Competent *E. coli* BL21DE3 Codon Plus cells were transformed with pET-15b carrying either the C112S or C112A mutant FabH insert. Transformants were grown in LB medium to an absorbance of 0.4–0.6, induced with 0.1 mM isopropyl-β-d-thiogalactopyranoside, and incubated for an additional four hours at 37 °C. Cells were harvested by centrifugation at 10,000 ***g*** for ten minutes at 4 °C and stored at –20 °C overnight. After lysis with lysozyme on ice for 30 minutes, cells were sonicated on ice and then centrifuged at 12,000 ***g*** for 30 minutes at 4 °C. The supernatant was loaded onto a Hitrap chelating 5 ml column and washed with a gradient step from 0 mM to 120 mM

imidazole in 50 mM sodium phosphate buffer (pH 8.0) with 300 mM sodium chloride. FabH was eluted with 1 M imidazole under the same buffer conditions. The high concentration of imidazole employed in the washing step improves the homogeneity of the mtFabH band as assessed by SDS-PAGE analysis. The mtFabH was desalted in 100 mM sodium phosphate buffer (pH 7.0), and kept at 4 °C overnight. Protein was concentrated in centricon tubes and assayed by Bradford assay using BSA as standard. For crystallization, the concentration of mtFabH used was in the range of 4–15 mg/ml.

3.3.4 Crystallization, data collection and structure determination

Note: This part of the project was kindly performed by Dr. Faik Musayev, Dr. Tonie H. Wright and Dr. J. Neel Scarsdale.

Crystallization conditions were initially screened at room temperature using the Hampton crystal screen kits and the hanging drop method. Small crystals of apo-mtFabH (C112A) were obtained with a number of precipitants, and further refinement of conditions gave promising diffracting crystals from ammonium formate and sodium chloride as precipitants. Optimal crystals were obtained from drops made from 3 µl of protein solution at 4 mg/ml in 100 mM sodium phosphate buffer (pH 7.5) to which was added 3 µl of reservoir solution consisting of 2 M NaCl and 100 mM sodium Mes buffer (pH 6.5). Crystals were cryoprotected in solutions containing 100 mM sodium Mes buffer (pH 6.5), 2 M NaCl and 28% glycerol, the final concentration of glycerol being reached in two steps of 45 seconds each before flash cooling in the liquid nitrogen stream. Crystals diffracted to a resolution limit of 1.85 Å on a Rigaku rotating anode X-ray

source run at 50 kV, 100 mA equipped with Osmic confocal optics. A total of 110 frames of 1.3° oscillations were measured using an RAxisII image plate detector. Oscillation data were integrated with MOSFLM and merged with SCALA. Data collection statistics are summarized in Table 4.

The complex of mtFabH (C112A) with lauroyl-CoA was prepared by mixing a mtFabH solution with 50 mM lauroyl-CoA in doubly distilled H_2O. The best crystals of the C112A–lauroyl-CoA complex were obtained from 1.6 M ammonium formate in 100 mM sodium Hepes buffer (pH 6.5). The plate form crystals reached maximum size of about 0.05 mm×0.1 mm×0.15 mm in two to three days. To minimize the effect of hydrolysis during crystallization, data were collected on crystals as soon as they reached sufficient size. Crystals were cryoprotected for a few seconds in a solution containing 2.7 M ammonium formate, 0.4 mM lauroyl-CoA, 14% glycerol, 100 mM sodium Hepes (pH 6.5), followed by quick transfer to a similar solution containing 3.5 M ammonium formate and 28% glycerol and freezing at 100 °K in the nitrogen stream. The crystals diffracted beyond 2.3 Å resolution and data sets of 135 oscillation frames were collected with a step size of 2.5°. Oscilllation data were integrated and merged with BIOTEX.

A model consisting of the biological dimer from our structure of mtFabH (RCSB entry 1HZP)[27] was used as a search model for molecular replacement for both the liganded and unliganded data sets. A cross-rotation search was carried out using the fast direct search protocol as implemented in CNS version 1.0.[71] For the unliganded data set, solutions corresponding to the highest peaks from the cross-rotation search were used as input to a translation search as implemented in CNS version 1.0. Inspection of initial

Table 4: Data collection and refinement statistics for mtFabH C112A and C112A.lauroyl-CoA (C112A/LCOA) structures

	C112A	C112A●LCOA
Data Collection		
Space Group	$P2_12_12_1$	P1
Unit Cell	55.25,109.01,110.98, 90.,90.,90.	55.57,63.19,55.33,113.2,100.8,92.7
Resolution (Å)	1.85	2.3
R_{merge}[1] overall/highest resolution shell	0.044/0.14	0.073/0.26
$\langle I \rangle / \langle \sigma(I) \rangle$ overall/highest resolution shell	9.1/5.0	8.7/1.9
Completeness overall/highest resolution shell	0.98/0.98	0.92/0.90
N_{obs}	56576	28398
Multipliciity	4.6	2.9
Wilson Plot B ($Å^2$)	26.7	46.6
Optical Resolution (Å)[2]	1.44	1.77
Refinement		
R_{work}[3] overall/highest resolution shell	0.186/0.219	0.206/0.333
R_{free}[c] overall/highest resolution shell	0.208/0.247	0.247/0.412
Completeness, overall/highest resolution shell[c]	0.975/0.809	0.950/0.757
$\langle B \rangle$($Å^2$)	13.2	37.3
N_{work}	50770	26967
N_{free}	5143	1431
N_{atoms}	5391	5203
$N_{degrees\ of\ freedom\ Torsion\ Angle\ Dynamics}$	2277	2321
Rmsd from ideal:		
bond length (Å)	0.007	0.008
bond angles (^{o})	1.085	1.323
Ramachandran Plot		
Most favored(%)	90.4	89.5
Additionally Allowed(%)	8.9	9.8
Generously Allowed(%)	0.4	0.7
Forbidden(%)	0.4	0.0
Cruickshank's Diffraction Precision Indicator[4]	0.167	0.493
Estimated Maximal Coordinate Error	0.059	0.218

[1] $R_{merge} = \Sigma\Sigma_i \left| I_h - I_{hi} \right| / \Sigma\Sigma_i I_h$ where I_h is the mean intensity of reflection h. All data with $I > -3\sigma$ are included.

[2] $W = (\sigma^2_{Patterson} + \sigma^2_{sph})^{1/2}$ the expected minimum distance between two resolved atom peaks

[3] Calculated with all reflections

[4] $\sigma(x) = (N_{atoms}/N_{obs})^{1/2} c^{-1/3} d_{min} R_{free}$

$2mF_o-dF_c$ maps generated with phases from the molecular replacement solutions indicated the presence of broken density in the putative acyl and pantetheinate channels of both monomers consistent with the binding of lauroyl-CoA in the C112A-lauroyl-CoA crystal. No significant density was observed in maps generated for the unliganded crystal. Models were refined iteratively using simulated annealing and torsion angle dynamics as implemented in CNS version 1.0 coupled with TLS[71] and positional refinement in REFMAC5[72] followed by manual rebuilding into $2mF_o-dF_c$, mF_o-dF_c and $2mF_o-dF_c$ composite omit maps using the programs O,[73] TOM or Xfit.[74] In the final stages of refinement, 556 and 197 water molecules were added to the unliganded and liganded structures, respectively, on the basis of the presence of peaks with heights $>3\sigma$ in the mF_o-dF_c maps. During iterative rebuilding, residue geometries were monitored *via* PROCHECK, WHATCHECK[75] and OOPS2,[76] while van der Waals contacts and hydrogen bonds were monitored using PROBE[77] as integrated with Xfit. Model coordinate errors were estimated using Cruikshank's diffraction precision indicator as implemented in SFCHECK.[78]

Accession Numbers:

*Coordinates for the mtFabH C112A mutant and C112A + lauroyl-CoA have been deposited in the Protein Data Bank (accession codes **1U6E** and **1U6S**)*

3.4 Results

3.4.1 Electron density interpretation

To obtain a stable complex of lauroyl-CoA with mtFabH, we made both C112A and C112S mutants to suppress transacylation activity to the active-site cysteine. Complexes of lauroyl-CoA with both the C112A and C112S mutants were made in solution and crystallized under significantly different conditions in similar but non-identical lattices. Both electron density maps showed density in the CoA channel and in the putative acyl-binding channel of each subunit of the homodimer, but the density for the C112S mutant was weaker than that for C112A. Only the structure of the C112A ligand complex is described and discussed here. The structure of the unliganded mtFabH (C112A), whose conditions of crystallization and lattice type are completely different from those of the wild-type, is essentially identical with that of the wild-type mtFabH previously described with one minor exception. The higher resolution of this structure revealed a bend in helix Cα1 (for nomenclature, see Davies *et al.*[62]) between residues 218 and 221 not reported earlier.[27] This bend is not present in the corresponding helix of *E. coli* FabH and may be a consequence of lattice interactions in the mtFabH (C112A) structure (see next section). Crystal parameters and statistics for data collection and refinement of the unliganded and liganded crystal forms of mtFabH (C112A) are shown in Table 4.

Electron density for the lauroyl-CoA ligand in complex with C112A mtFabH was readily fit to each subunit of the homodimer in the omit and $2F_o–DF_c$ maps. Electron density for the adenosine-3′-phosphate moiety of CoA is almost complete in the A

subunit, but is broken in several places in the composite omit map of the corresponding site of the B subunit. There is a break in electron density at the pyrophosphate-ribose linkage of the CoA in both subunits (Figure 17). The descriptions that follow pertain to the model for lauroyl-CoA in the A subunit binding site, but those of the B subunit are very similar. There are no significant differences in conformation between the two subunits of the biologically functional homodimer of either the unliganded or complexed mtFabH, as was also observed for complexes of *E. coli* KAS I covalently[66] bound to C10 and C12 acyl groups and *E. coli* FabH[64] with bound CoA.

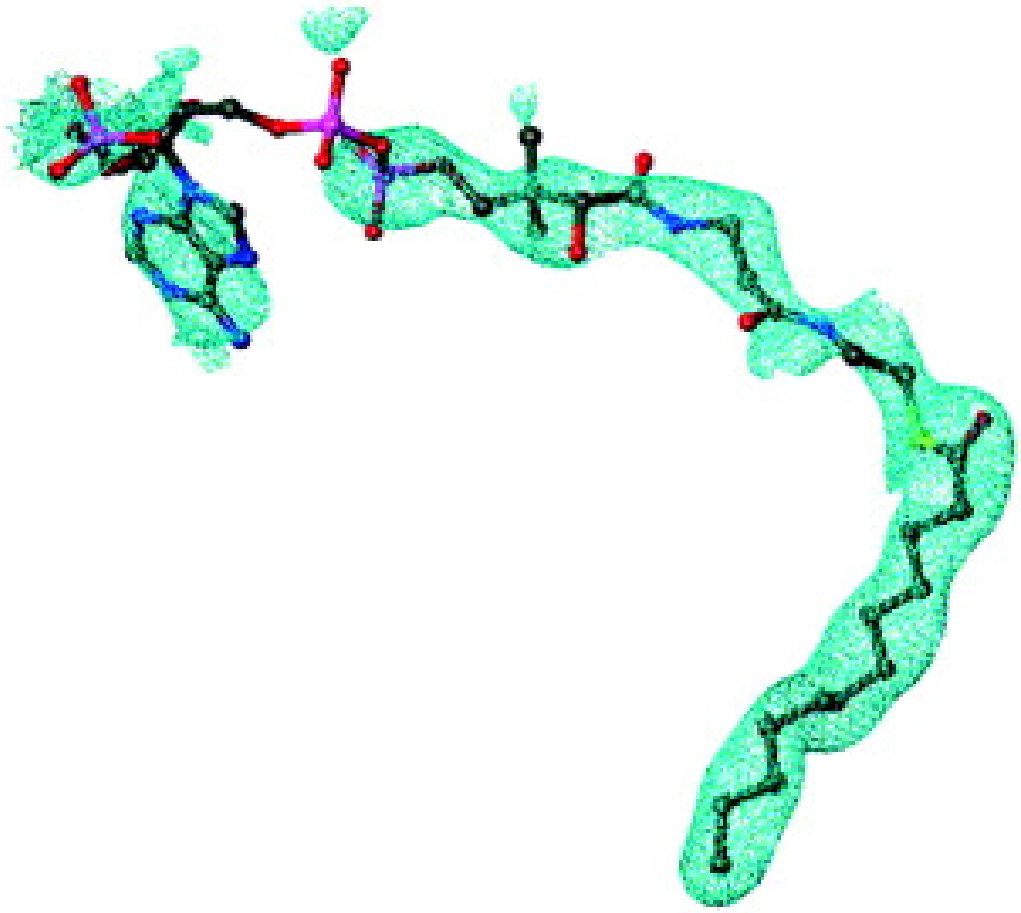

Figure 17: Composite omit map electron density for lauroyl-CoA bound to subunit A of mtFabH homo-dimer.

3.4.2 Packing of FabH dimers in the crystal lattice

The tight functional FabH homodimers are related to each other in the triclinic lattice by a pseudo-dyad axis parallel with the dyad of the functional homodimer (Figure 18 (a)). Although much smaller in area than the contact surface between the monomers of the biological homodimer, the contact area between non-crystallographic dimers is not negligible (1535 $Å^2$). It is formed across a local dyad by pairwise interactions between helix Cα1 of one monomer (residues 210–231) and helix Cα2 (residues 248–259) and part of helix L1α2 (28–35) of an adjacent monomer. A consequence of this interaction is that the 3′-phosphoryl-adenosine pyrophosphate groups of CoA in monomer subunits of different functional dimers are in close proximity across this local pseudo-dyad (Figure 18 (b)). The CoA adenosine nucleotide group of subunit A lies immediately next to this pseudo-dyad, which appears to force a displacement of the corresponding part of the ligand in the opposing B subunit. We infer that the local static disorder in the 3′-phosphoadenosine pyrophosphate groups of the CoA in each monomer is a consequence of this close approach of polyanionic groups.

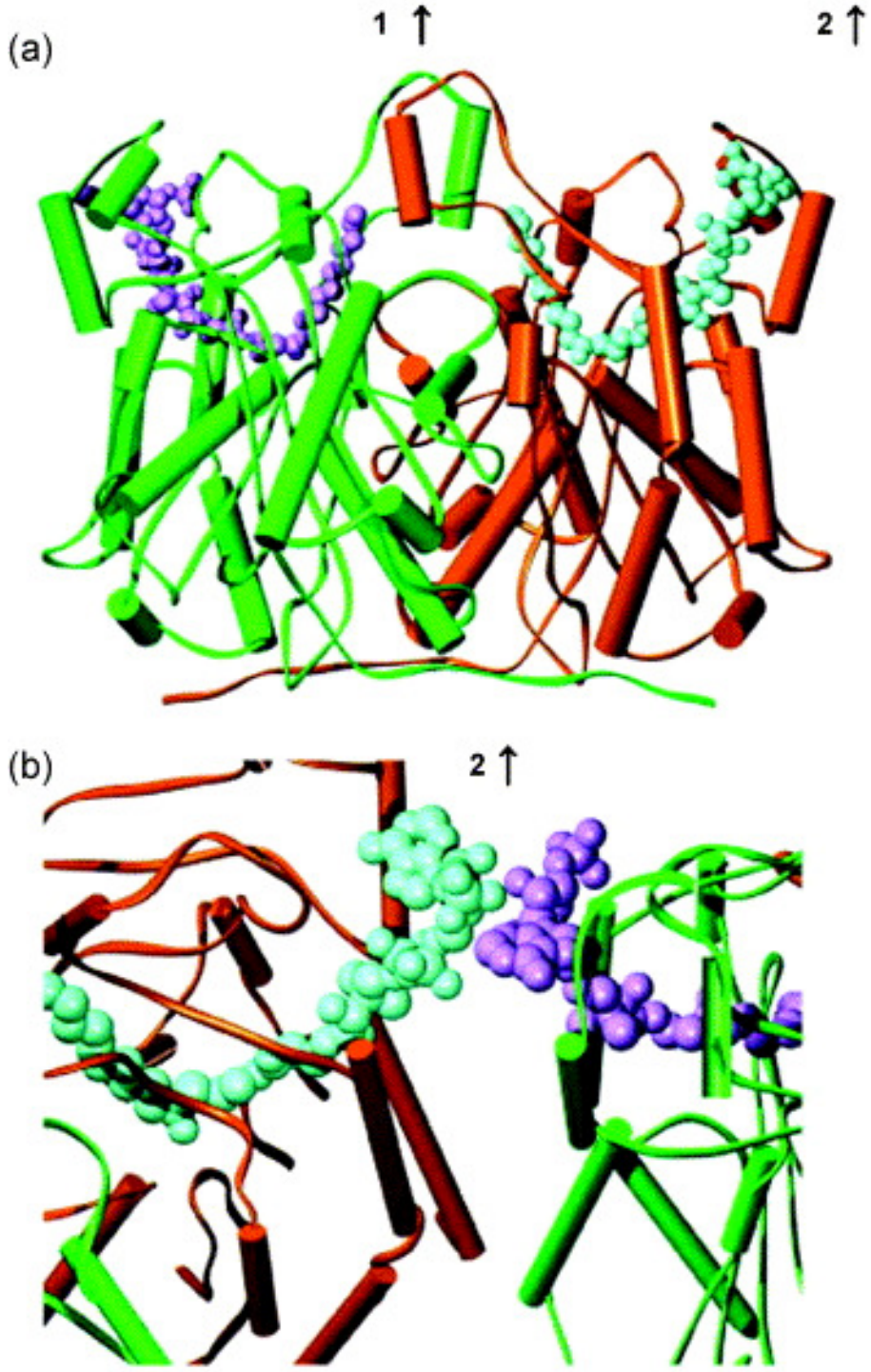

Figure 18: (a) Model of the mtFabH dimer with lauroyl-CoA (ball and stick models: blue in subunit A and magenta in subunit B). Arrow 1 denotes the non-crystallographic 2-fold rotation axis relating the monomers of the functional dimer; arrow 2 denotes a distinct pseudo-2-fold rotation axis relating the functional dimers. (b) **Contact region of two functional homodimers of the asymmetric unit**: The proximity of adenosine triphosphate groups of lauroyl-CoA is depicted at the non-crystallographic 2-fold rotation axis (2) displayed in (a).

3.4.3 The lauroyl binding channel

Electron density for the lauroyl group in the mtFabH–lauroyl-CoA structure is clear and shows this chain lying in the channel hypothesized from the unliganded mtFabH structure (Figure 17). The lauroyl chain is extended, but with a bend at C7–C8 which lies between Thr (B87) and Thr (A145). A similar bend at C6 was observed in structures of decanoyl and dodecanoyl groups in complex with KASI and was attributed to the presence of Phe201 in the acyl channel.[66] As noted earlier,[27] Thr87 plays a permissive role in opening this channel to longer acyl chains, in contrast to *E. coli* FabH, in which residue 87 is a phenylalanine, which restricts the acyl chain length to four carbon atoms or less. There is sufficient room at the distal end of the lauroyl chain to accommodate four more carbon atoms, consistent with the observed *in vitro* activity of mtFabH toward myristoyl- and palmitoyl-CoA substrates, as well as lauroyl-CoA.[26] The acyl carbon of the lauroyl group is juxtaposed at a distance of 2.20 Å to the modeled Cys112 S^{γ} of wild-type mtFabH overlaid on the Ala112 mutant structure, and the carbonyl oxygen makes hydrogen bonds of unequal length (3.01 Å and 2.66 Å) to the main-chain –NH– of A112 and A306 (Figure 19). This oxyanion hole is a conserved feature of the ketoacyl synthases and stabilizes the inferred tetrahedral intermediate.

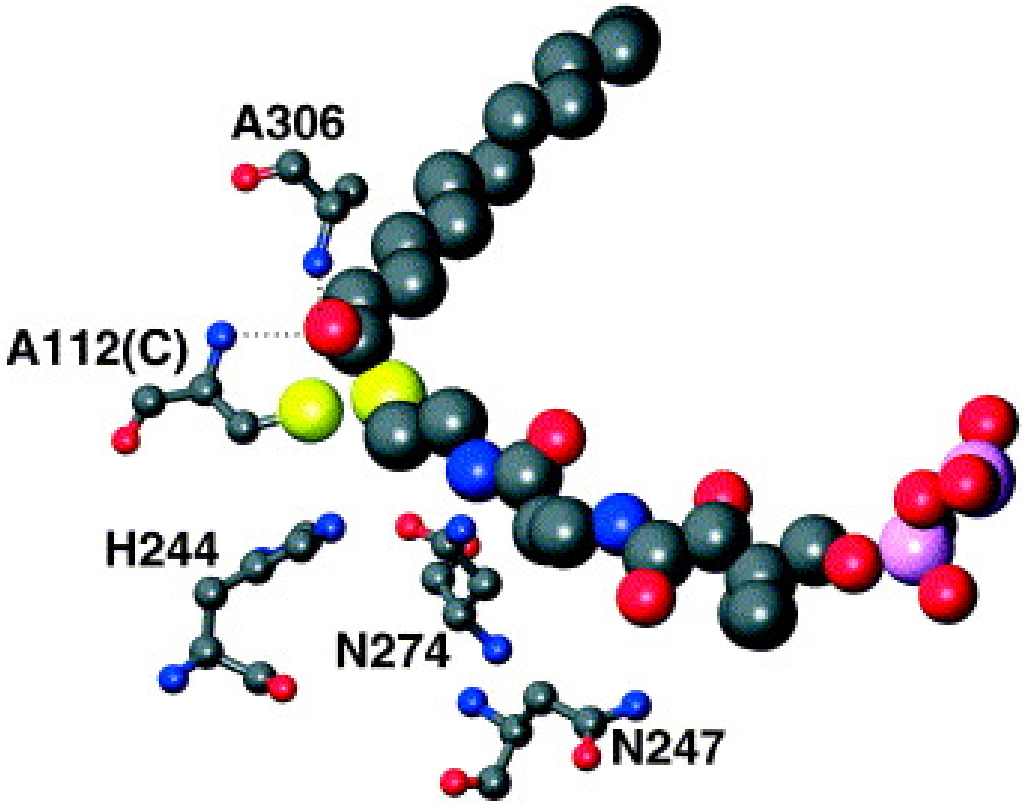

Figure 19: Model centered on the lauroyl acyl group linkage to CoA in subunit A showing the mutant active-site alanine overlaid on the wild-type active-site cysteine A112(C)). Dotted lines are hydrogen bonds from proton donors of the oxyanion hole to oxygen of the acyl group.

3.4.4 Conformation and interactions of coenzyme A

The CoA part of lauroyl-CoA lies in the channel in which a putative lauric acid binds to the unliganded wild-type mtFabH structure. Although this density is contiguous, except at the pyrophosphate linkage, and has structural features through most of its length, it is not sufficiently well resolved to be unambiguously fit by the CoA model. The model of the CoA from the ecFabH complexes cannot be fit throughout to the electron

density of the mtFabH–CoA structure: the mercaptoethylamine and nucleotide pyrophosphate portions of the CoA in the mtFabH–lauroyl-CoA complex differ significantly in position and conformation from those observed in the ecFabH–CoA complexes, while the pantetheinate parts appear to be more similar (Figure 20).

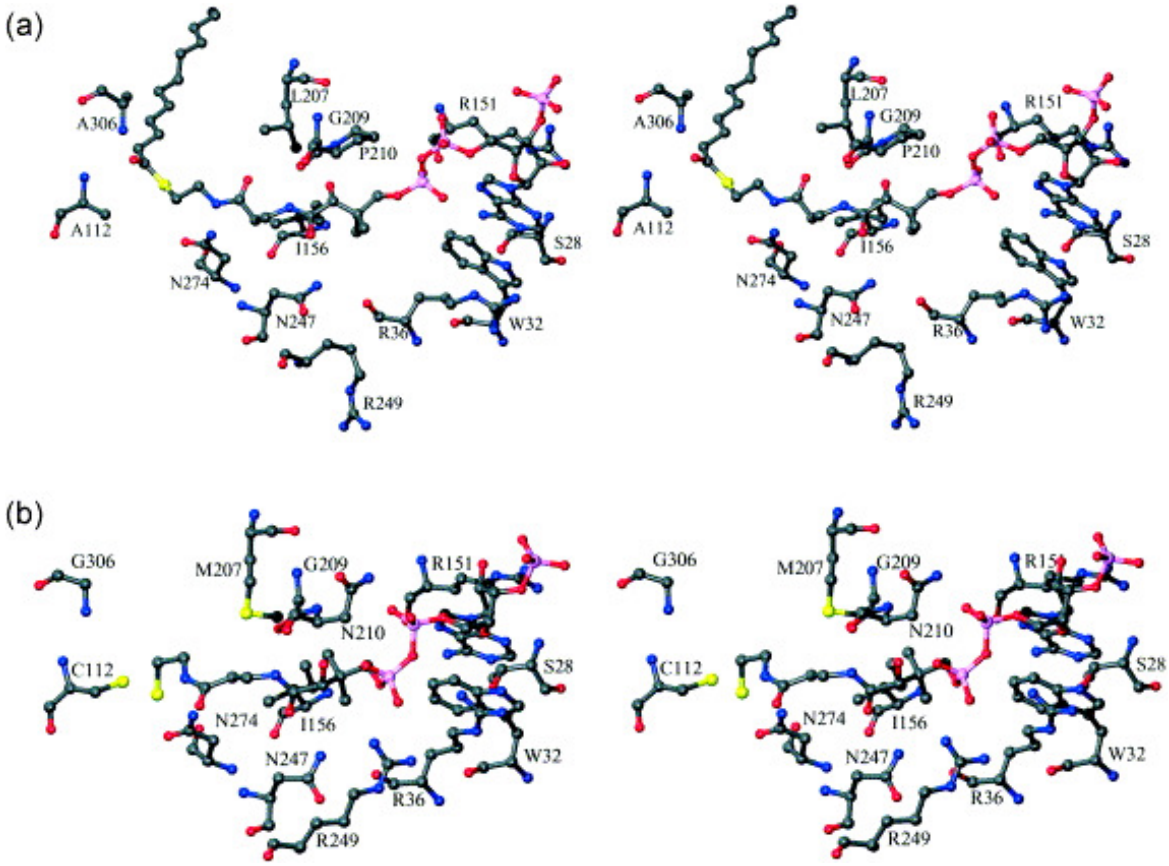

Figure 20: Stereo view of amino acid residues in proximity to the bound CoA portion of lauroyl-CoA in the A subunit of mtFabH (a) and of CoA bound to *E. coli* FabH (b).

Most of the interactions of CoA with mtFabH occur at the distal adenosine nucleotide terminus, which lies at the mouth of the CoA binding channel. The adenine ring of CoA is sandwiched between the planes of Trp32 and the guanidinium group of Arg151, as was observed for the ecFabH–CoA complex,[63] and the adenine amino group makes a hydrogen bond to O^{γ} of Ser28. This intercalation of the adenine ring requires unstacking of the Trp32 and Arg151 side-chains of the unliganded FabH structure on binding of the cofactor ligand. The 3′ phosphoryl groups of the CoA in the A subunit interact with Arg151 from the A subunit and also from a lattice-related B subunit across the non-crystallographic-dyad axis (2) described above. Density for the ribose pyrophosphate of the CoA in the mtFabH–lauroyl-CoA complex is broken at the pyrophosphate, but it is clear that the model of CoA derived from the ecFabH–CoA complexes cannot be fit to it. This is likely due to the close crystal lattice contacts across the non-crystallographic dyad described above in the mtFabH–lauroyl-CoA complex. This dyad lies between the 3′-ribose phosphate groups of CoA in different dimers in the lattice and the juxtaposition of these two anionic groups appears to induce static disorder at this site. The high temperature factors for the CoA in the mtFabH complex indicate some disorder in the cofactor and are consistent with the paucity of interactions between the cofactor and the protein. The temperature factors for protein groups lining this channel are near the mean for the overall structure, further confirming that the disorder is confined to the cofactor. The temperature factors for the CoA moiety in the channel are not an artifact of erroneous occupancies, since the temperature factors for the lauroyl group are much lower than those of the CoA. In the structure of the ecFabH–CoA

complexes, the temperature factors for those parts of the cofactor visible in the electron density map are only slightly higher than those for the protein. These observations are consistent with a loosely bound CoA in the mtFabH–lauroyl-CoA complex. The possible origins and implications of this are discussed below.

3.5 Discussion

As a regulated catalyst of the first step in an essential biosynthetic pathway, FabH has been identified as a potential target for development of new antibacterial agents. The distinctions between the monomeric type I FAS of animals and the type II dissociated FAS of bacteria offer the prospect that a target-specific antibiotic would discriminate between host and pathogen. The crystal structure described here is the first of an intact substrate complex of FabH with an acyl-CoA, and provides a template for the design of possible inhibitors of this vulnerable class of enzymes.

Previous attempts to determine the structure of complexes of ecFabH with acyl-CoA (acetyl and malonyl) prepared by incubation either failed to show electron density for the acyl group or were transacylated.[63] Electron density was visible, however, for the CoA ligand in these structures and it provided information on the mode of cofactor binding in the product complex. Crystal structures for two acetyl–CoA complexes with ecFabH (1HNH, 1HND) have been determined. In one, the acetyl group is covalently bound to the active-site cysteine S^{γ}, but is missing in the other, though the CoA is retained in the binding channel of both. In the malonyl–CoA complex with ecFabH

(1HNJ), the malonyl group is not observed and was inferred to be disordered or to have hydrolyzed during preparation, but CoA is observed in the binding channel. The acetyl–CoA complex with ecFabH is therefore a product complex of the initial transacylation step of the reaction, probably stabilized by the retention of bound CoA, which prevents ingress of water that would hydrolyze the thioester linkage. The other two ecFabH complexes, while not on the reaction pathway, confirm the observed conformation of the CoA as that for product complex, except for variation in the tail from C7 of the pantetheinate through the mercaptoethylamine group.

In contrast to ecFabH–CoA complexes, formation of CoA crystal complexes with mtFabH, either by soaking or cocrystallization, has been problematic. When lauroyl–CoA is used as substrate to try to prepare substrate or product complex with wild-type mtFabH, only lauric acid is observed to bind in the acyl channel. This latter result suggests that the lauroyl-thioester intermediate is hydrolyzed by water that can enter the active-site in the absence of bound CoA and is consistent with a low affinity of CoA for its binding channel in mtFabH relative to ecFabH. By utilizing a catalytically disabled FabH mutant, C112A, we have been able to visualize the intact lauroyl–CoA substrate bound to mtFabH. The acyl linkage between the lauroyl group and the β-mercaptoethylamine of the CoA is clearly visible in our electron density map. The length of the acyl channel in the mtFabH–lauroyl-CoA complex is consistent with the substrate specificity of this enzyme in solution and confirms our hypothesis for the unique role of this type II FabH in the biogenesis of long chain fatty acids in *M. tuberculosis*.[27]

Of the few known structures[64,69,70] and inferred models[79] of CoA complexes with ketoacyl-synthases, the CoA of the mtFabH–lauroyl-CoA complex described here appears to be the least stabilized in its binding site. The observed difference in binding mode of CoA between the *E. coli* and mtFabH complex structures could arise from any of several sources: (i) differences in the residues that interact with the CoA in the two FabHs; (ii) effects of the CoA-linked lauroyl group; (iii) distinctions between substrate and product complexes; (iv) the influence of lattice interactions on the conformation of CoA.

There are two amino acid differences between ecFabH and mtFabH in the pantetheinate binding part of the CoA channel: L189, which is Ile in mtFabH, and M207, which is Leu in mtFabH. HINT analysis[80] of the ecFabH and mtFabH complexes with CoA shows that these two residues make unfavorable polar-hydrophobic interactions with the pantetheinate as built in the mtFabH complex. These two unfavorable contacts, plus several favorable ones in the ecFabH–CoA complex that are not made in the mtFabH–lauroyl-CoA complex are consistent with more stable binding of CoA in the ecFabH–CoA complex than in the mtFabH.

It is possible that binding of the lauroyl group affects the conformation of the CoA in the mtFabH–lauroyl-CoA complex relative to that observed in the ecFabH–CoA complex. This seems unlikely for substrate acyl–CoA complexes, since the stereochemical requirements for acylation will be the same for small and large acyl groups. However, because we are comparing a substrate complex (mtFabH–lauroyl-CoA) with a product complex (ecFabH–CoA), differences in structure could be a consequence

of differences between these chemically distinct intermediates on the reaction pathway. The apparent higher stability of the CoA in the ecFabH complexes than in the mtFabH–lauroyl-CoA complex may reflect differences in the energetics of binding substrate *versus* product. These differences are most likely to be manifested at the mercaptoethylamine part of the CoA where chemical bonding differs in the two complexes. This could explain the major differences in conformation of this part of the CoA between the ecFabH–CoA and mtFabH–lauroyl-CoA complexes. In this connection, we note that the overall conformation of the lauroyl–CoA ligand in the mtFabH complex differs from that of two other long-chain acyl–CoA complexes in the RCSB database (*1H9G, 1IYK*). This is consistent with a relatively flat energy surface for CoA conformers and a dominant role for the protein binding site in determining the conformation of bound CoA.

Finally, the close lattice contacts involving the nucleotide ends of CoA in the mtFabH–lauroyl-CoA complex are likely to induce changes in conformation of the CoA in each copy of the complex. This is a probable cause for the difference in conformation of the ribose pyrophosphate group in the ecFabH–CoA complex *versus* that in the mtFabH–lauroyl-CoA complex. The electron density for this part of the CoA in the latter complex is broken, which is consistent with disorder imposed by the close contact of anionic groups. Nevertheless, density for the adenine ring is complete in subunit A and substantial though incomplete in subunit B, indicating that this interaction is a highly stabilizing one and can tolerate disorder in immediately contiguous groups.

The difference in apparent stability of bound CoA between the mtFabH–lauroyl-CoA and the ecFabH–CoA complex may reflect compensating contributions of the acyl and CoA moieties that result in isoenergetic binding of both long and short acyl-CoA substrates. The longer acyl chain of mtFabH substrates will be more stable in its extended, sequestered hydrophobic binding channel than an acetyl group and could thereby anchor the CoA portion of the substrate, which may have lower stability bound to the mtFabH than to ecFabH. It may be more important to note that neither the ecFabH product complex nor the mtFabH substrate complex described here shows numerous or strong stabilizing interactions of bound CoA in the CoA channel. This may reflect a requirement for facile dissociation of the product CoA ligand after the initial transacylation step of the reaction and could help drive this reaction, which is a ground state exchange with little intrinsic energy difference between substrate and product.

These arguments and the structure of the complex of lauroyl-CoA with mtFabH raise two questions relating to the trajectory and energetics of long chain acyl group binding to FabH. For instance, how does the long acyl chain enter the seemingly restricted binding channel in mtFabH. If the acyl group threads through the CoA channel past the active-site cysteine to reach the buried acyl channel, what drives that translocation? And how is a long chain ketoacyl-ACP product dissociated from the enzyme? In the case of long chain acyl-CoA binding, differential stability of the acyl group in its highly hydrophobic specificity pocket could promote its migration beyond the CoA channel, culminating in a substrate complex stabilized primarily by the sequestered acyl group and the nucleotide end of the CoA. An alternate mechanism

where the substrate entry is facilitated by conformational changes in the enzyme is also possible. Following transacylation to the active-site cysteine, the paucity of interactions of the CoA in the pantetheinate binding channel would permit its ready dissociation. This might be further assisted by disruption of the adenine nucleotide interaction of CoA at the mouth of the channel through competition with incoming malonyl-ACP. However, following decarboxylation and condensation by mtFabH, a long-chain ketoacyl-ACP product complex would be stabilized in its bound state due to the buried position of the acyl group in the hydrophobic channel. Dissociation of this long-chain ketoacyl-ACP product would seem to require facilitating mechanisms.

3.6 Conclusions:

The crystal structure of this complex confirms our identification of the acyl binding channel and shows the mode of binding of the acyl group in this channel and of CoA in the other channel. This supports the hypothesized function for this FabH as an initiator of mycolate biosynthesis utilizing acyl-CoA chains of length 12–16 carbon atoms. This structure also suggests distinctions from the ecFabH in its interactions with CoA and poses several important questions regarding the binding of substrates and energetics of the FabH reaction mechanism.

4. Probing reactivity and substrate specificity of both subunits of the dimeric *Mycobacterium tuberculosis* FabH (mtFabH) using alkyl-CoA disulfide inhibitors and acyl-CoA substrates

4.1 Summary

The dimeric *Mycobacterium tuberculosis* FabH (mtFabH) catalyses a Claisen-type condensation between an acyl-CoA and malonyl-Acyl Carrier Protein (ACP) to initiate the Type II Fatty Acid Synthase cycle. To analyze the initial acylation of mtFabH with acyl-CoA, we challenged it with a mixture of C_6-C_{20} -CoAs and the ESI-MS analysis showed reaction at both subunits and 'a strict specificity for C_{12}-CoA. Crystallographic and ESI-MS studies of mtFabH with decyl-CoA disulfide inhibitor revealed the decyl chain bound in acyl-binding channels of both subunits through disulfide linkages to the active site cysteines. These data provide the first unequivocal evidence that both subunits of mtFabH can react with substrate or inhibitor. The discrepancy between the observed C_{12}-CoA substrate specificity in the initial acylation step and the higher catalytic efficiency of mtFabH for C_{18}-C_{20} -CoA substrates in the overall mtFabH catalyzed reaction suggests a role for *M. tuberculosis* ACP as a specificity determinant in this reaction.

4.2 Introduction:

Enzymological studies have shown that mtFabH can utilize a wide range of C_{12}-C_{20} acyl-CoA substrates,[26,27,57] which distinguishes it from FabH in other type II FAS systems that typically utilize C_2-C_6 acyl-CoA substrates.[26,81] Initial studies using malonyl-*E. coli* ACP (ecACP) as the malonyl-ACP substrate of mtFabH indicated a broad C_8-C_{20} acyl-CoA substrate specificity.[26] The C_{10}-C_{12} acyl-CoA substrates were processed most efficiently (6-8 nmol/min/mg), while the reaction rates using the putative, physiological longer chain (C_{18}-C_{20}) acyl-CoA substrates were significantly lower (<0.6 nmol/min/mg).[57] This same pattern has recently been observed in assays using malonyl-CoA in place of malonyl-ACP [data in publication]. However, mtFabH has a higher turnover number toward longer chain C_{14}-C_{20} acyl-CoA substrates (9-10.5 nmol/min/mg) in the overall reaction when cognate ACPM is used in the assay.[57] The basis for this differential efficiency in processing longer chain acyl-CoA substrates remains unclear.

The crystal structures of mtFabH and an array of mutants have raised other questions relating to processing of longer chain C_{18}-C_{20} acyl-CoA substrates. (see chapter 3 and ref. [27,57]) mtFabH has a closely similar topology and active site architecture to that of *E. coli* FabH (ecFabH). However, whereas ecFabH has a small acyl binding pocket contiguous with the pantetheinate binding channel, the substrate binding pocket of mtFabH is L-shaped, consisting of a solvent accessible pantetheinate binding channel connected to a closed, elongated acyl binding channel. The active site catalytic triad (Cys112-His244-Asn274) lies at the junction of the two arms of the "L". The closed

distal end of the acyl binding channel imposes an upper length limit of C_{16} for acyl-CoA substrates in the static mtFabH structure. An mtFabH crystal structure of the Michaelis complex of dodecanoyl-CoA with an inactive C112A mutant (chapter 3) clearly shows substrate bound in the "L" shaped channel of each monomer, with the dodecanoyl group in the acyl binding channel. The length of this channel raises the as yet unanswered question of how longer C_{18}-C_{20} acyl-CoA substrates bind and acylate mtFabH.

Previous observations made with both the ecFabH and mtFabH raise a third question of whether both monomers of the mtFabH homodimer are acylated. In the case of the ecFabH crystal structures,[63,82] including an unliganded tetragonal form of ecFabH in which several polypeptide segments that contribute to the structure of the substrate binding site and to the dimer interface are disordered, indicate structural equivalence of the two monomers. However, we have recently obtained a crystal structure of the inhibition complex of ecFabH with a methyl-CoA disulfide (MeSSCoA) in which there is a methyl disulfide linkage to the active site cysteine in only one monomer of the dimer.[83] Attempts to obtain a crystal structure in which both subunits are modified have thus far been unsuccessful. Kinetic analysis of MeSSCoA inhibition suggests that both subunits of ecFabH are modified via a biphasic process in which one subunit is modified quickly and the second more slowly. A similar biphasic acylation of the ecFabH with acetyl-CoA substrate was also observed. These observations have led to the proposal that ecFabH exists in an open form that orders around either a substrate or inhibitor in one subunit, and in so doing retards binding of ligand to the second subunit.[83] Similar asymmetry of ligand binding and disorder→order transitions may occur in mtFabH and may severely

hamper ligand binding and reaction at the second subunit. Indeed, it has been reported that acylation studies carried out using the mtFabH and radiolabeled decanoyl-CoA (in a molar ratio of 1:2.3) result in only 23% acylation of the protein[57]. Our complex of the mtFabH C112A mutant with lauroyl-CoA indicates structural identity of the two monomers (as seen for all mtFabH structures) and also that under prolonged incubation dodecanoyl CoA can bind in both subunits of the enzyme (chapter 5)

In this work we have addressed these questions of mtFabH specificity and mechanism using ESI-MS and crystallography to monitor the reaction of the wild type mtFabH with both a decyl-CoA disulfide inhibitor and a wide range of C_6-C_{20} acyl-CoA substrates. We have shown conclusively that substrate and inhibitor react with the active site cysteines in both subunits of the mtFabH dimer. We have also probed for the first time the substrate specificity of the acylation step catalyzed by mtFabH (previous analyses have only assessed this step indirectly by analysis of the overall reaction), and shown clear preferential formation of a modified enzyme using a C_{12} dodecanoyl-CoA. These findings imply a role for ACPM in determining the specificity of the mtFabH reaction and the profile of the product pool and provide new and essential data for the formulation of a model for mtFabH catalysis.

4.3 Experimental procedure

4.3.1 Materials

Long chain acyl-CoAs, coenzyme-A, imidazole, dithiothreitol (DTT) (Sigma); Crystal screens I and II (Hampton Research).

4.3.2 Enzyme expression and purification

The wild type and C112A mtFabH proteins were overexpressed in *E. coli* as discussed in chapter 3.

4.3.3 Synthesis of decylSSCoA

DecylSSCoA was synthesized using standard procedures[83] and generously provided by Dr. Mamoun Alhamadsheh.

4.3.4 ESI-MS analysis

A solution of wild type or mutant mtFabH in sodium phosphate buffer (50 mM, pH 7.0, 15 % glycerol) was incubated at room temperature for 40 min with either an equimolar mixture of C_6, C_8, C_{10}, C_{14}, C_{16}, C_{18}, and C_{20} acyl-CoAs (ratio of mtFabH monomer to each substrate was 1:5) or decylSSCoA (ratio of mtFabH monomer: inhibitor of 1:5). Excess ligand in both incubations was then removed using Pierce spin desalting columns and the enzyme concentrated in a Microcon concentrator (50 kDa cutoff) and stored at –20˚C until the ESI-MS analysis was performed. The thawed samples were diluted to a concentration of approximately 1 pm/µl with 50% methanol/0.1% formic acid and analyzed by ESI-MS using a Quadrupole Time-of-flight mass spectrometer under standard procedures and the peaks were deconvoluted by the Bayesian protein reconstruct tool (in the Bioanalyst QS 1.1 software package).

4.3.5 Crystallization conditions (Kindly performed by Dr. Faik Musayev)

Prior to crystallization trials, the protein solution was concentrated to approximately 15mg/ml by ultrafiltration using a Microcon concentrator (Amicon) with a 30 kDa cutoff. The enzyme (15mg/ml in 100mM sodium phosphate buffer, pH 7.0) and inhibitor (13mM in methanol) solutions were mixed in a 1:3 molar ratio and incubated on ice for 2 hours. Crystallization of the mtFabH- C_{10}SSCoA was achieved using the hanging-drop vapour-diffusion technique. Initial crystallization conditions were screened using Crystal Screen and Crystal Screen II from Hampton Research at 290K. Crystals grew within two-three weeks from PEG-4K and PEG-10K and further variation of conditions yielded two optimal crystal forms. Both were obtained by mixing 2µl of protein-inhibitor complex solution with an equal volume of reservoir solution and equilibrated over the precipitant well at 295K. The first crystal form was obtained in 25% (w/v) PEG-8K, 0.1 M ammonium sulfate and 100mM Na Cacodylate, pH 6.5 and grew to maximum dimensions of ~ 0.04 x 0.02 x 0.06 mm within three weeks. These crystals have space group P1, with unit cell parameters a = 49.06, b = 55.76, c = 63.16 A, α = 92.8, β = 98.8, γ = 111.8^0. The second crystal form was crystallized in the presence of 18% PEG-10K (w/v) and 100mM Na Hepes, pH 7.0 and grew to 0.05 x 0.03 x 0.3mm within three weeks. These crystals have space group C2221 with unit cell parameters a = 67.65, b = 89.36, c = 232.01 A.

Data sets for both crystal forms were collected at 100°K on an R-Axis IV++ image-plate detector using CuK α X-rays (λ = 1.54 A) from a Rigaku MicroMax ™ 007 X-ray source equipped with MSC Varimax confocal optics operating at 40kV and

20mA. The crystals were transferred with a cryoloop into corresponding mother liquor solutions containing additional 15-20% glycerol and 0.1mM inhibitor for ~10s and subsequently flash-cooled in a cold nitrogen-gas stream from an X-stream cryosystem (MSC). Both crystal forms diffracted to 2.5Å resolution, but the data-collection statistics were better for the second crystal form, which was used for structure determination and refinement. *Coordinates of the final refined structure were deposited in the RCSB with accession number 2QX1*.

4.4 Results and discussion.

4.4.1 Acylation of mtFabH by a mixture of acyl-CoA substrates

mtFabH was treated with a mixture of acyl-CoA substrates ([C_6-C_{20}]-CoA) in the absence of ACP and the resultant acylated mtFabH was analyzed using ESI-MS. The ratio of each acyl-CoA to the mtFabH monomer is ~ 5:1. The experimental ESI mass value for native mtFabH monomer is 36903 Da (compared to a theoretical value of 36904.7 Da) (Figure 21a). Treatment of mtFabH with this mixture of acyl-CoAs for 40 minutes at room temperature resulted in total modification of the enzyme as evident from the complete absence of native mtFabH at 36903 Da (Figure 21b). These data provide the first evidence that both monomers of the mtFabH dimer are acylated during reaction. The appearance of a major peak at 37085.0 Da corresponds to the addition of one dodecanoyl group (from dodecanoyl-CoA) to the mtFabH enzyme (experimental mass shift of +182 Da compared to theoretical mass value of +183 Da). Surprisingly, under our assay conditions, we did not observe mtFabH acylation with any other acyl-CoAs.

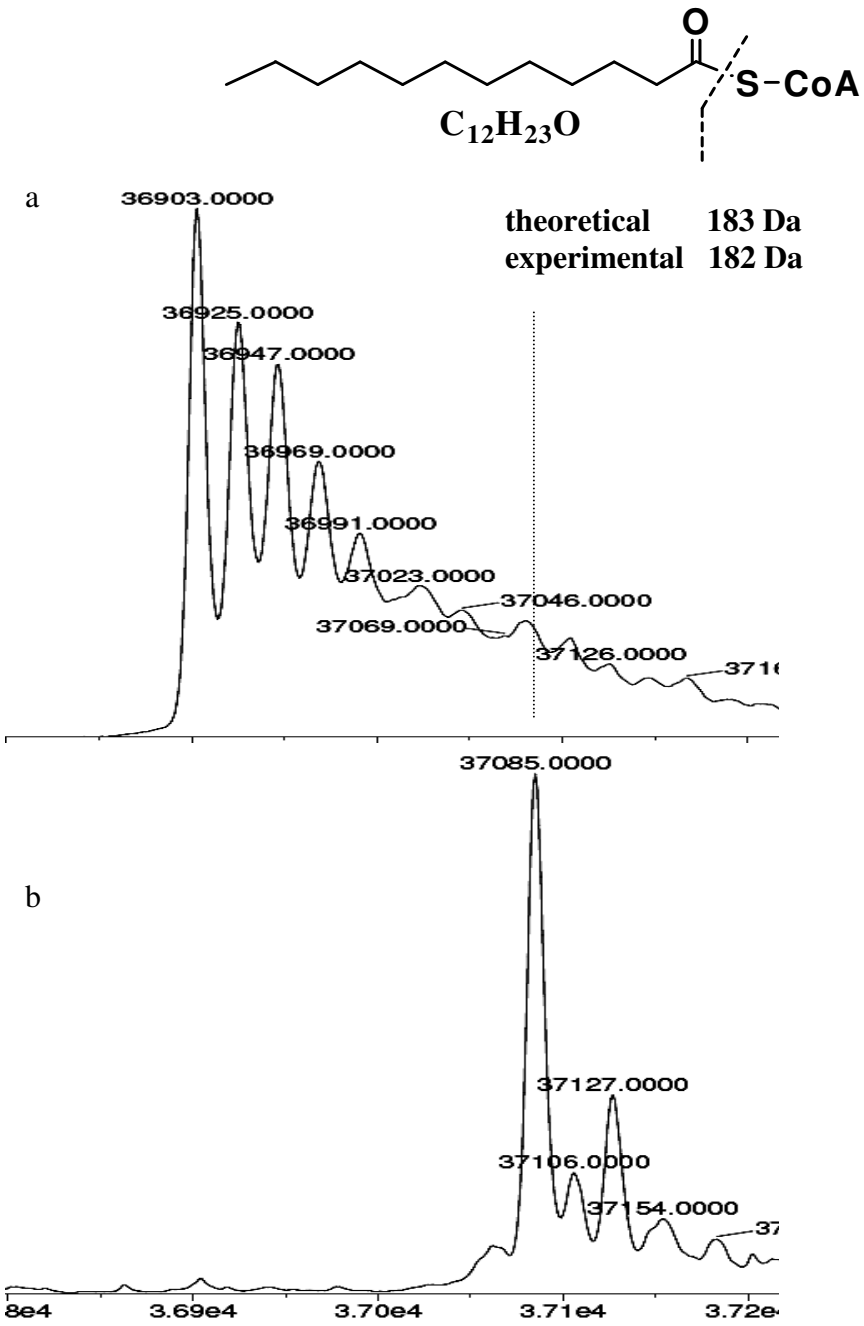

Figure 21: Reconstructed ESI-TOF mass spectra of the incubation products of WT mtFabH with a mixture of acyl-CoAs (C_6-C_{20}). (a) Mass spectrum of untreated WT mtFabH (control). (b) Mass spectrum of WT mtFabH treated with acyl-CoA mixture.

The apparent selective formation of the dodecanoyl product is puzzling given the relatively similar rates of reaction for the overall mtFabH catalyzed reaction with a range of acyl-CoA substrates.[57] However, it is consistent with our repeated observation of adventitiously bound dodecanoic acid in the substrate binding channel of crystal structures of recombinant mtFabH expressed in *E. coli*. Also, in trying to prepare Michaelis complexes of mtFabH C112A mutant with either tetradecanoyl-CoA or hexadecanoyl-CoA for co-crystallization, we have invariably obtained a complex with dodecanoyl-CoA in the binding site (unpublished data). We cannot exclude the possibility that the tetradecanoyl- or hexadecanoyl- groups are present in the determined crystal structures but are disordered at their terminal pairs of methylene groups. However, this is made less likely by the determination from HPLC analyses of these longer chain acyl-CoA substrate preparations, that a dodecanoyl-CoA impurity (≤2%) is present, which we infer binds preferentially to the mtFabH during crystallization. Together these observations suggest that the mtFabH Michaelis complex and subsequent acyl-enzyme intermediate thermodymamically favor the dodecanoyl-CoA substrate.

4.4.2 Thio-Alkylation of mtFabH by decylSSCoA

As noted above, MeSSCoA inhibits ecFabH through a disulfide exchange mediated transfer of the MeS- group to the sidechain sulfur of the active site Cys112 of the enzyme. We also prepared decylSSCoA, which in preliminary experiments did not inhibit ecFabH but was effective against mtFabH.[83] To determine whether this class of inhibitors acts by the same mechanism on mtFabH as on ecFabH, the inhibition of

mtFabH by decylSSCoA was analyzed using ESI-MS under similar conditions to those described above for the acylation reaction (Figure 21).

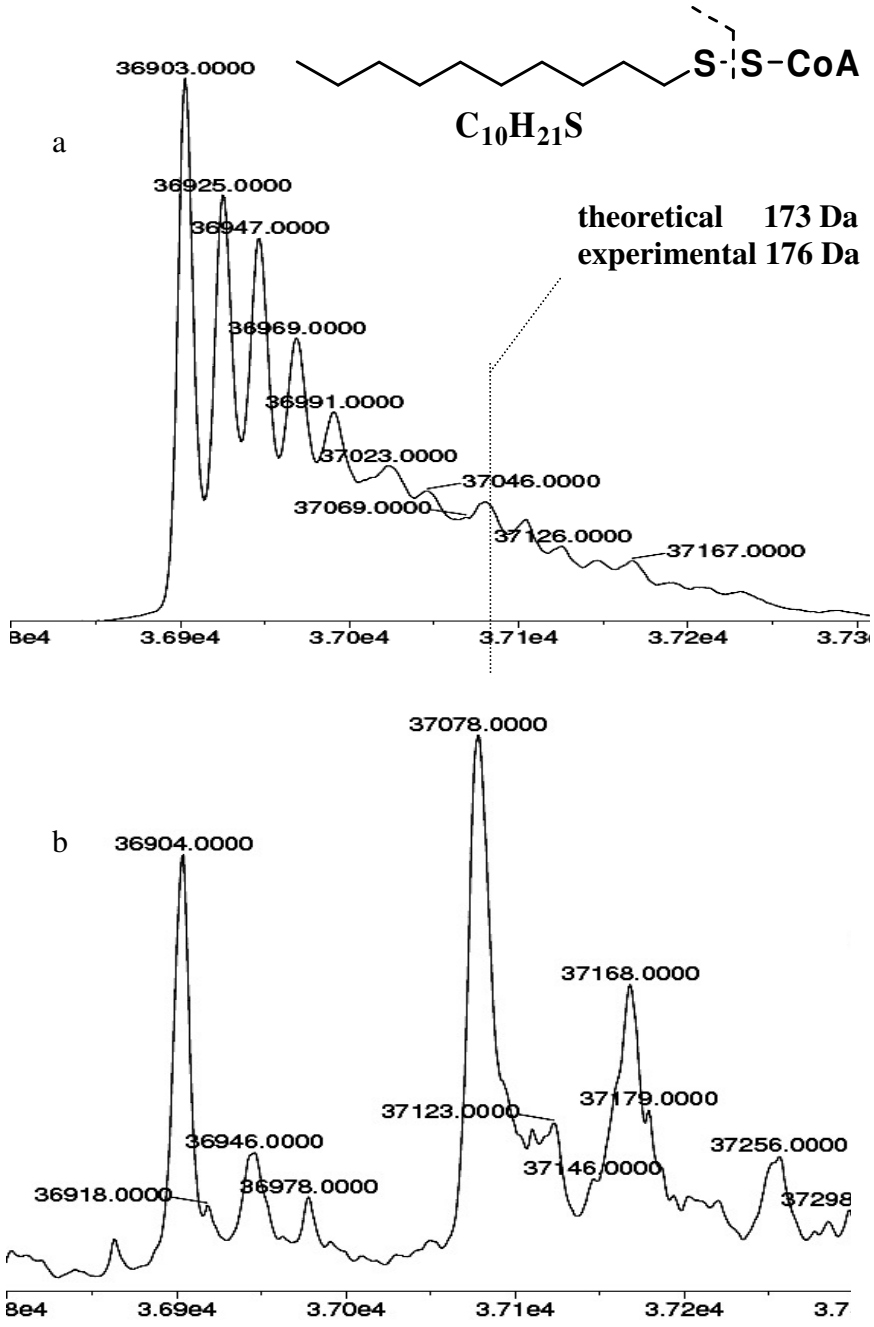

Figure 22: Reconstructed ESI-TOF mass spectra of the incubation mixture of WT mtFabH and decylSSCoA. (a) Mass spectrum of untreated WT mtFabH (control) (b) Mass spectrum of WT mtFabH treated with decylSSCoA disulfide inhibitor.

Treatment of mtFabH with decylSSCoA resulted in formation of a modified mtFabH species (Figure 22B) that correlates well with the addition of a $C_{10}S$- fragment (a theoretical mass increase of 173 Da to the mtFabH monomer fragment). The absence of this peak in C112A mtFabH mutant confirmed that this modification occurs at the active site cysteine in WT mtFabH (data not shown). Only a fractional modification of the mtFabH with decylSSCoA was observed, in contrast to the full modification observed using dodecanoyl-CoA. This observation, taken with the 23% extent of reaction for decanoyl-CoA with mtFabH,[57] confirm a specificity preference for C_{12} over C_{10} ligand binding in the acyl binding channel, but probably also reflects in part a slower reaction rate of the inhibitor relative to the substrate. This latter is the case for acetyl-CoA and methylSSCoA inhibitors with ecFabH.[83]

A co-crystal structure of mtFabH and decylSSCoA showed both of the active site cysteines of the mtFabH dimer to be modified through disulfide linkage to the decylthio-group. The decyl group has full occupancy in one subunit and slightly less than full occupancy in the second subunit. As we and others have frequently observed, CoASH product is only weakly retained in the pantetheinate channel of FabH – ligand complex structures. No interpretable density for CoASH was observed in one subunit of the decylSSCoA complex, while density in the other subunit was largely complete except for breaks around the pyrophosphate group. CoASH is probably preferentially retained in this latter channel as a consequence of an interaction of the pyrophosphate group of the nucleotide with Arg214 of a symmetry-related molecule. The terminal thiol of the pantetheinate group of this CoASH is 6.1Å from the Cys112 decyl-disulfide and the

terminal adenine nucleotide group stacks on Trp32 and Arg151 at the mouth of the binding pocket (Figure 23), as has been observed in other CoASH complexes with FabH.

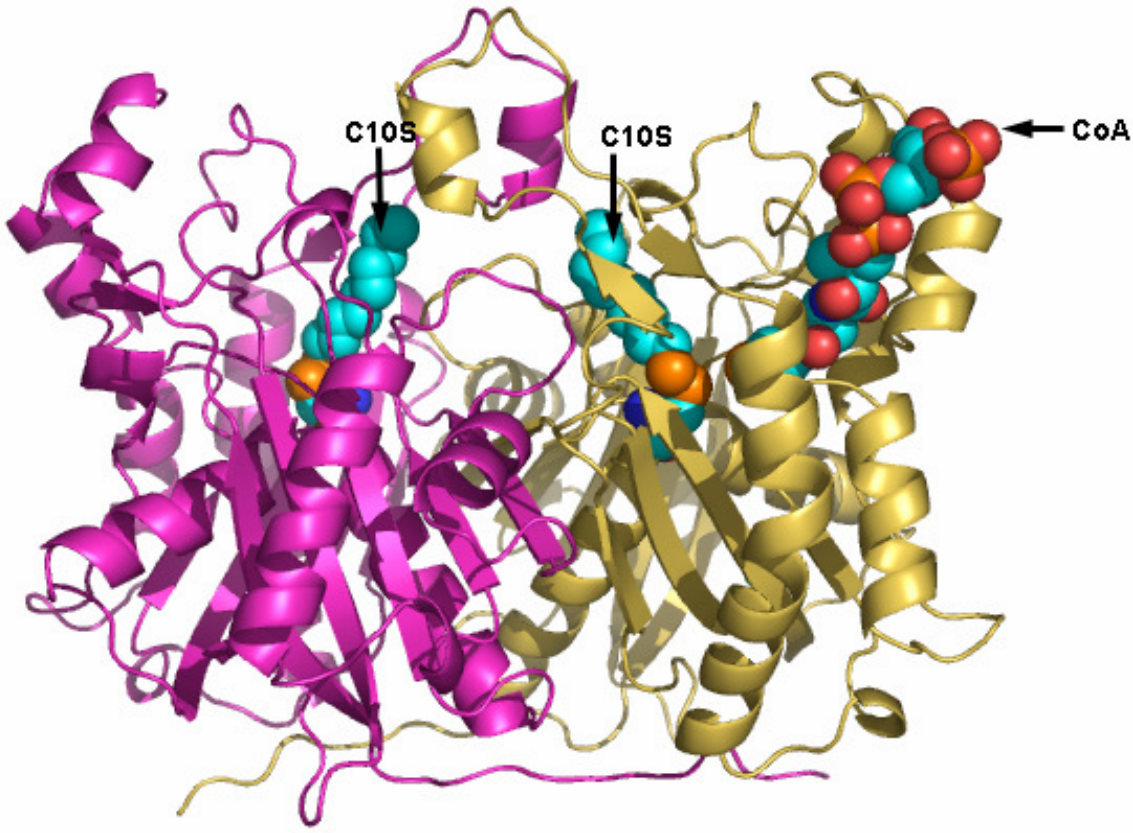

Figure 23. Backbone structure of mtFabH homodimer (subunits in gold and magenta ribbon) in complex with $C_{10}S$- (space filling, cyan = carbon, red = oxygen, blue = nitrogen, orange = sulfur) covalently linked to the sidechain sulfur of Cys112 (also space filling) in both subunits. CoA is shown bound in only the A-subunit (gold) also in space filling model.

4.5 Conclusion

We provide the first evidence that the active site cysteine in both subunits of the wild type mtFabH dimer is able to react with either a dodecanoyl-CoA substrate or a decylSSCoA inhibitor. The data clearly demonstrate that binding and reaction at one subunit does not preclude reaction at the other, but we cannot determine whether binding and reaction occur at the same rate in both subunits. In the case of ecFabH, reaction at the second subunit is slower than that at the first.[83]

In the static crystal structure of wild type mtFabH modified by formation of a disulfide product with the decylSSCoA inhibitor, the CoA binding channel is the only obvious access path to the buried acyl-binding channel. Binding and reaction of one of the mtFabH subunits with substrate or inhibitors via a reptational threading through this pantetheinate channel and past the active site residues would be energetically unfavorable. The data however show that this occurs readily to both subunits suggesting that there is likely an alternative more favorable pathway for binding of substrate or inhibitor ligand to mtFabH. These observations support the existence of a hitherto unobserved 'open' form of mtFabH, like that proposed for ecFabH,[63,83] which provides a direct, low energy path for substrate or inhibitor entry to the acyl binding channel.

The overall mtFabH catalyzed reaction using malonyl-ACPM has been shown to use C_{14}-C_{20} acyl-CoAs at least as efficiently as dodecanoyl-CoA.[57] In this current work we have shown that in the acylation reaction performed with a range of acyl-CoAs (carried out in the absence of malonyl-ACPM) the mtFabH selectively forms a product with the dodecanoyl CoA. It has been previously proposed that ACPM modulates the

substrate specificity of the mtFabH.[57] Our current data support this hypothesis and we propose that ACPM assists in formation of an open mtFabH structure, which facilitates both binding of longer chain acyl-CoA substrates and also release of the long chain β-ketoacyl-ACP products.

In conclusion, this and other recent analyses of FabH enzymes suggest that the model for catalysis provided by current crystal structures is incomplete, and must be expanded to include significant protein conformational changes which are associated with the acyl–CoA and specific malonyl-ACP substrates. Further experiments are discussed in future direction (chapter 7).

5. Separate entrance and exit portals for ligand traffic in *Mycobacterium tuberculosis* FabH

5.1 Summary

Mycobacterium tuberculosis FabH initiates type II fatty acid synthase-catalyzed formation of the long chain (C_{16} – C_{22}) acyl-CoA precursors of mycolic acids, which are major constituents of the bacterial cell envelope. Crystal structures of mtFabH (as discussed in chapter 3) show the substrate binding site to be a buried, extended L-shaped channel with only a single solvent access portal. The distal, dead end arm of this channel binds the acyl moiety of the substrate and the arm proximal to the solvent portal binds the CoA moiety. Entrance of an acyl-CoA substrate through the solvent portal would require energetically unfavorable reptational threading of the substrate to its reactive position. Using a new class of FabH inhibitors, we have tested the alternative hypothesis that FabH exists in an 'open' form during substrate binding and product release, and a closed form in which catalysis and intermediate steps occur. This hypothesis is supported by mass spectrometric analysis of the product profile and crystal structures of complexes of mtFabH with these inhibitors.

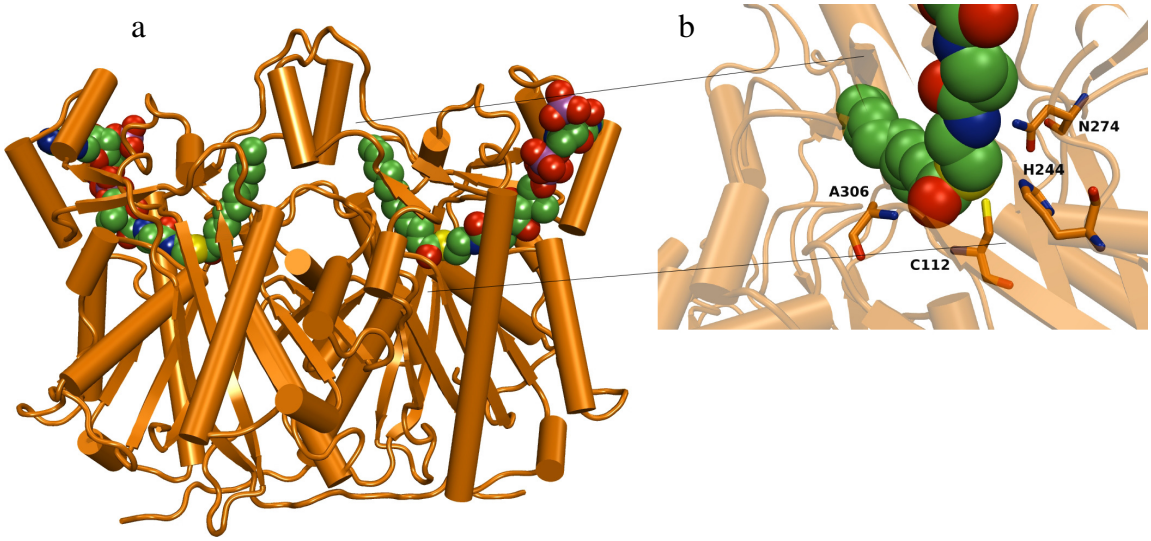

Figure 24: (a) Backbone structure of C112A mtFabH homodimer (gold ribbon) in complex with lauroyl-CoA (space filling, green = carbon, red = oxygen, blue = nitrogen, yellow = sulfur, magenta = phosphorous) bound in the buried, L-shaped binding site of each monomer of the dimer. (adopted from chapter 3)
(b) Expansion of active site residues (gold stick) in 24 (a) with functional atoms (color coded as in Figure 24 a) and Cys112 modelled from wt mtFabH structure for the lauroyl-CoA (space filling atoms color coded as in Figure 24 (b) with bound lauroyl-CoA.

5.2 Introduction:

The crystal structure of the Michaelis complex of lauroyl-coenzyme A with an inactive C112A mtFabH mutant (chapter 3) clearly shows substrate bound in an "L" shaped channel of each monomer (Figure 24a), with the active site triad (Cys112-His244-Asn274) at the junction of the two arms of the "L" (Figure 24 b). Coenzyme A occupies the solvent accessible, pantetheinate arm of the "L", while the acyl group occupies the distal, dead-end arm of the "L", an extended hydrophobic channel that appears accessible

only through the pantetheinate channel. Binding of lauroyl-CoA substrate would thus appear to require migration of the hydrophobic lauroyl chain through the pantetheinate binding channel and around the bend of the "L" past the hydrophilic and charged catalytic residues. Formation of the complex in this manner would present formidable stereochemical and energetic barriers, and dissociation of long chain β-ketoacyl-ACP reaction product from this buried hydrophobic site via a reversal of this process would appear to be equally unfavorable.

These considerations have led us to hypothesize that native mtFabH adopts a hitherto unobserved 'open' conformation which offers an alternate pathway with lower energy barriers for initial substrate binding and final product release. To test this hypothesis, we prepared inhibitors with one or two hydrophobic arms that occupy either one or both binding channels, and a reactive group that targets the active site cysteine (Figure 25). The binding modes of these inhibitors with the wild type mtFabH have been established by mass spectrometry and x-ray crystallography. These same analyses with an mtFabH A246F mutant, whose pantetheinate binding channel is blocked, reveal that inhibitor binding and reaction still proceed efficiently, but only with one arm inhibitors that bind exclusively in the acyl channel. These experiments provide strong evidence that mtFabH exists in an open conformation that accepts ligands directly into the acyl binding channel without entry to the single solvent portal and passage through the pantetheinate channel of the closed form of the enzyme. These results support a new model for substrate binding, catalysis and product release in mtFabH.

5.3 Experimental procedures

5.3.1 Materials

All general chemical supplies not listed below are ordered from standard companies and were reagent grade or better. The source of specific supplies are as follows: [2-^{14}C] malonyl-CoA (ARC-528, specific activity 55mCi/mmol) was purchased from American Radiolabeled Company and lauroyl-CoA (trilithium salt) was purchased from Sigma. The Reverse Phase (RP) HPLC studies were performed on Amberchrom C_{18} RP columns from Rohm and Hass Company; trypsin enzyme used was proteomic grade and was bought from Sigma; Pepclean^{TM} C_{18} Spin Columns were from Pierce. All Electrospray Ionization Mass spectrometry (ESI-MS) experiments were performed on Quadrupole time-of-flight mass spectrometer (model QSTAR XL) from Applied Biosystems/MDS Sciex which is equipped with a standard ion source from MDS Sciex, Concord, Canada. The glu-fibrinopeptide used for externally calibrating the QSTAR instrument in positive ion mode was from Sigma. Grafit 4.012 (Middlesex, United Kingdom) for data plotting is bought from Sigma.

5.3.2 Enzyme expression and purification:

WT mtFabH and C112A mtFabH are cloned, expressed and purified as described in chapter 3. The A246F mutations were made on the open reading frame Rv0533c (mtFabH), which was cloned into the expression vector pET-15b as described previously.[27] Mutants were made according to the protocol provided for the Quikchange

XL site-directed mutagenesis kit and primers designed to substitute Phe for Ala246. Primers were ordered from Integrated DNA Technologies and were, forward 5'-GTG TTC GTC CCT CAT CAG TTC AAT AGC CGC ATC AAC GAG - 3' and reverse 5' – CTC GTT GAT GCG GCT ATT GAA CTG ATG AGG GAC GAA CAC– 3'. Mutations were confirmed by sequence analysis of the final constructs. The plasmid was purified using the QIAprep miniprep kit.

Competent *E. coli* BL21DE3 Codon Plus cells were transformed with pET-15b carrying A246F FabH insert. Transformants were grown in LB medium to an absorbance of 0.4 – 0.6, induced with 0.2 mM isopropyl-beta-D-thiogalactopyranoside, and incubated for an additional 4 hrs at 37º C. Cells were harvested by centrifugation at 10,000 g for 10 min. at 4 °C and stored at -80 °C until used. After lysis with lysozyme on ice for 30 minutes, cells were sonicated on ice and then centrifuged at 12,000 g for 30 min. at 4 °C. The supernatant was loaded onto a Hitrap chelating 5-ml column and washed with a gradient step from 0 to 120 mM imidazole in 50mM sodium phosphate buffer, pH 8.0 with 300mM sodium chloride. FabH was eluted with 1 M imidazole under the same buffer conditions. The high concentration of imidazole employed in the washing step improves the homogeneity of the mtFabH band as assessed by SDS-PAGE analysis. The mtFabH was desalted in 100mM sodium phosphate buffer pH 7.0, and kept at 4 °C overnight. Protein was concentrated in Centricon tubes and assayed by Bradford assay using BSA as standard. For crystallization, the concentration of mtFabH used was in the range of 4 - 8 mg/ml.

5.3.3 Synthesis of compounds 1-3:

The syntheses of inhibitors 1-3 were carried out by Dr. Alhamadsheh and kindly provided in ample amount for this study.

5.3.4 Enzyme assays:

The mtFabH assay was performed as described in chapter 2.

5.3.5 Electrospray Ionization-Mass Spectrometry (ESI-MS) analysis:

5.3.5.1 Sample preparation:

Wild type or mutant mtFabH in sodium phosphate buffer 50 mM, pH 7.0, 15 % glycerol were first desalted with HPLC grade water using Hitrap desalting column. The aliquot of enzyme (10-40 μM) and inhibitors 1, 2 or 3 separately (mtFabH dimer: inhibitor ~ 1:10) were incubated at room temperature for 60 minutes and then excess or non-covalently adhered inhibitor was desalted using a Pierce spin desalting columns. The enzyme was concentrated using Microcon concentrator (50 kDa cutoff) that also works as second desalting step and then stored at –20˚ C until the ESI analysis.

5.3.5.2 ESI-MS analysis conditions:

The sample was diluted to 1 pm/µl with 50 % methanol/0.1 % formic acid and analyzed by a quadrupole time-of-flight mass spectrometer. The instrument was externally calibrated in the positive ion mode using two fragment ion peaks (*m/z* 175.1190 and *m/z* 1285.5444) from the tandem mass spectrum of Glu-fibrinopeptide. The samples were directly infused into the ion source using a 500 μl syringe at a flow rate of 5 µl/min through red peek tubing (Upchurch). The following parameter settings were used to acquire mass spectra from *m/z* 600-1600 in the positive ion TOF/MS mode: spray voltage, 5500V; curtain gas, 20; GS1 gas, 15; declustering potential (DP), 85 V; declustering potential 2 (DP2), 15 V; focusing potential (FP), 265 V; accumulation time, 1 s. Typically, spectra were averaged over 120 scans, and the series of multiply charged ion peaks were deconvoluted by the Bayesian protein reconstruct tool (in the Bioanalyst QS 1.1 software package) to determine the zero charge masses of the intact proteins. For all mass calculations, 0.01 % mass accuracy was set as tolerance limit; ie about 3.7 Da for mtFabH whose monomeric molecular weight is about 37,000.

5.3.5.3 ESI-MS data analysis:

The theoretical mass of His-tagged WT mtFabH monomer by DNA deduced amino acid sequence is calculated to be 36904.7 Da. The experimental mass is found to be 36903 as shown in Figure 26 a. Treatment of mtFabH with inhibitors resulted in appearance of multiple new species along with their sodium adducts (Figure 26b). The mtFabH was purified and initially prepared in sodium phosphate buffer and thus up to 4 sodium adducts were readily obtained as evident from the control experiment (untreated WT mtFabH deconvoluted spectrum, Figure 26 a). All calculations were performed based on guidelines set forth as described below. The area of most abundant species was identified and all species with areas encompassing up to 10% of its area was taken into consideration for calculation of total area. Mass value of control mtFabH (36903 Da) was subtracted from each mass value obtained and the positive mass difference as indicative of a particular species being present. Each species and its sodium adducts was categorized as a single species and percent area of each species was calculated. Mass differences of more than 1 kDa and negative mass differences were discarded as non-mtFabH related species. The final data was presented with nature of species (unmodified, trimodified, dimodified, mono-modified and others, for those which can't be assigned) on X-axis and percentage of particular species observed is plotted on Y-axis.

5.3.6 Crystallization, x-ray data collection and structure determination. (This work was carried out by Dr. Faik Musayev, Dr. Tonie Wright and Dr. J. Neel Scarsdale)

Crystals were obtained by the hanging-drop vapor diffusion method using 4µl drops consisting of a 1:1 ratio of protein to reservoir solution equilibrated against 600µl of reservoir solution at room temperature. Protein concentration varied from 4-15mg/ml in 100mM sodium phosphate buffer, pH 7.0. Inhibitor molecules were dissolved in methanol to a final concentration of 34mM (**1**)**,** 25mM (**2**) and 23mM (**3**) and mixed with protein solution at the molar ratios shown in Table 5. Before crystallization, protein-inhibitor complex mixtures were incubated on ice for 2 hrs. Crystallization conditions and lattice parameters for the structures are summarized in Table 5.

Table 5 Crystal conditions for structures determined in this study (chapter 5)

Inhibitor No.	Protein	Protein Conc. (mM)	Protein: Inhibitor molar ratio	Reservoir solution	Lattice Parameters (A)	Accession No.
1	WT	0.21	1:3.5	50mM Na Acetate, pH4.6, 2.4M Na Formate	68.03, 88.85, 229.74 sp.gr. C2221	2QNZ
1	A246F	0.11	1:4	100mM Na Hepes, pH 7.5, 1M K/Na Tartrate	67.70, 88.69, 229.90 sp.gr. C2221	2QNY
2	WT	0.15	1:5	100mM Na Mes, pH 6.5, 50mM NaH2PO4/KH2PO4, 1.8M NaCl	68.28, 88.98, 230.25 sp.gr. C2221	2QNX
3	WT	0.4	1:2.5	100mM Na Hepes, pH 7.5, 1M K/Na Tartrate	68.41, 89.12, 233.29 sp.gr. C2221	2QO1
3	A246F	0.21	1:4	100mM Na citrate, pH 5.6, 10% Isopropanol, 18% PEG-4K	55.30, 93.05, 104.72 sp.gr. P212121	2QO0

For x-ray data collection, crystals were cryoprotected in their mother liquid solution supplemented with 25-30% glycerol, and where appropriate, with inhibitors, before flash cooling in a liquid nitrogen stream. X-ray data were collected at 100^{o}K using a Molecular Structure Corporation (MSC) X-Stream Cryogenic Crystal Cooler System and an R-Axis IV++ image plate detector with a Rigaku MicroMax^{TM}–007 X-ray source equipped with MSC Varimax confocal optics operating at 40 kv and 20 mA. Data were processed and scaled with D*Trek. Structures were determined via molecular replacement with AMORE, using pdb entry 1HZP[27] as a search model, and refined via alternating cycles of manual fitting into SigmaA weighted $2mf_{o}df_{c}$ electron density maps in COOT[84] and computational refinement in CNS[71] and Refmac5[85]. Ligand topology and parameter files used in refinement were generated using the prodrg server.[86] Data collection and refinement statistics are summarized in Table 6.

Table 6: Data Collection and Refinement Statistic for MtFabh Crystal Structures					
	2QNZ	**2QNY**	**2QNX**	**2QO1**	**2QO0**
Data Collection					
Resolution(Å)	48.3-2.3 (2.3-2.3)[5]	39.2-2.1 (2.2-2.1)[5]	29.0-2.7 (2.8-2.7)[5]	39.7-2.6 (2.7-2.6)[5]	38.0-1.8 (1.9-1.8)[5]
Unique Reflections	31228 (2987)[5]	35143 (2605)[5]	19219 (1913)[5]	20938 (2193)[5]	46884 (4610)[5]
Redundancy	12.43 (7.98)[5]	3.17 (1.95)[5]	3.65 (3.69)[5]	2.54 (2.84)[5]	6.37 (6.17)[5]
R_{merge}[6]	0.089 (0.206)[5]	0.075 (0.150)[5]	0.120 (0.264)[5]	0.108 (0.244)[5]	0.095 (0.314)[5]
Completeness(%)	99.3 (96.7)[5]	92.2 (69.6)[5]	97.3 (98.0)[5]	93.2 (98.8)[5]	99.8 (99.9)[5]
I/σ(I)	19.6 (9.5)[5]	10.7 (4.4)[5]	8.7 (4.8)[5]	7.4 (4.1)[5]	11.3 (5.5)[5]
Refinement					
Resolution	14.8-2.3 (2.3-2.3)[5]	10.0-2.1 (2.2-2.1)[5]	15.0-2.7 (2.8-2.7)[5]	15.0-2.6 (2.6-2.6)[5]	25.0-1.8 (1.9-1.8)[5]
Number of reflections (work)	27984 (1943)[5]	31289 (1625)[5]	17172 (1209)[5]	18707 (1459)[5]	42064 (3050)[5]
Number of reflections (test)	3115 (207)[5]	3445 (182)[5]	1954 (147)[5]	2076 (146)[5]	4710 (368)[5]
R_{work}/R_{free}[7]	0.16/0.2 (0.19/0.25)[5]	0.19/0.24 (0.2/0.27)[5]	0.2/0.2 (0.2/0.3)[5]	0.2/0.29 (0.28/0.35)[5]	0.19/0.26 (0.31/0.37)[5]
Average B(Å^2)	28.9	30.2	26.8	40.5	22.9
DPI(Å)[8]	0.212	0.213	0.352	0.389	0.162

[5] Values in parentheses are for highest resolution shell.

[6] $R_{merge} = \sum |I_h - \langle I \rangle| / \langle I \rangle$ where I_h refers to the measured intensity for a given reflection and $\langle I \rangle$ refers to the average measured intensity for that reflection.

[7] $R_{work} = \sum |F_{obs} - F_{calc}| / \sum F_{obs}$ where F_{obs} and F_{calc} refer to the observed and calculated structure factors respectively.

[8] $DPI = (N_{atoms}/N_{obs})^{1/2} c^{-1/3} d_{min} R_{free}$ where N_{atoms} is the number of atoms in the refinement, N_{obs} is the number of reflections, c is the data set completeness expressed as a fraction, d_{min} is the resolution and R_{free} is the free R factor.

Deviations from Ideality	**2QNZ**	**2QNY**	**2QNX**	**2QO1**	**2QO0**
Bond Lengths	0.007	0.007	0.007	0.007	0.009
Bond Angles	1.11	1.08	1.11	1.10	1.22
Ramachandran Plot					
Most Favored (%)	90.7	90.1	88.1	88.8	90.5
Additional Allowed (%)	9.0	9.1	11.3	10.4	9.0
Generously Allowed (%)	0.2	0.4	0.4	0.5	0.4
Forbidden(%)	0.2	0.4	0.2	0.4	0.2

Table 6: Data collection and refinement statistic for mtFabh crystal structures in chapter 5 (continued…).

5.4 RESULTS

5.4.1 Inhibitor design and activity

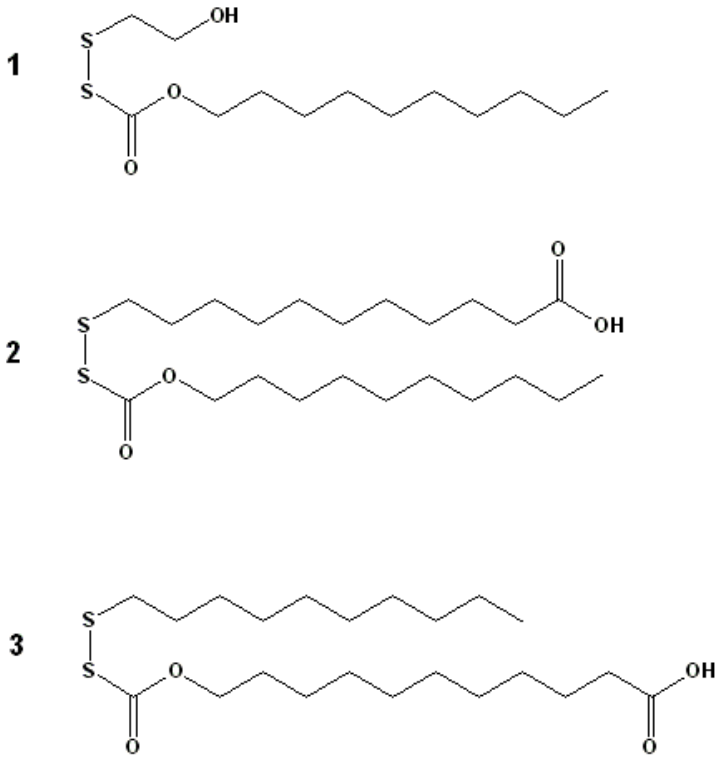

Figure 25: Chemical structures of inhibitor ligands used in this study

It has been demonstrated that alkyl-CoA disulfide inhibitors target the active site cysteine of both ecFabH and mtFabH and that inhibition of these enzymes is specific for short (C_2) or long (C_{10}) alkyl chains respectively, matching their acyl chain substrate

specificities.[83] To investigate the route for ligand binding and reaction with mtFabH, we synthesized linear inhibitors (Compounds **1-3**, Figure 25) composed of two arms linked by an oxycarbonyl-disulfide group, which can potentially react with the reactive site Cys112 by acylation or by thiol-disulfide exchange. The arms in the compounds used here are: ethanol, decyl and decanoic acid. Each pair of arms of a compound is potentially able to simultaneously bind in the acyl and pantetheinate binding channels of mtFabH. Preliminary analysis under standard conditions revealed similar levels of inhibition for mtFabH (IC_{50} values: **1,** 3.8 ± 0.5 μM; **2**, 2.4 ± 0.8 μM; **3**, 2.7 ± 0.2 μM).

5.4.2 Characterization of E-I complex:

We initially utilized the "reversibility studies" to analyze the nature of association between mtFabH and compounds **1-3** and the results are recorded in Appendix 1. The studies revealed the formation of a covalent adduct, most likely via a disulfide bond, between the two. We further utilized the "bottoms up" type proteomics approach (digestion of E-I complex with trypsin followed by HPLC/ tandem MALDI-MS) to investigate the specific mtFabH residue/s modified on reaction with 1 and 2. Indeed, we observed the modification at Cys23 residue (on the surface of the mtFabH), but could not prove the reaction at the active site Cys112 (as proposed), most likely due to the harsh and long digestion conditions (Appendix 1). We thus diverted our attention to intact protein ESI-MS techniques to investigate the reaction under relatively milder conditions. The ESI-MS data complemented with crystal structures revealed the reaction at active site Cys112 and also threw light on the mode of binding of the inhibitors.

5.4.3 Electrospray ionization mass spectrometry and crystal structure analysis:

5.4.3.1 Reaction products and crystal structures of mtFabH and C112A mtFabH with 1

Electrospray ionization mass spectrometry (ESI-MS) was used to follow the modification of the wild type mtFabH with an excess of **1**. Under these conditions the protein was completely modified (Figure 26b vs 26a and Figure 36a), the two major species exhibiting mass increases of either 230 or 338 Da. The former of these is consistent with addition of three 77 Da fragments of A (theoretical increase in mass of 231 Da) to mtFabH monomer, while the latter is consistent with addition of two 77 Da fragments of A, and one 185 Da fragment of B (theoretical increase in mass of 339). These analyses indicated that all three solvent accessible cysteines in wild type mtFabH (the active site Cys112, plus Cys23 and Cys154) can react with **1** through disulfide exchange and at least one through acylation.

The crystal structure of the inhibition complex of wt mtFabH with **1** showed extra electron density at the two surface cysteines (Cys23 and Cys154), consistent with disulfide linked beta-mercaptoethanols, and at the active site Cys112, consistent with acylation by the long B arm fragment of **1**. This crystal structure corresponds to the tri-modified reaction product denoted (A + A + B) identified by mass spectroscopy (the

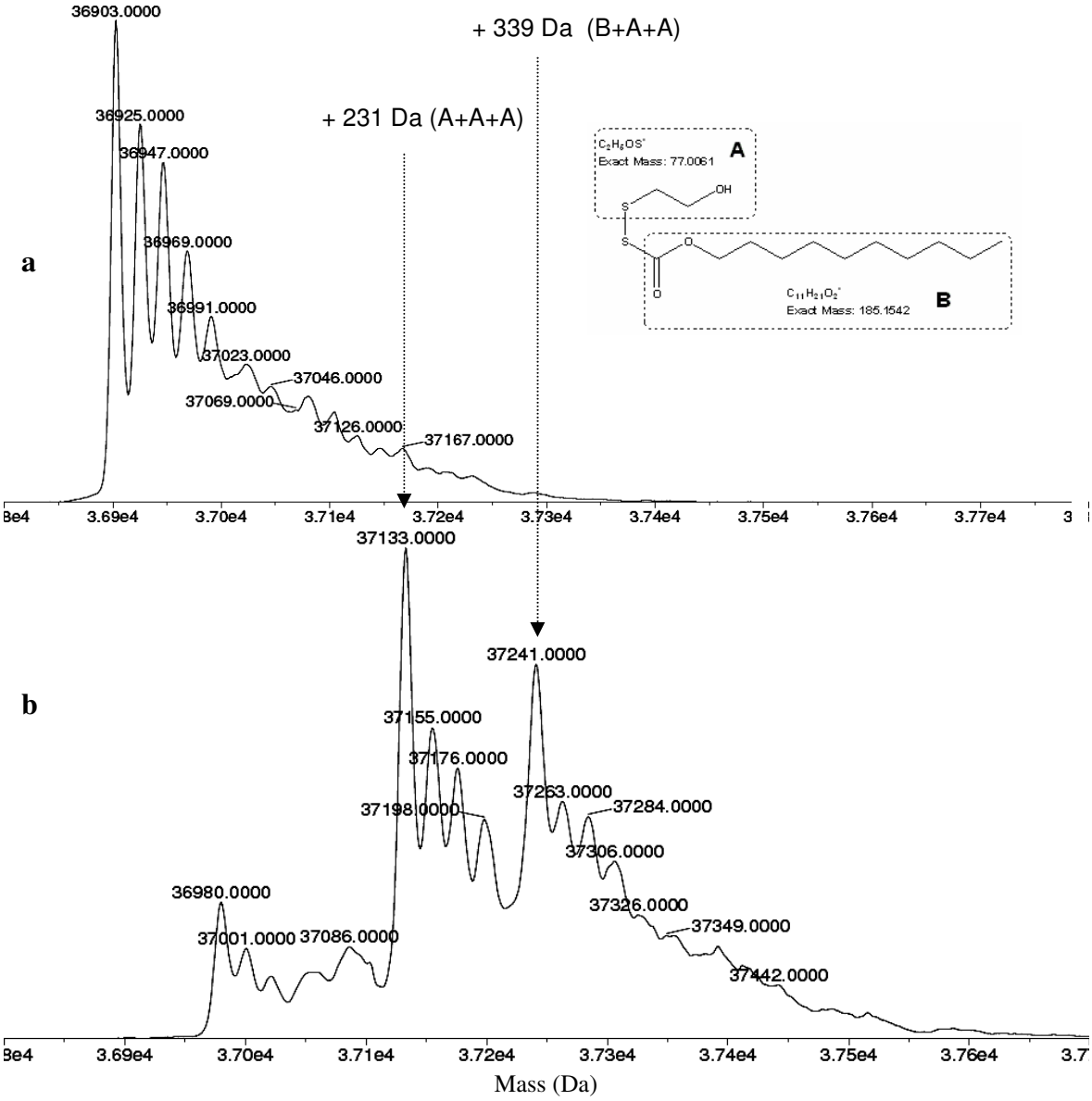

Figure 26: Reaction products of WT mtFabH with 1. a) Reconstructed ESI-MS spectrum of untreated WT mtFabH (Control) b) Mass spectrum of WT mtFabH treated with **1**. The mass shifts in WT mtFabH on treatment with **1** is correlated with proposed species (in bracket). WT mtFabH is treated with excess of **1** and incubated at room temperature for 60 minutes. The mixture is desalted to remove the excess inhibitor and the species formed are determined using direct infusion ESI-TOF mass spectrometry as determined in material and methods.

A + A + A tri-modified species did not crystallize). The contiguous electron density in both mtFabH subunits extending from the active site Cys112 into both acyl and pantetheinate binding channels (Figure 27a) was interpreted and refined as dual, conditional half occupancy of each channel by fragment B of compound **1**, whose carbonyl carbon forms a thioester with the active site Cys112 sidechain –SH.

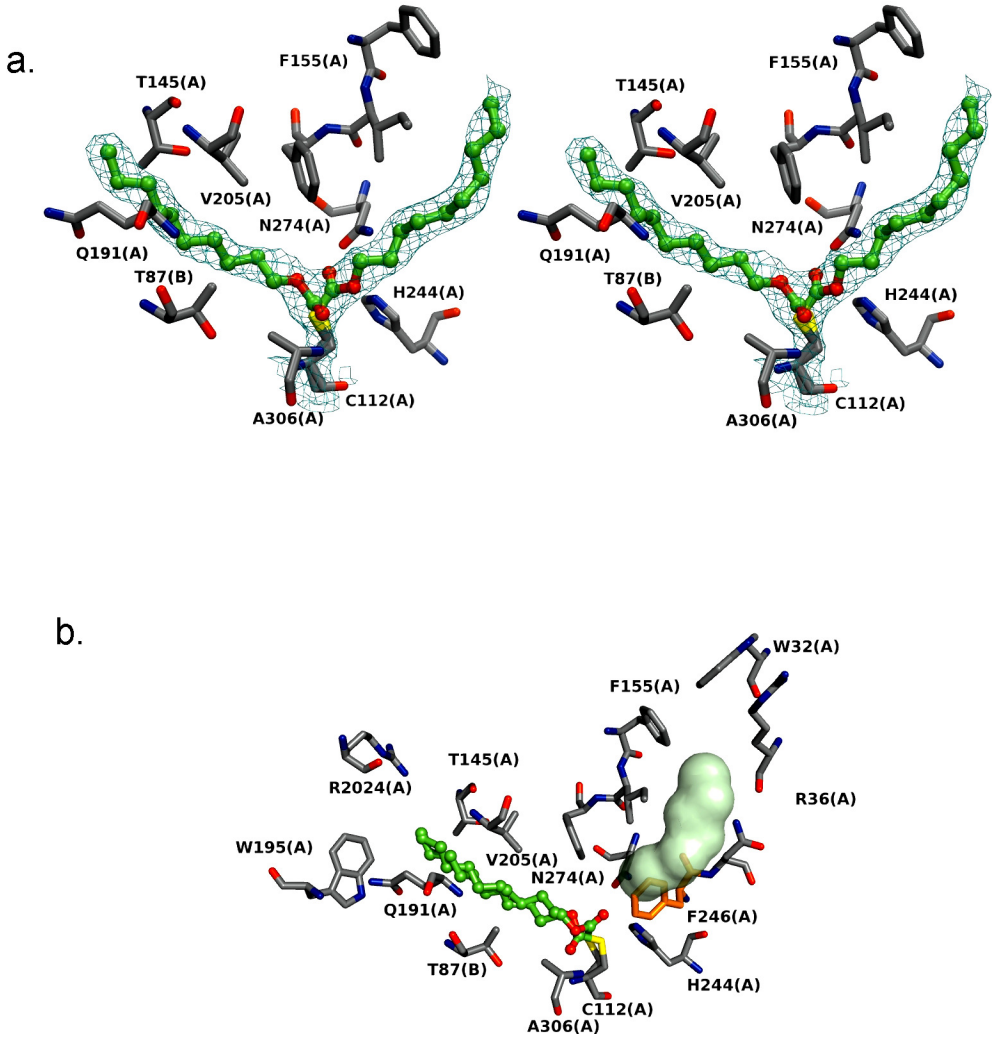

Figure 27 a: Stereoview of structure around the binding channel of the product complex of compound 1 with the wild type mtFabH, showing fragment B of its electron density alternately bound in each of the two arms, the acyl channel (A) and the pantetheinate channel (P), of the substrate binding channel. Contour level of electron density is 1σ. b). **Structure of the A246F mutant with a phenylalanine residue blocking the pantetheinate channel (gray space filling surface) and fragment B (2 conformations) of compound 1 bound in the acyl channel.**

The two complexes in the asymmetric unit (one with fragment B in the acyl channel, the other with B in the pantetheinate channel), both acylated on Cys112, differ from each other in the interactions they make at the active site. Furthermore, each differs in detail from its counterpart (with the ligand in the same channel) in the other subunit of the mtFabH homodimer complex.

The carbonyl group of the complex with fragment B in the acyl channel of one of the two subunits of the asymmetric unit is oriented toward the oxyanion hole, but does not make the full complement of hydrogen bonds. The carbonyl oxygen makes a hydrogen bond to the main chain –NH- of Ala306 but not to the –NH- of Cys112 in either subunit. In one subunit this oxygen makes a long hydrogen bond to the sidechain of Ser276. In the other subunit the Ser276 sidechain has alternate conformations, both of which make favorable (2.6Å) hydrogen bonds to the ester oxygen of the ligand in the acyl channel. These hydrogen bonds to the Ser276 sidechain –OH may compensate for the absence of the hydrogen bond to the main chain –NH- of Cys112 in the oxyanion hole.

For the complex with the ligand bound in the pantetheinate channel, the carbonyl oxygen in one subunit makes a hydrogen bond with the sidechain $–NH_2$ of Asn274 (3 Å), but not to His244, the two residues that constitute the malonyl anion-binding site. In the second subunit this oxygen makes tenuously long hydrogen bonds (3.3 Å and 3.6 Å respectively) to these groups in the malonyl anion site, but makes a favorable hydrogen bond (2.5 Å) to the sidechain of Ser276 in one of its two alternate conformations.

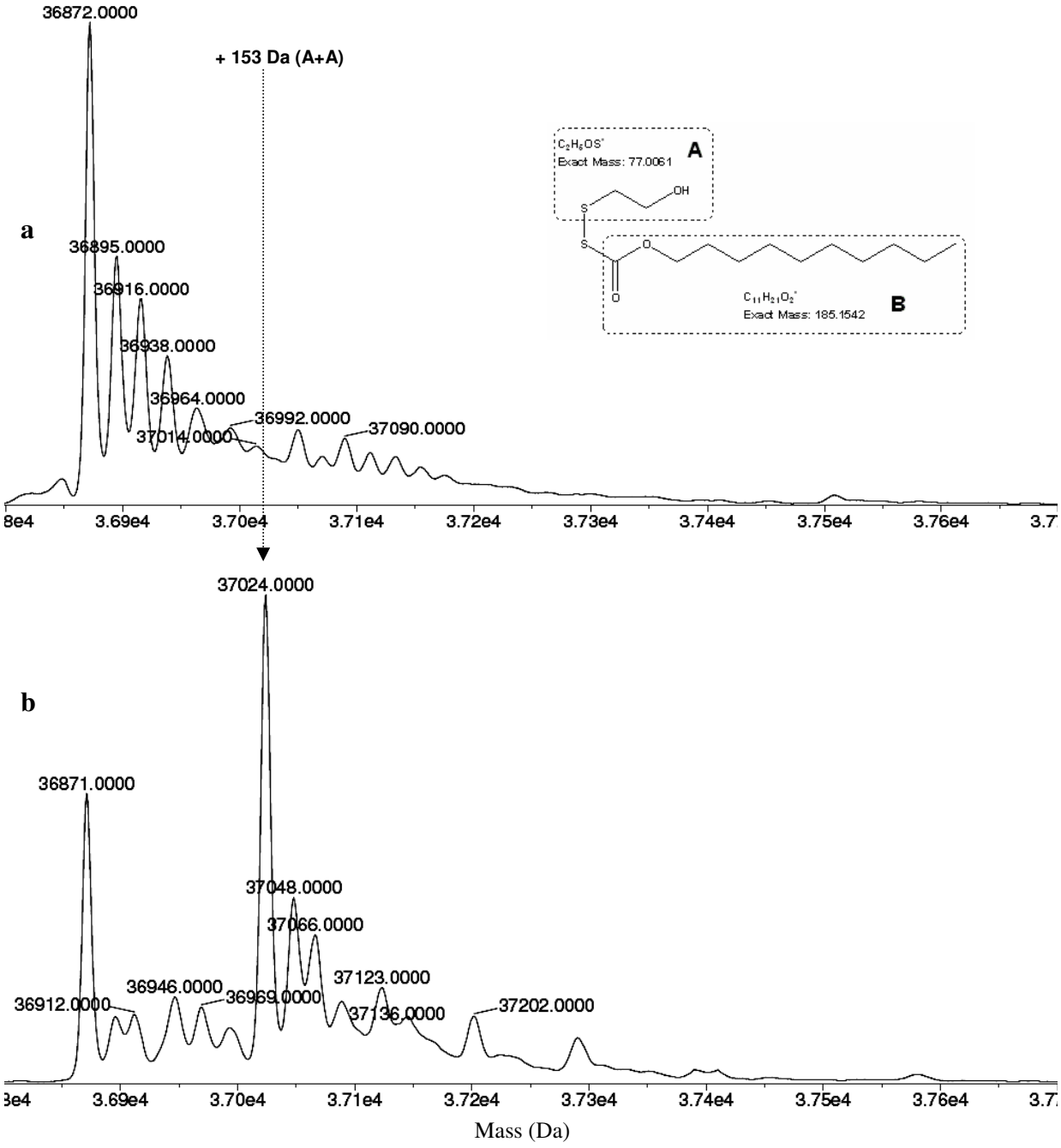

Figure 28: Reaction products of C112A mtFabH with 1. a) Reconstructed ESI mass spectrum of untreated C112A mutant mtFabH (Control) b) Mass spectrum of C112A mutant mtFabH treated with excess of **1**.

ESI-MS analyses of the C112A mutant complex prepared under the same conditions showed no tri-modified species (Figure 28 and 36a). Instead, a predominant di-modified species (mass increase of 152 Da) was observed, consistent with addition of two 77 Da fragments of A. Two less abundant species (mono- and di-modified), consistent with the addition of a single B fragment and an A+B respectively, that together approximated the unmodified species in abundance (Figure 36 a), were also observed. This decrease in the number of cysteine modifications coincident with mutation of the active site Cys112 indicates that it is this residue in the wild type mtFabH that can undergo modification with either fragment A or B.

5.4.3.2. Reaction of A246F mtFabH with 1

The alternate occupancy of the acyl- and pantetheinate channels of wild type mtFabH by the $C_{10}H_{21}OCO$ groups in the above structures could be realized by two binding orientations of **1** prior to reaction with the active site Cys112. The alternate occupancy might also arise if there was only one binding orientation which permitted reaction with C112, with a subsequent equilibration of the covalently-linked $C_{10}H_{21}OCO$ chain between the two channels.

In either case, migration of the inhibitor into the pantetheinate channel with passage through the active site residues into the acyl channel, presents similar formidable energetic barriers to those facing the natural acyl-CoA substrate, which suggested to us that there may be alternative modes for substrate and ligand entry to the extended mtFabH binding site.

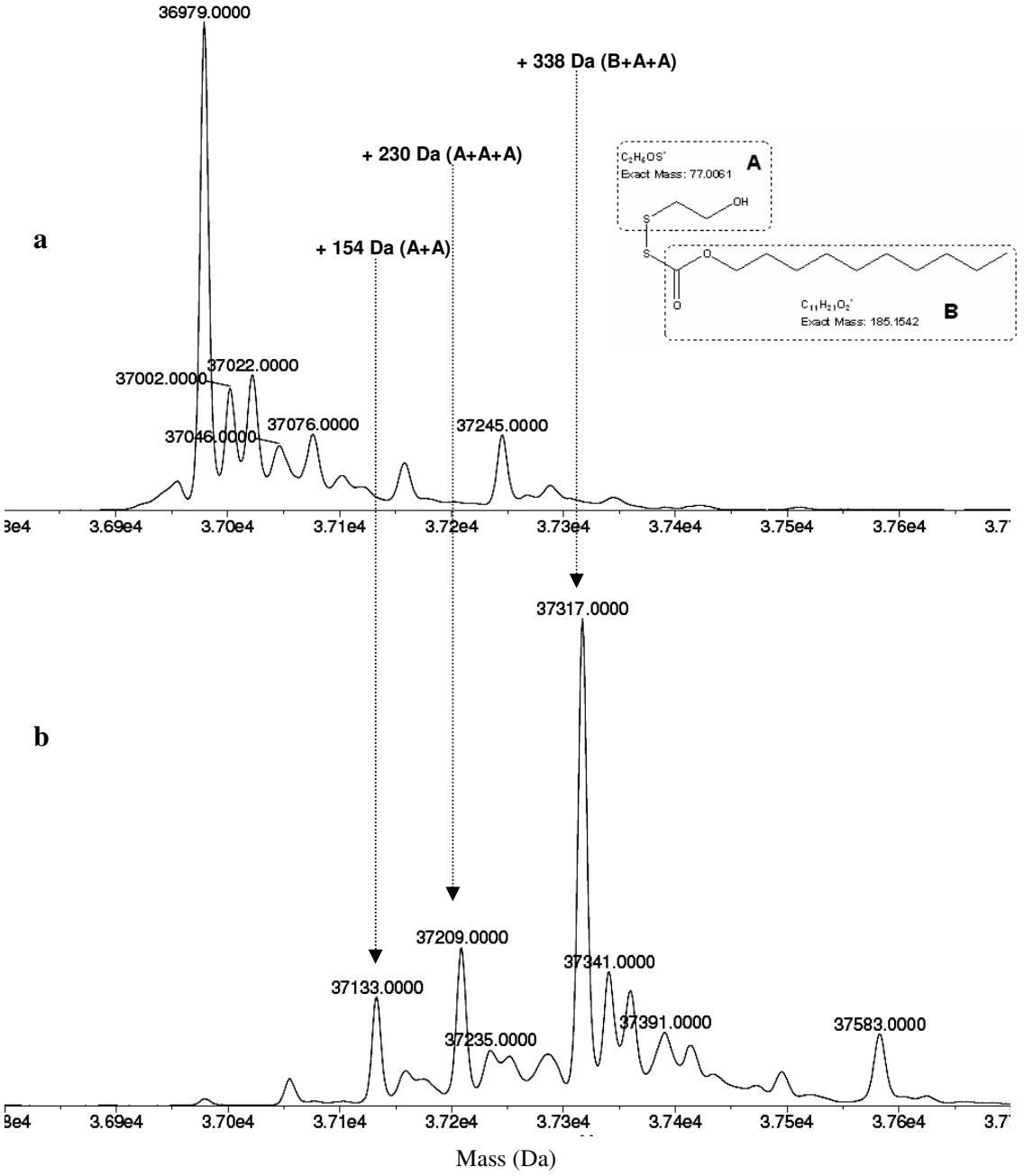

Figure 29: Reaction products of A246F mtFabH with 1. a) Reconstructed ESI mass spectrum of untreated A246F mutant mtFabH (Control) b) Mass spectrum of A246F mutant mtFabH treated with excess of **1**.

To test this hypothesis we created an A246F mutant mtFabH, which introduces a large obstructive group into the pantetheinate channel about 8 – 9Å out from the active site Cys112. This A246F mtFabH mutant had no detectable catalytic activity in an elongation assay with lauroyl-CoA and malonyl-ACP. Mass spectrometry (Figures 29 and 36a) revealed that an incubation of **1** with this A246F mutant resulted in the same tri-modification seen with the wild type enzyme. Both tri-modified species (A + A + A) and (A + A + B) were observed, with an apparent greater abundance of the latter.

The crystal structure of the unliganded A246F mutant showed no significant differences in structure relative to the wild type except for the presence of the bulky phenylalanine, which clearly blocks access to the active site cysteine via the pantetheinate channel. Electron density was observed in the acyl channel that can be fit with a free laurate (not linked to the active site cysteine). Like other mtFabH structures crystallized in the absence of ligands, including the wild type, the electron density in the acyl channel that can be fit with a free laurate is probably taken up during expression and purification of the recombinant mtFabH.

The co-crystal structure of A246F mtFabH with **1** (Figure 27b) shows the overall structure of the protein to be virtually identical to the unliganded mutant. The hydrophobic ligand, modeled as laurate in the acyl binding channel of the unliganded A246F crystal structure, is replaced in the liganded form by electron density contiguous with Cys112 that can be well fit by fragment B of **1** in thioester linkage with Cys112 (Figure 27b). There was no ligand electron density in the blocked pantetheinate channel. In contrast to fragment B in the acyl channel of wt mtFabH, the carbonyl group of B in

the A246F mtFabH complex assumes two alternate orientations, one toward the oxyanion hole and the other toward the malonyl anion binding site. In one subunit, the carbonyl oxygen makes hydrogen bonds with optimal stereochemistry to –NH- of Cys112 and Ala306 in the oxyanion hole of the acyl- binding site, while in the other subunit the hydrogen bond to –NH- of Cys112 is too long to be significant. In both subunits of the dimer, the alternative conformation of the carbonyl oriented toward the malonyl anion binding site positions the oxygen at long hydrogen bond distance from the His244 and Asn274 proton donors.

The vacant pantetheinate channel in the A246F mutant confirms that this channel is blocked by the phenylalanine mutation and indicates that **1** must enter the acyl binding channel by a path other than the pantetheinate channel. We hypothesize that this alternative path exists in an 'open' form of the enzyme in which the extended binding site consisting of the two channels is accessible to ingress of the inhibitor as a result of the lifting of a loop that covers both binding channels (see Discussion below).

5.4.3.3 Reaction of mtFabH, C112A mtFabH and A246F mtFabH with 2 and 3

Inhibitor **1** contains only one long hydrophobic arm, which as shown above can occupy either channel of wt mtFabH, or just the acyl binding channel of the A246F mutant. To probe how inhibitors with two hydrophobic arms, in principle competent to bind both channels, would react with the A246F mutant, we synthesized **2** and **3**, both with two long arms differing only in the addition of a carboxylate group to the C_{10} alkane chain. In addition to providing potential full occupancy of both channels of the enzyme,

the anionic carboxylate of **2** and **3** was expected to both inhibit the putative transit of the long chain through the pantetheinate channel and into the acyl channel and to direct ligand orientation according to the relative hydrophobicities of the two arms and the two arms of the binding channel.

The reaction of wt mtFabH with **2** (Figures 30 and 36b) resulted in two tri-modified products with mass increases of either 617 Da or 648 Da. The former is consistent with addition of two 217 Da A' fragments and one 185 Da B' fragment and the latter to addition of three 217 Da A' fragments (an overall increase in theoretical mass of 619 Da or 651 Da respectively) per mtFabH monomer. There was no detectable unmodified protein. Reaction of **3** with wt mtFabH gave predominantly the tri-modified products exclusively with A" chain fragment (some A" + A" di-modified species was also observed).

Crystal structures of the wild type enzyme with **2** and **3** showed that in both cases a disulfide species was formed between the A' or A" fragments and the active site Cys112 (Figures 37a and 37 b respectively). In the structure of mtFabH with **2**, the undecanoic acid group surprisingly is in the acyl channel and the *O*-undecylcarbonothioate lies in the pantetheinate channel, detached from the C112-disulfide-linked undecanoic acid, and with its carbonyl oxygen oriented towards the malonyl anion binding site of His244 and Asn274 (Figure 37a). Hydrogen bonds in this binding site are close to optimal in one subunit (2.72Å and 2.74Å), but are long in the other subunit (3.34Å and 3.45Å). The crystal structure of wild type mtFabH complexed with **3** (Figure 37b) shows the decyl

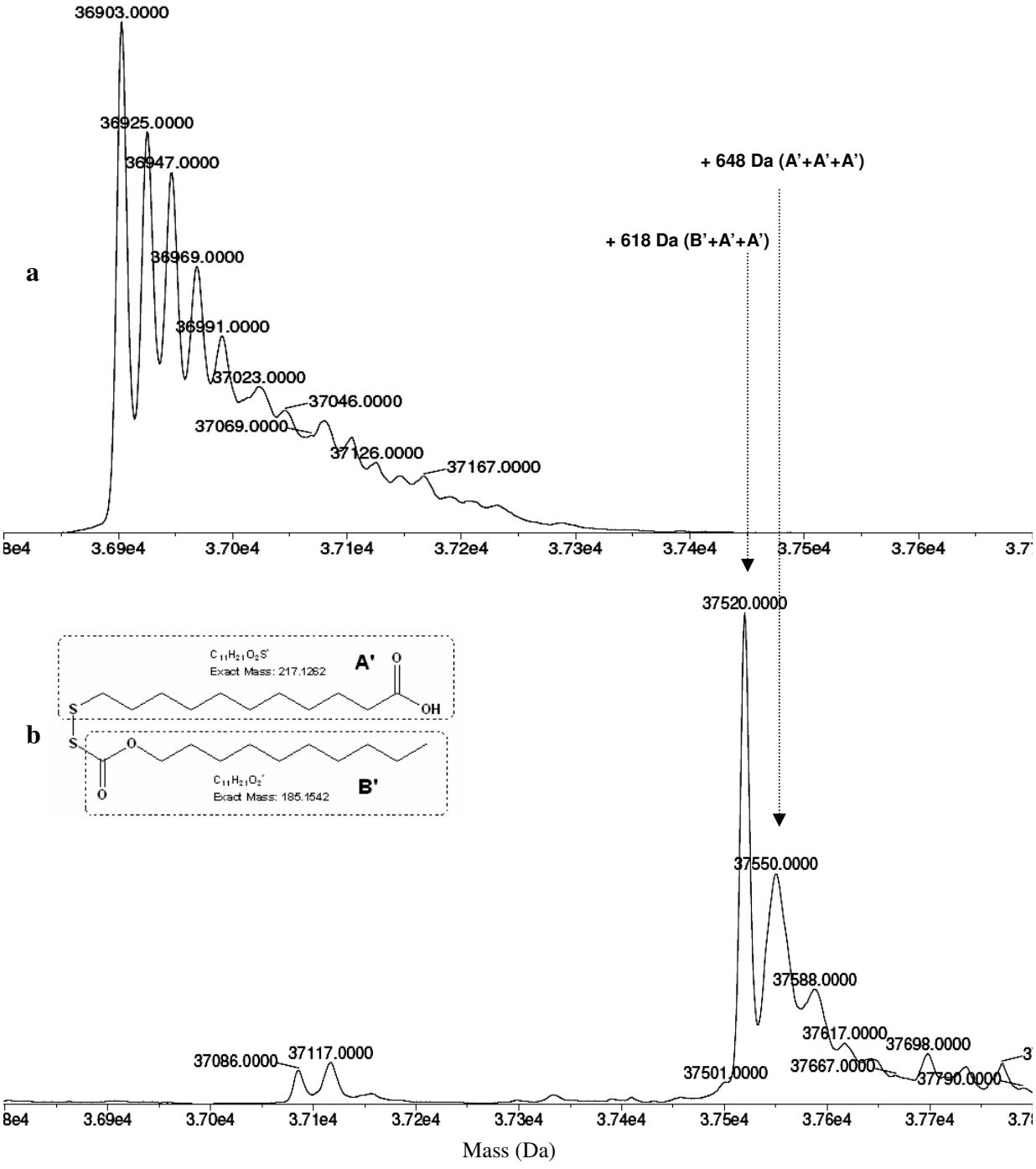

Figure 30: Reaction products of WT mtFabH with 2. a) Reconstructed ESI mass spectrum of untreated WT mtFabH (Control) b) Mass spectrum of WT mtFabH treated with excess of **2**.

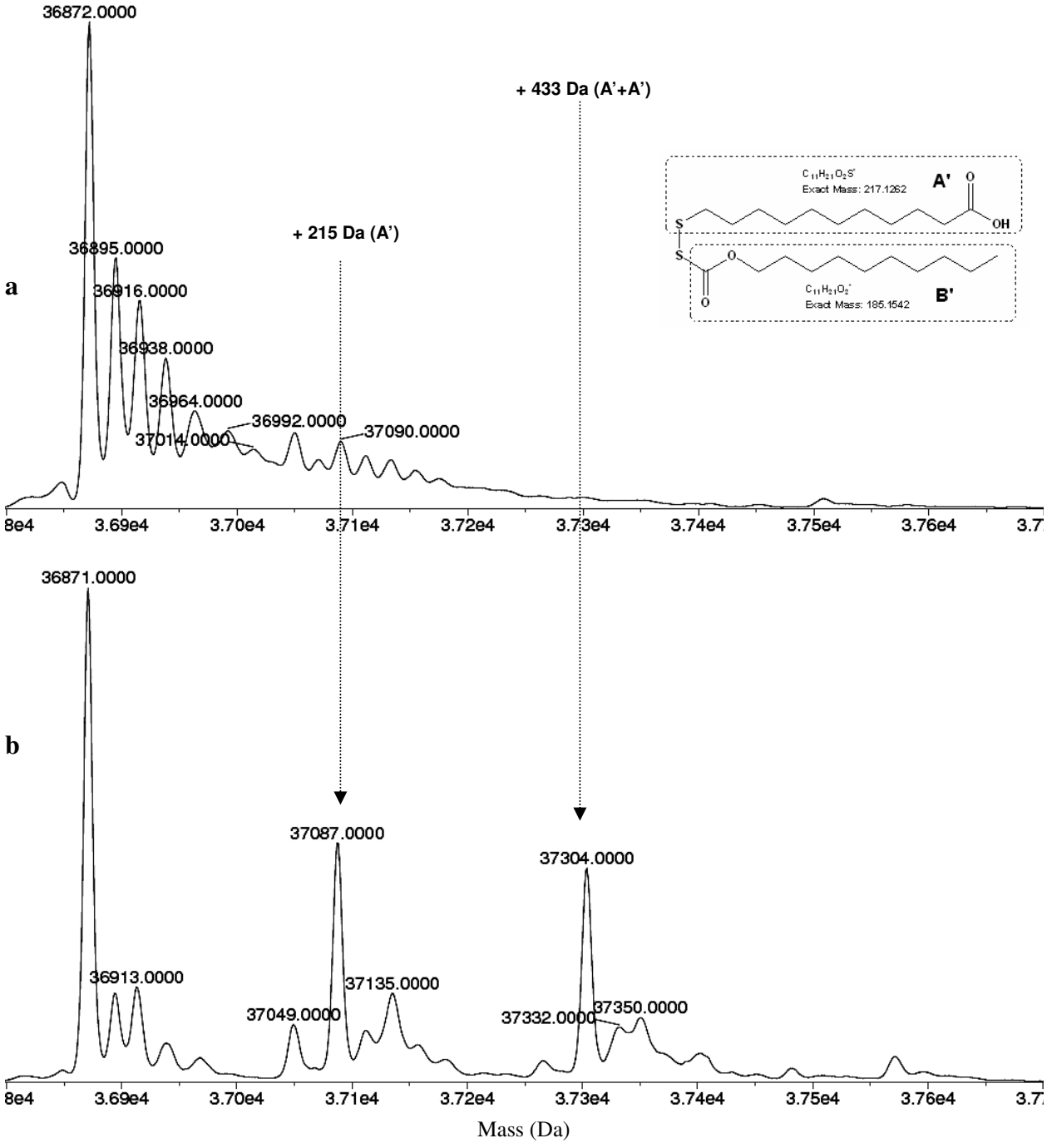

Figure 31: Reaction products of C112A mtFabH with 2. a) Reconstructed ESI mass spectrum of untreated C112A mutant mtFabH (Control) b) Mass spectrum of C112A mutant mtFabH treated with excess of **2.**

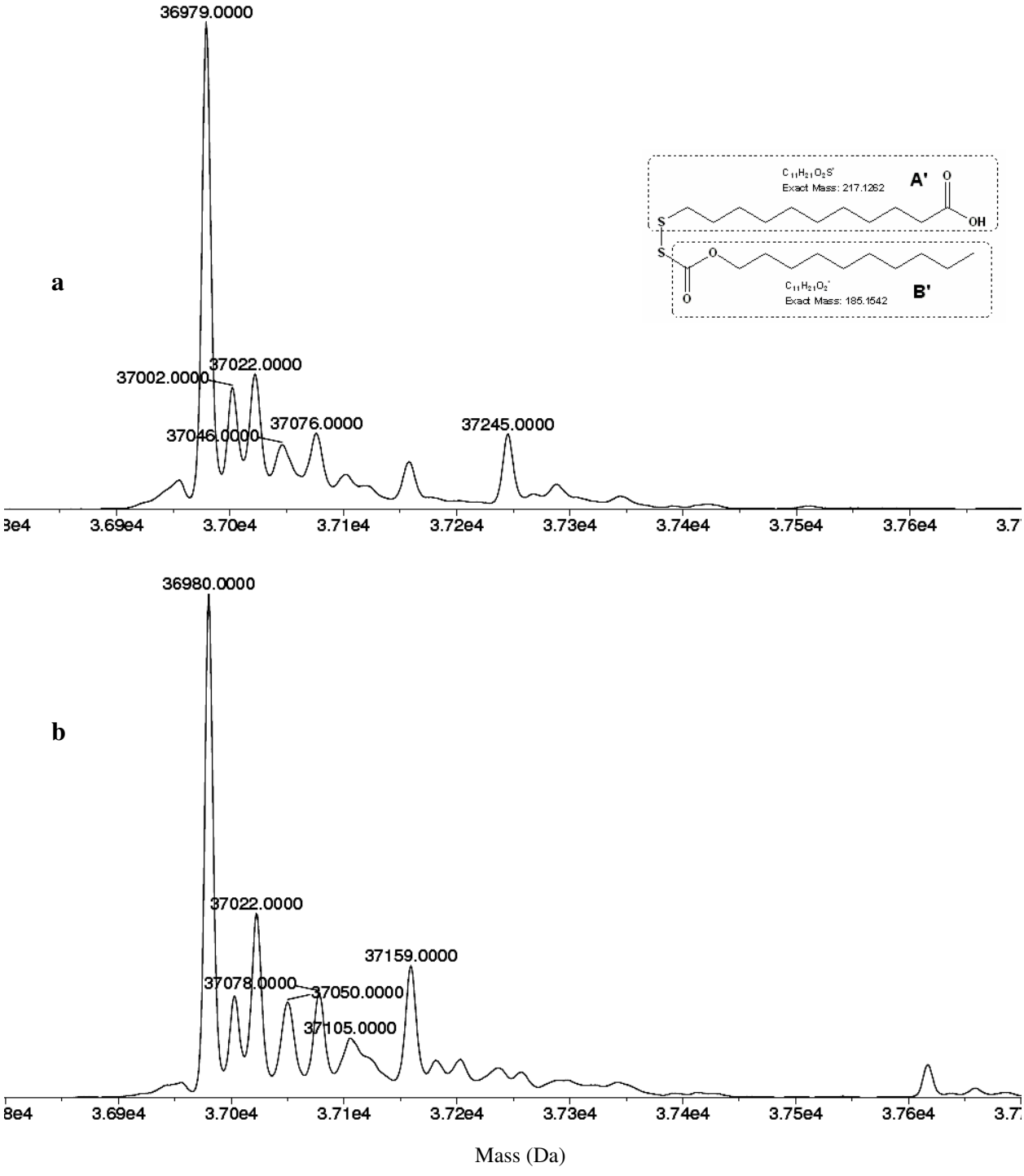

Figure 32: Reaction products of A246F mtFabH with 2. a) Reconstructed ESI mass spectrum of untreated A246F mutant mtFabH (Control) b) Mass spectrum of A246F mutant mtFabH treated with excess of **2**.

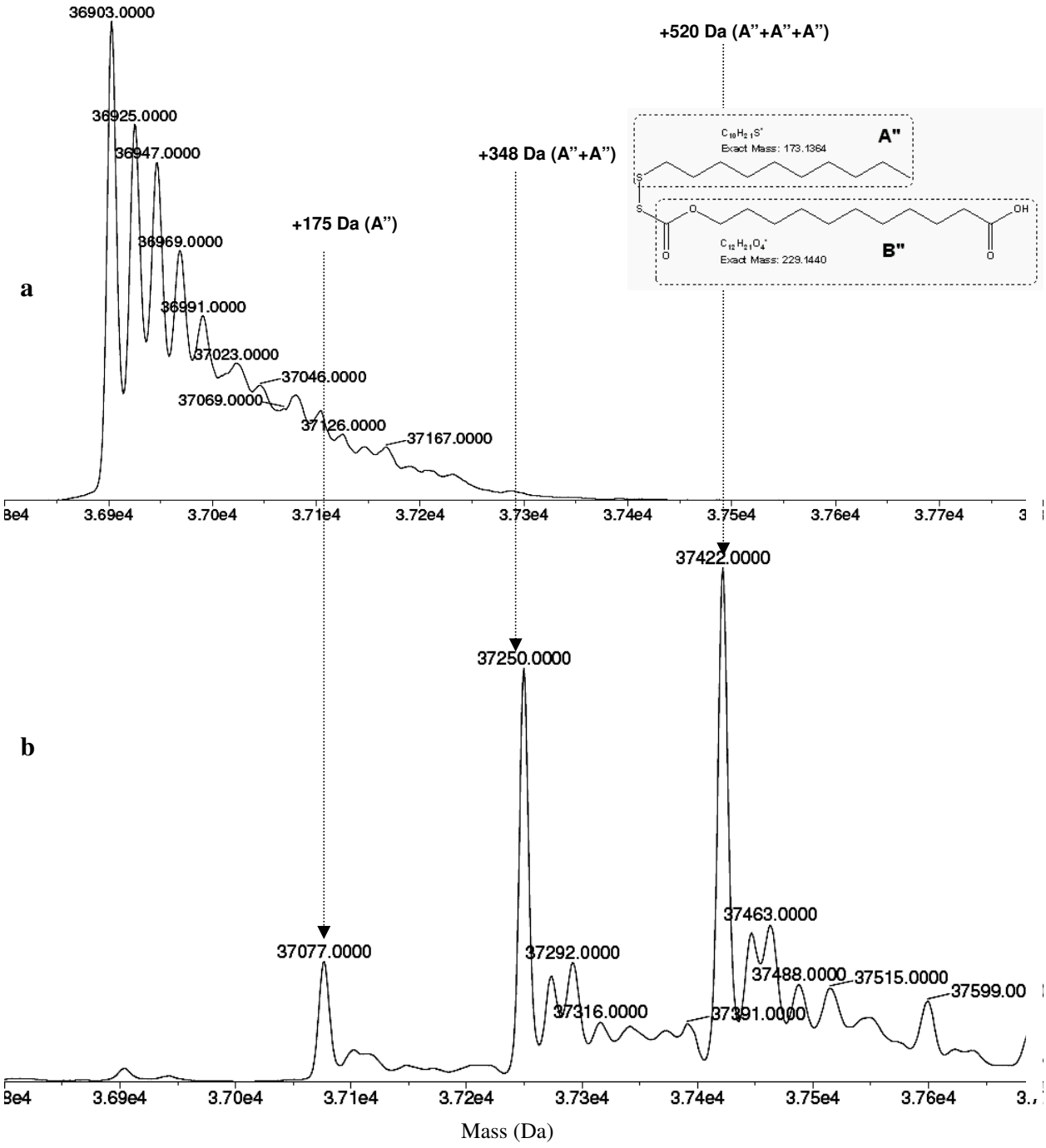

Figure 33: Reaction products of WT mtFabH with 3. a) Reconstructed ESI mass spectrum of untreated WT mtFabH (Control) b) Mass spectrum of WT mtFabH treated with excess of **3**.

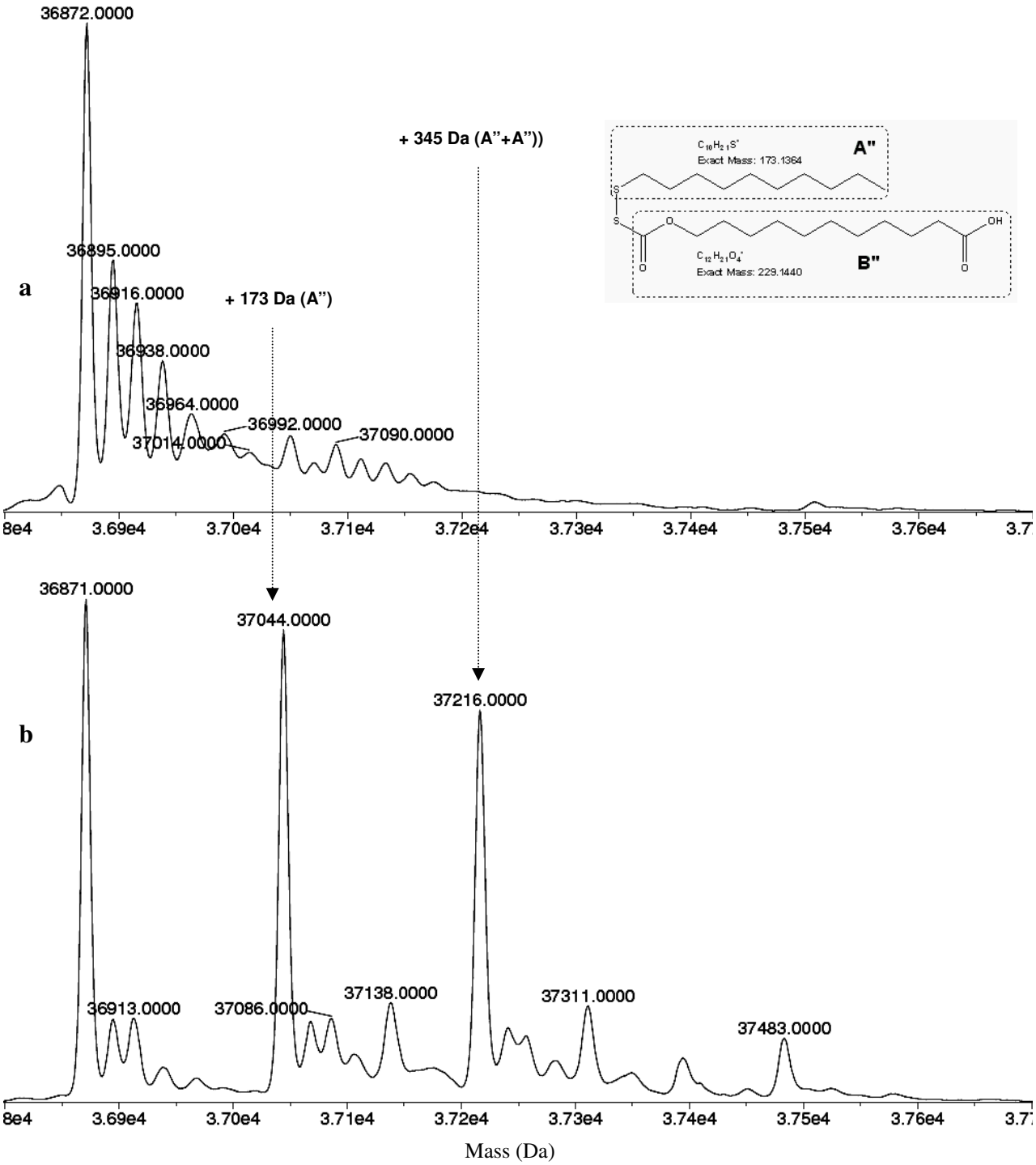

Figure 34: Reaction products of C112A mtFabH with 3. a) Reconstructed ESI mass spectrum of untreated C112A mutant mtFabH (Control) b) Mass spectrum of C112A mutant mtFabH treated with excess of **3**.

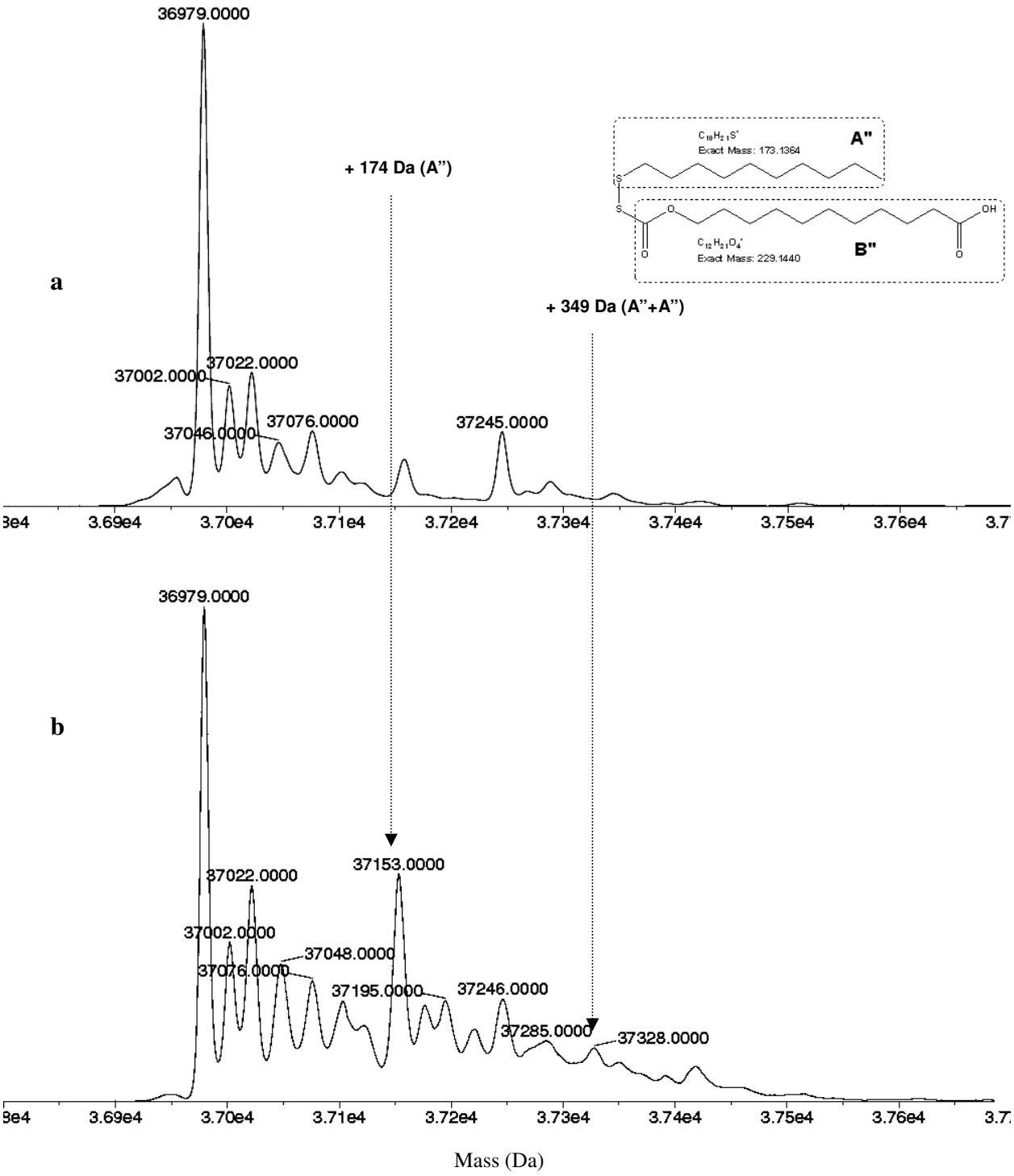

Figure 35: Reaction products of A246F mtFabH with 3. a) Reconstructed ESI mass spectrum of untreated A246F mutant mtFabH (Control) b) Mass spectrum of A246F mutant mtFabH treated with excess of **3**.

chain in the acyl channel disulfide linked to Cys112. The *O*-carboxyundecylcarbonothioate in the pantetheinate channel is present in the same orientation as the *O*-undecylcarbonothioate group in the complex with **2** with its carboxylate at the mouth of the pantetheinate channel and its carbonyl oriented toward the malonyl anion binding site, but too far from His244 and Asn274 in both subunits to make hydrogen bonds. This latter difference vis a vis the complex with **2** may be a consequence of lattice interactions of the carboxylate that are transmitted to the other end of the chain in the malonyl anion binding site.

These observations demonstrate that the linkage positions of the undecanoic acid chain and the decyl chain in **2** and **3** do not determine the orientation of binding these compounds in the acyl site of mtFabH. For **2** the binding of the undecanoic acid in the acyl binding channel is possibly stabilized by the presence of the Arg2024 side chain at the top of the acyl channel in both subunits (4 – 5Å from the carboxylate). In one subunit, there is also a hydrogen bond between one of the carboxylate oxygens (inferred to be in the protonated state) and the amido oxygen of the side chain of Gln191. The recurrence of disulfide exchange products in both cases where the inhibitor has two long arms suggests that orientation in binding is determined primarily by the positioning of the oxycarbonyl-disulfide group in the active site. The crystal structures show that the carbonyl oxygen of this group is directed toward the malonyl anion binding site, and this may be the principal determinant of ligand orientation. For a mechanism involving transit through the pantetheinate into the acyl channel, there is no obvious basis for discrimination in the orientation of the oxycarbonyl-disulfide group. This and the

a

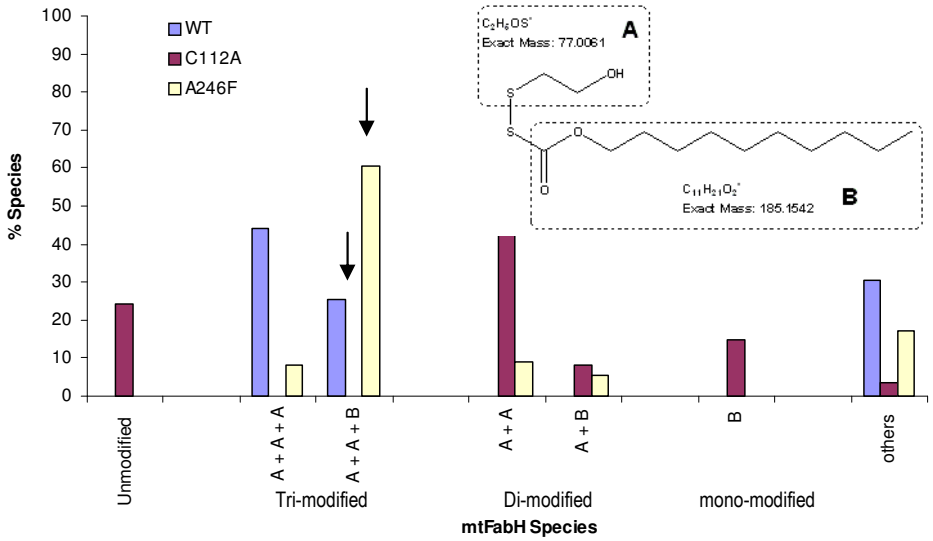

b

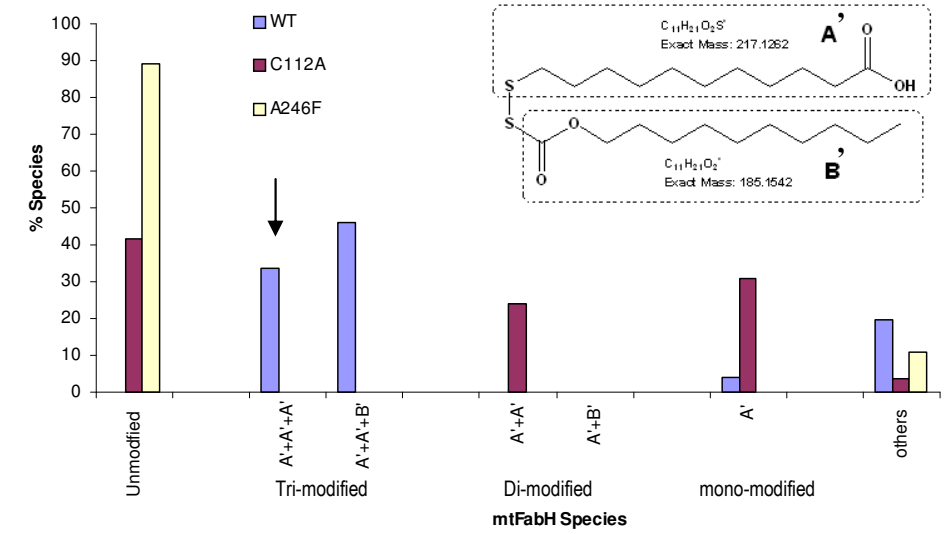

c

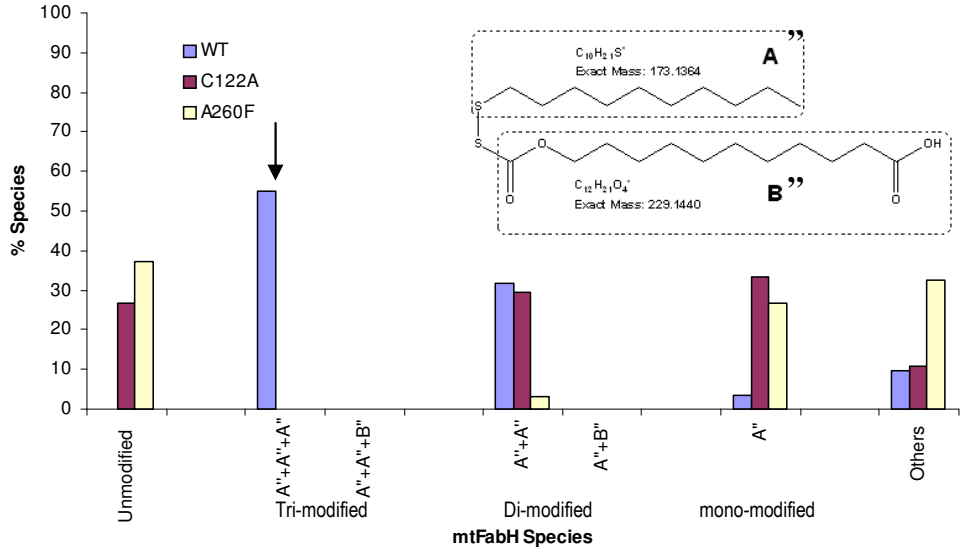

Figure 36: ESI-MS analyses of products of the reactions of compounds 1 (a), 2, (b), and 3 (c) with the wild type, C112A, and A246F mtFabH. Arrows indicate species for which a crystal structure was obtained.

presence of the carboxylate in the acyl channel argue against a threaded transit of the ligand into its final reactive position and for a lower energy pathway of entry.

Reaction of **2** and **3** with the C112A and A246F mutants leads to no detectable tri-modification of the protein (Figures 31, 32, 34, 35, and 36 b and c). For both inhibitors **2** and **3,** a major reaction product species was the unmodified mutated proteins. These results contrast with those of the wild type FabH where there was no unmodified protein and the major species observed with either inhibitor was the tri-modified species. A striking observation from these ESI-MS studies is that the A246F mutant behaves like the C112A mutant with **2** and **3**, but like the wild type mtFabH with **1**. The presence of the phenylalanine mutation dramatically affects reaction of the active site cysteine, but only with inhibitors having two long chain hydrophobic arms.

A co-crystallization of **3** with the A246F mutant revealed a complex with the A" fragment linked by a disulfide to Cys112 and lying in the acyl channel like the ligand complexes with wt mtFabH (Figure 37c). Fragment B", which is observed in the pantetheinate channel of wt mtFabH, is absent in this A246F mutant and this channel remains blocked by the phenylalanine mutation (Figure 37c). Thus, while the ESI-MS results indicate that efficient reaction of the active site cysteine with **3** is affected by this mutation, the crystallization studies indicate that the reaction occurs. Formation of this product by entry of **3** through the pantetheinate channel, which is blocked, seems unlikely. The most parsimonious hypothesis for its formation is that **3** binds to an 'open' form of the enzyme through interaction of its oxycarbonyl-disulfide group at the malonyl anion binding site; this orients A" in the acyl channel for disulfide exchange with

Fig. 37

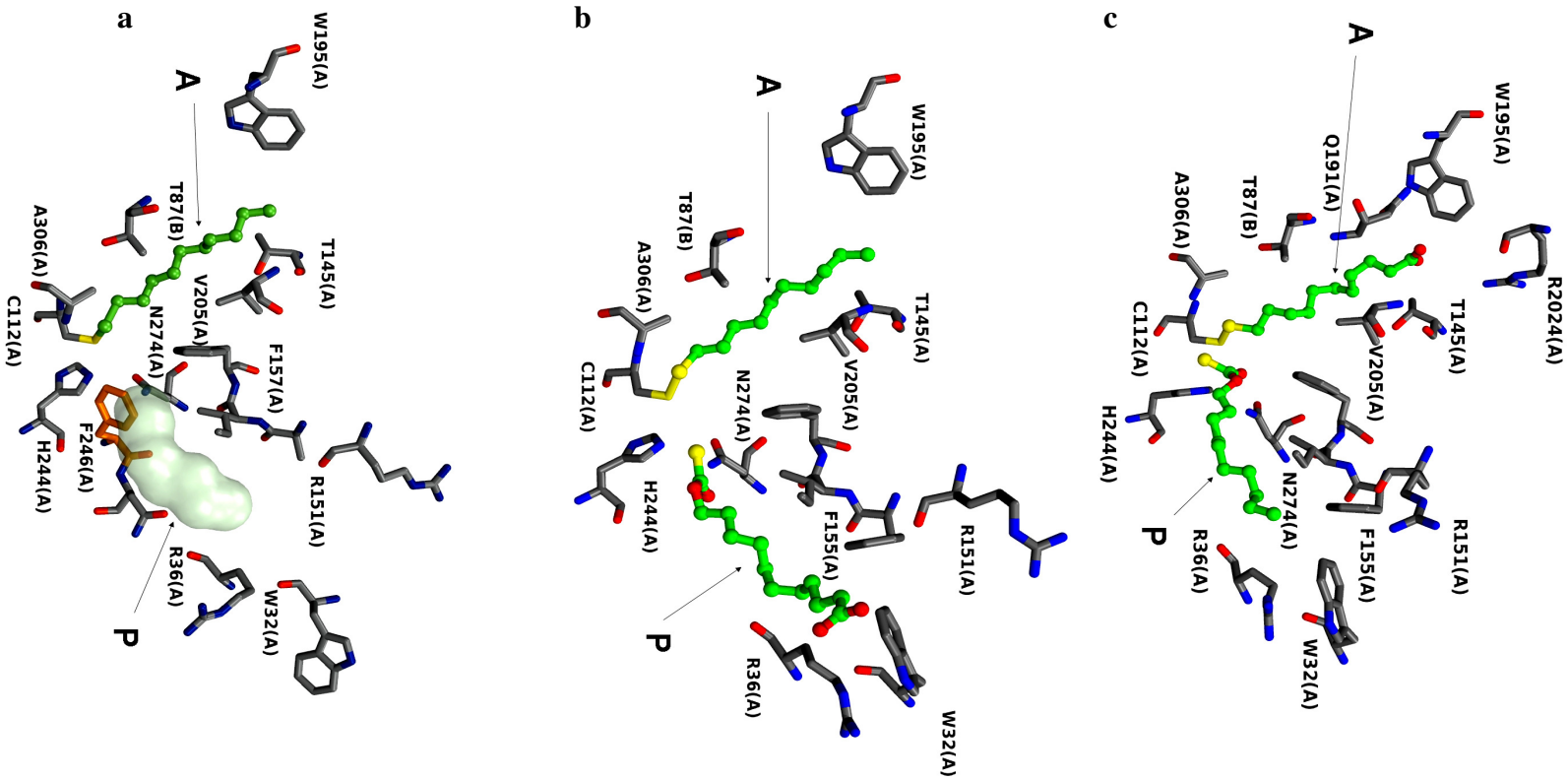

Figure 37. a. Structure of the product of compound 2 with mtFabH showing fragment A' in the acyl channel disulfide linked to Cys112, and fragment B' in the pantetheinate channel. Arrows from A and P point to acyl channel and pantetheinate channel.
b. **Structure of the product of compound 3 with wt mtFabH** showing fragment A" in the acyl channel disulfide linked to Cys112 and fragment B" in the pantetheinate channel.
c. **Structure of the product complex of compound 3 with A246F mtFabH** showing fragment A" in the acyl channel disulfide linked to C112. The surface shape of the empty pentetheinate channel is shown blocked by F246.

Cys112, while B" extends into solvent from the 'open' form in lieu of binding in the pantetheinate channel, and dissociates when the thiol-disulfide exchange reaction occurs.

5.5 Discussion:

5.5.1 Unresolved aspects of *M. tuberculosis* FAS II enzyme mechanisms:

The *M. tuberculosis* type II FAS pathway for synthesis of long chain ($>C_{54}$) fatty acid precursors of the mycolic acid component of the bacterial cell wall [87] is a proven target for existing Tb treatments and offers other opportunities for development of new treatments. Binding and transfer of long chain acyl reactants and products almost certainly require enzyme conformational changes and specific protein-protein interactions, some of which may be vulnerable points for therapeutic development. In particular, it is not clear how some well characterized enzymes of this pathway can accommodate substrates of widely variable acyl chain length and how the protein components of the pathway interact.

Characterization and structure determination of individual enzymes[37,88-91] and acyl-carrier protein in this pathway[92] provide evidence that conformational changes of the proteins play an important role in some individual steps. For instance, conformational changes on substrate binding to InhA (FabI) provide an accessible acyl binding crevice to which a C_{16} thioester binds in a U-shaped conformation.[93] For the reductive enzyme β-ketoacyl reductase (MabA), an open and closed form of the enzyme have been observed and docking studies suggest that an L-shaped binding pocket in the open form can accommodate substrates up to C_{16},[89] but it is unclear how physiological substrates with

acyl chains longer than C_{16} bind to either InhA or MabA. An acyl binding region for C_{10} and C_{12} substrates in the condensing enzyme mtKasB has been identified and is U-shaped. While this binding pocket is larger and more occluded than the corresponding binding region of the *E. coli* FabB (which catalyzes the analogous reaction during palmitate biosynthesis in this microorganism),[91] there is no data suggesting how the much longer physiological substrates bind to mtKasB.

There is less information on protein-protein interactions both in the *M. tuberculosis* type II FAS and also with type I FAS, but there is evidence that such interactions are essential for mycobacterial viability.[94,95] Formation of a type II FAS complex, possibly with some features resembling those in the type I FAS,[96-98] is likely required to facilitate passage of the extremely long chain fatty acid substrates between enzymes.

To date there is no information on conformational changes or protein-protein interactions of mtFabH. The linear acyl binding pocket appears to be capable of accepting substrates only up to about C_{16} in length, (chapter 3) while experiments have shown that the enzyme can process C_{22} substrates.[57] The crystal structure of mtFabH also raises the question of how substrate (and product) enter (and leave) the extended L-shaped binding site consisting of two long, tandem channels, which are roughly perpendicular to each other. The distal, buried acyl-binding channel in the mtFabH structure appears accessible only through the pantetheinate channel, which opens to solvent. However, a binding process in which lauroyl- or other long chain acyl-CoA is threaded first through the pantetheinate channel into the acyl channel seems implausible.

5.5.2 A model for substrate binding and product release in mtFabH

An alternative to this substrate-threading model is a mechanism in which mtFabH exists in an 'open' conformational state, where both the acyl and pantetheinate binding channels are accessible. To test this hypothesis, we used active-site directed oxycarbonyl-disulfide inhibitor ligands flanked on each side by alkyl or carboxyalkyl chains.

Since existing crystal structures of both liganded and unliganded mtFabH are inferred to be in the 'closed' conformational state of the enzyme, we combined solution ESI-MS and crystal structure data to analyze the reaction pathways and product complexes of these inhibitor ligands with mtFabH. These results provide evidence that these compounds do not bind to mtFabH by passage through the pantetheinate channel into the acyl channel. Inhibitor **1** efficiently enters the acyl-channel of the mtFabH A246F mutant, blocked in the pantetheinate channel, and the carboxylated C_{10} arm of compound **2** binds in the acyl channel of wt mtFabH despite the inferred energetic obstacle to migration of a charged (or possibly protonated) group through two hydrophobic channels. These data argue strongly for an 'open' form of mtFabH that binds acyl substrates or inhibitors in a single step.

A crystal structure of a disordered ecFabH[63]and recent kinetic data for inhibition of this enzyme with alkyl-CoA disulfide inhibitors[83] support a model in which 'open' dimeric protein becomes ordered on binding of an acetyl-CoA substrate or methyl-CoA disulfide inhibitor. For the mtFabH there is no experimental crystal structure in a disordered or 'open' form, and a large structural change in the observed 'closed' crystal

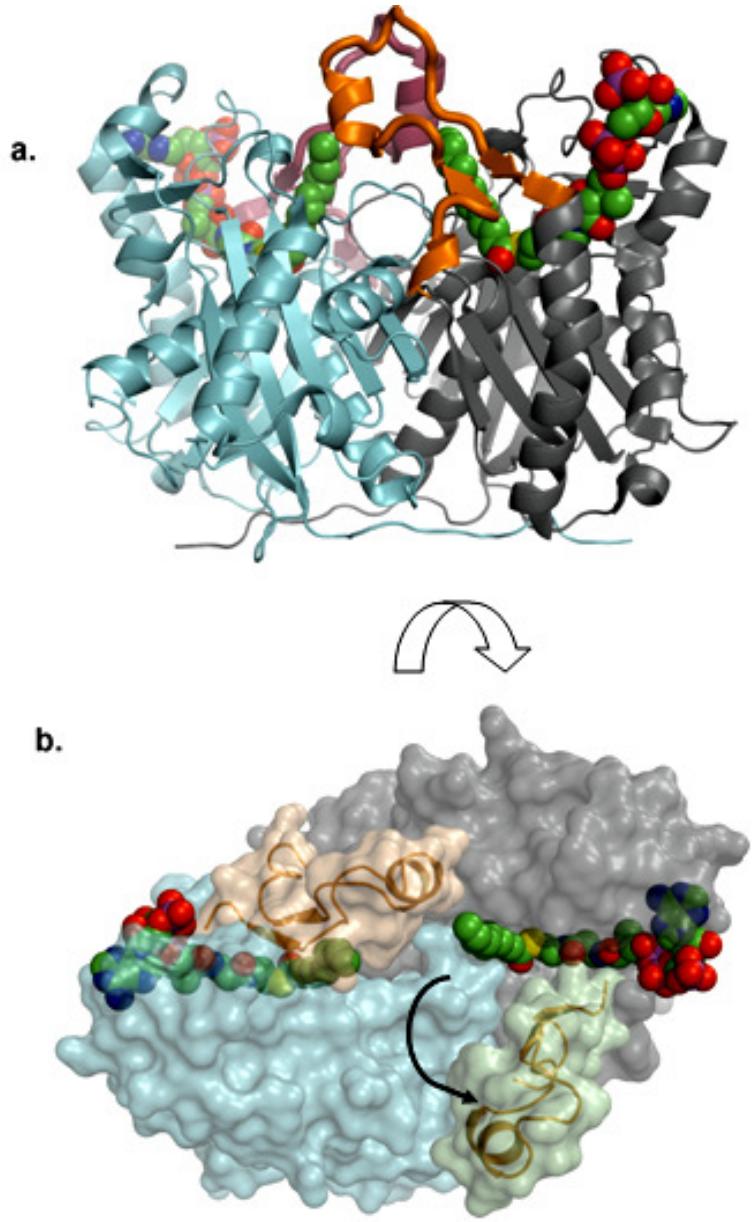

Figure 38: (a) Backbone ribbon model of the dimeric C112A mtFabH complex with lauroyl-CoA (color-coded space filling) bound in active sites of both monomers. The putative flap that covers the extended L-shaped binding site is colored gold (front) in the right-hand (gray) monomer and magenta (back) in the left-hand (blue) monomer subunit.
(b) Surface figure of dimer in Figure 6a rotated approximately 90° about the horizontal axis showing the two flap covers (gold) of each of the two binding sites (defined by lauroyl-CoA (color coded space filling). The flap in the blue left monomer is in the 'closed' conformation, thereby burying the lauroyl-CoA ligand; the flap in the gray right monomer is in the 'open' conformation (movement shown by arrow), opening the lauroyl-CoA binding site to solvent.

structure would be required to provide direct access to the long hydrophobic acyl channel. Inspection of the mtFabH structure reveals how the extended binding site of this enzyme could be exposed for concerted binding of long chain acyl-CoA substrates. A single polypeptide segment (residues 183 – 209, ecFabH numbering) forms most of the top of the acyl channel and part of the top of the pantetheinate channel in mtFabH (Figure 38a). We note that this flap includes an insertion sequence in mtFabH relative to ecFabH that mediates intersubunit interactions in the mtFabH dimer. The extremities of this polypeptide segment coincide with glycine residues (181 and 207) that are almost completely conserved across 5 FabH sequences. Synchronized hinge motions at each of these glycines could raise this polypeptide flap to expose most of the substrate binding site of mtFabH to solvent and to the binding of substrates and ligands (Figure 38b).

This proposed 'open' conformation of mtFabH provides an understanding of how both acyl-CoA substrates and the ligands **1-3** bind and react with the wild type enzyme and how **1** reacts with the A246F mutant. The proposed 'open' conformation of the mtFabH also offers a solution to the dilemma of how mtFabH utilizes substrates longer than palmitoyl-CoA (the maximum permitted chain length suggested by the 'closed' mtFabH structure). Exposure of the acyl binding channel would allow longer chains to extend outward from the channel, possibly interacting with the exposed hydrophobic underside of the opened flap in a modified 'closed' conformation of mtFabH that is necessarily slightly different from that observed with lauroyl-CoA substrate (chapter 3). We propose that ordering or closing of the mtFabH on the substrate or inhibitor is required for efficient reaction with the active site cysteine and that this is why 2 and 3

react poorly with the A246F mutant. Reaction of this mutant with 3 results in loss of fragment B" whose only plausible position during this reaction is extended outward from the binding site, since the pantetheinate channel is blocked.

In this model for acyl-CoA binding to mtFabH, the acyl-CoA reactants synchronously bind both arms of the substrate binding site and CoA product is released from the mouth of the pantetheinate channel in the first stage of the reaction. In the second stage of the mtFabH reaction these different paths for substrate binding and product release would be reversed: the phosphopantetheine arm of ACP carrying the malonyl thioester would enter the mouth of the closed pantetheinate channel after CoA dissociation, and following decarboxylative condensation of malonyl-ACP, transition back to the 'open' form of the enzyme would permit egress of the hydrophobic 3-ketoacyl ACP product. This open form could also facilitate transfer of the long, hydrophobic acyl chain from the acyl channel binding site of mtFabH to a putative binding site on ACP. This latter step is supported by kinetic analyses of the complete mtFabH reaction that indicate an apparent difference in acyl group specificity when using *E. coli* vs *M. tuberculosis* ACP (ACPM),[57] and by the structure of butyryl-ACP in which the acyl group is sequestered in a site on the ACP.[99] We have observed ACP-dependant changes in substrate specificities of other FabH enzymes and kinetic data for inhibition of ecFabH on binding a MeSSCoA inhibitor are consistent with conformational transitions on malonyl-ACP binding.[83]

5.6 Conclusions

In conclusion, the work described here demonstrates that large scale dynamic motions in mtFabH are likely required for ligand binding. Such conformational changes may be critical for the synchronization of binding and dissociation steps, not only in mtFabH but also in other enzymes of the FAS pathways, including transfers between the FASI and FASII components. They require consideration and may also offer alternative approaches in developing new therapeutics that target mycolic acid biosynthesis.

6. CHARACTERIZATION OF NAPHTHALENE-BASED COMPOUNDS AS NOVEL INHIBITORS OF FabH

6.1 Summary

A naphthalene based compound (A) (Figure 39) was previously identified as an effective inhibitor of pfFabH in a screening program at WRAIR (Walter Reed Army Research Institute). A number of structure based analogs were synthesized and found to be effective against purified pfFabH with IC_{50} values in the range of 0.027 μM to >500 μM (unpublished data). In this study, we have tested these analogs against FabH from *M. tuberculosis* and reported a similar SAR with IC_{50} values ranging from 0.6 μM to 138 μM. A comparison of the two sets of IC_{50} values was utilized to deduce a preliminary pharmacophore for this series of inhibitors.

6.2 Introduction

The emergence of multidrug resistance in recent times has shifted the impetus of anti-microbial research from lead discovery towards target discovery. β-ketoacyl-ACP synthase (FabH) is one such enzyme which, owing to its key role in type II fatty acid synthesis, has recently attracted considerable attention as a good anti-microbial drug target. Consequently, it has been characterized from a number of species including highly pathogenic microbes such as *M. tuberculosis*[27,57,88,100] and *S. pneumonia*.[101] Further, the

availability of crystal structures from various species has added enormously to the mechanistic knowledge of this enzyme and various research groups have directed significant efforts towards the design of selective FabH inhibitors in the recent past.

Daines et al.[102] utilized a combination of high throughput screening and homology modeling to identify a series of indole-based inhibitors found to be active against spFabH and ecFabH. These inhibitors were shown to bind non-covalently in the CoA/malonyl-ACP pocket close to the active site triad. A computational search of National Cancer Institute (NCI) database for compounds structurally similar to thiolactomycin resulted in identification of several 1,2-dithiole-3-ones as potent inhibitors of both *E. coli* FabH and *S. aureus* FabH.[81,103] In contrast to the indole-based FabH inhibitors the mode of binding of these inhibitors could not be determined. Recently, Nie et al. have used a structure-based drug design approach which afforded a series of benzoylaminobenzoic acid compounds as potent inhibitors of *E. faecalis* FabH.[58] Some of these compounds demonstrated good antibacterial activity against Gram-positive and some Gram-negative organisms.

Here we have explored the inhibitory activity of a series of naphthalene-based compounds, which were found effective against pfFabH and ecFabH (unpublished data), on mtFabH. The lead compound "A" (Figure 39) was initially identified in a screening effort by Division of Experimental Therapeutics branch of Walter Reed Army Institute of Research (WRAIR) for inhibitors of the *P. falciparum* FabH. This was later found to be active against FabH from *E. coli* and *M. tuberculosis* which led to the synthesis of fourteen analogs of inhibitor A (series 1-4; synthesis was carried out by Dr.

Alhamedsheh). These compounds were tested against purified pfFabH enzyme and the IC_{50} values are listed in Table 7 (pfFabH IC_{50} column). The compounds were also tested against chloroquine (CQ)- sensitive (D6) *P. falciparum* strain (pf D6 IC_{50} column). In this study, we have tested these compounds against purified mtFabH (mtFabH IC_{50} column) and deduced a generalized SAR based on IC_{50} values from the two FabHs.

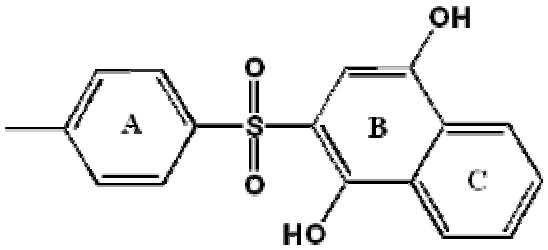

Figure 39: **Structure of the lead compound A.** The rings are labeled as discussed in the text.

6.3 Results and Discussion

The series of analogs 1-4 (see table 7) were tested against purified *M. tuberculosis* FabH using the ACPM independent assay described in chapter 2 and the IC_{50} values are listed in table 7 along with IC_{50} values for *P. falciparum* FabH and in-vivo inhibitory activity against chloroquine (CQ)- sensitive (D6) *P. falciparum* strain for comparison (pf D6 IC_{50} values).

We initiated our SAR analysis with the variation of the 'A' ring. Removal of the methyl group from ring 'A' of our lead compound 1a led to ~ 4 times decrease in inhibitory activity in compound 1b in mtFabH. Further substitution of the methyl group to larger propyl and chloro groups and much bulkier phenyl group (compounds 1c, 1d

and 1g respectively) resulted in ~2-5 times decrease in inhibitory activity in mtFabH. Replacement of methyl to amine (1e) resulted in prominent 50-fold decrease in inhibitory activity in mtFabH while the relatively bulkier acetamide substitution (1f) had a meager effect on the activity. Total removal of 'A' ring of the lead compound 1a to 1h led to a small decrease in inhibitory activity indicating the non-essential nature of the 'A' ring. A very similar pattern in IC_{50} values on varying the ring "A" was noted for pfFabH enzymes with series 1.

The SAR analysis of the ring "B" of the lead compound 1a was concentrated mainly on the importance of 1, 4 di-hydroxyls. Removal of the two hydroxyls (1j) resulted in > 200 fold decrease in inhibitory activity against mtFabH with an IC_{50} value of 138 μM. The oxidation of di-hydroxyls to di-keto groups (2a) resulted in a slight decrease in inhibitory activity but not nearly as drastic as their removal. We noticed a ~ 5 times decrease in inhibitory activity on mtFabH and a ~ 20 fold decrease in inhibitory activity against pfFabH for compound 2a. Lastly, we tried the variation of the 'C' ring by removing the 'C' ring of compound 1a and 1f to 3a and 3b respectively. A complete loss of inhibitory activity against pfFabH enzyme and parallel 50-fold decrease in mtFabH IC_{50} values strongly suggested the necessity of ring 'C'. Substitution of naphthalene-1,4-diol (1a) to anthracene-1,4-diol (4a) resulted in a ~ 10 fold decrease in activity indicating the steric limit on ring 'C'.

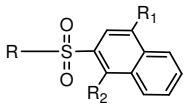

1

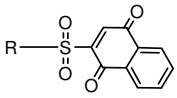

2

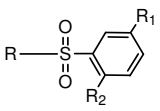

3

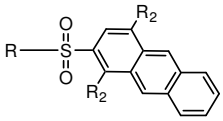

4

Compound	R	R_1	R_2	pfFabH IC_{50} (µM)	pf D6 IC_{50} (µM)	mtFabH IC_{50} (µM)
1a		OH	OH	0.07	24.5	0.61 ± 0.1
1b	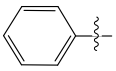	OH	OH	0.2	90.5	2.84 ± 0.1
1c	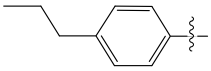	OH	OH	0.07	102	3.09 ± 0.6
1d	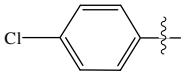	OH	OH	0.12	9.7	3.61 ± 0.9
1e	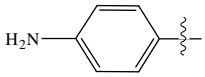	OH	OH	115.9	16	28.96 ± 3.3
1f	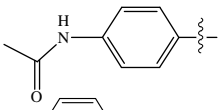	OH	OH	0.03	14	3.76 ± 0.6
1g	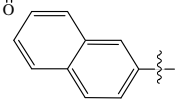	OH	OH	0.4	15	1.49 ± 0.1
1h		OH	OH	0.03	20.3	3.53 ± 0.1
1i	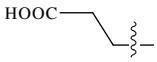	OH	OH	nd	nd	3.53 ± 0.1
1j		H	H	>500	31	138.1 ± 6.4
2a		na	na	1.4	21.4	1.99 ± 0.2
3a		OH	OH	>500	14	34.35 ± 2.8
3b	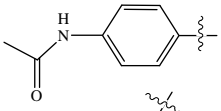	OH	OH	>500	24.5	31.38 ± 2.7
3c	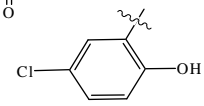	Cl	OH	145.9	75	2.75 ± 0.3
4a	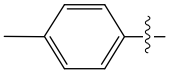	OH	OH	0.3	15.6	8.47 ± 1.6

Table 7: IC_{50} values of compounds 1-4 against pfFabH and mtFabH. The mtFabH IC_{50} values determined in this study are highlighted.

The preliminary inhibitory analysis showed a clear similarity between the inhibitions of two FabHs by this series of compounds. The summary of SAR based on the above analysis is as follows. A wide range of substitution as well as the complete removal was well tolerated on ring 'A', which strongly suggests a large flexibility of this part of molecule. The di-hydroxyl groups on the ring 'B' are required for activity but can be replaced with di-keto groups too. The Ring 'C' was noted to be absolutely essential for activity as its absence led to drastic decrease in inhibitory activity in both enzymes. Finally, in-vivo activity was also tested in chloroquine (CQ)- sensitive (D6) *P. falciparum* strain and the results are shown in table 7. The "ineffective" in-vitro inhibitors (series 3 and 1j) showed comparable inhibition level (14 –75 μM) to the "effective" in-vitro inhibitors (1a, 1c, 1h). The absence of any co-relation between the in-vivo and in-vitro values strongly suggests that FabH is certainly not the sole enzyme target for this class of inhibitors.

6.3.1 Mode of binding

The available structural data depicts two distinct channels for ligand binding in all FabHs. The first channel, leading up to the active site Cys112 is shown to accommodate the pantetheinate arm of both CoA and ACP. The second channel, located at the distal end of the active site cysteine is shown to accommodate the variable acyl chain of the first substrate acyl-CoA. mtFabH contains the largest acyl pocket in FabH class of enzyme and consequently it can catalyze the condensation of the long acyl-CoAs (C_6-C_{20} CoAs) with malonyl-ACP to form the β-ketoacyl-ACP product. The inhibition pattern of

this series of compounds tested on mtFabH and pfFabH enzymes strongly indicates that these inhibitors would most likely bind in the common CoA/malonyl-ACP pocket considering the large difference in size of acyl pockets in two enzymes. Unfortunately, despite several co-crystallization attempts we were not able to determine the absolute mode of binding of these compounds in mtFabH enzyme. In addition, docking of the most potent analogs resulted in unconvincing results. Further biochemical studies such as mutational analysis are required to elucidate the mode of binding.

6.4 Conclusions

A novel class of naphthalene based compounds is tested against clinically important mtFabH enzyme and the IC_{50} values were compared with pfFabH IC_{50}. Although the inhibitory activity of the analogs based on the lead compound did not improve much, a basic pharmacophore was established based on available data. This pharmacophore can be further utilized to search for related structures in the vast chemical libraries available and also can be further improved by conventional chemical synthesis and QSAR technique.

7. Conclusions and Future directions

1. *M. tuberculosis* FabH (mtFabH) is claimed to be a key enzyme for its proposed regulatory role in the biosynthesis of mycolic acid, an essential component of the mycobacterial cell wall responsible for imparting rigidity and virulence to the bacterium. The methods to assay mtFabH, thus far, have been very tedious and costly due to technical difficulties associated with physical separation of its substrate from its product. We have designed a simpler and more cost efficient assay in this study.

   This assay utilizes malonyl-CoA instead of malonyl-ACP and thus is the first ACP independent assay designed for mtFabH. We propose to utilize this assay in conjunction with the analogous malonyl-ACP-dependent mtFabH assay to investigate the molecular interaction between the mycobacterial acyl carrier protein (ACPM) and mtFabH. This study will involve mtFabH mutants mutated at key amino acid residues that are likely to be involved in interaction with ACPM. The relative condensation activity in ACP-dependent versus our ACP-independent assay can help us understand the role of those residues in their interaction with ACPM.

2. Fatty acid enzymes in *M. tuberculosis* are responsible for synthesizing the long acyl chain component of the mycolic acids. Although mycobacterium enzymes share functional and structural similarities with FAS enzymes from other species, they have structural features, which make them unique. mtFabH is known to process much longer acyl-CoA substrates than its analogous enzymes in other bacterial species. In this study we solved the crystal structure of mtFabH with its substrate dodecanoyl-CoA. We observed that there is room for no more than four more carbons (maximum of hexa-decanoyl CoA) in the acyl pocket, which does not agree with its physiological substrate specificity. Although a possible hypothesis to resolve this paradox is set forth in chapter 5, a stable crystal structure of mtFabH complexed with C_{18}-C_{24} CoA would be helpful in understanding the molecular dynamics involved in long acyl chain binding in the acyl pocket of mtFabH. In our previous attempts to obtain a co-crystal of mtFabH with tetradecanoyl-CoA or hexadecanoyl-CoA, we observed that a small impurity of dodecanoyl CoA in the preparation resulted in crystallization of density corresponding to doecanoyl CoA in the acyl pocket. We propose to achieve a pure preparation of longer acyl-CoAs (C_{18}-C_{24} CoA) using the HPLC technique, and use it to prepare stable co-crystals with mtFabH. This will help us greatly in understanding the dynamics of substrate binding and possibly also the ligand trafficking in mtFabH.

3. Fatty acid biosynthesis (FAS) has been recently identified as an excellent drug target for bacteria in the wake of rising drug resistance. Although some clinically and commercially available compounds (eg isoniazid, triclosan) do target FAS, the full aptitude of this system is not yet utilized as many enzymes with no inhibitors in the clinical pipeline are likely to be good targets. FabH is one such enzyme with a proposed regulatory role in fatty acid biosynthesis in bacteria. While FabH from bacterial species such as *E. coli* is important for investigational purposes, FabH from clinical species such as *M. tuberculosis and H.pylori* hold more promise clinically. With only a handful of drugs that are effective against TB, and with the rise of MDR, it is imperative to develop new effective TB drugs. We plan to fully characterize mtFabH using the ACP dependent and ACP independent assay to have better understanding of the enzyme, which further can aid in discovery of novel anti-tubercular drugs.

4. The ligand trafficking in mtFabH is one of the many unanswered questions which are critical to understanding the physiological functioning of this enzyme at the molecular level. In this study, we attempted to answer this question using a series of oxycarbonyl-disulfide ligands and a "CoA channel blocked" mtFabH mutant. We developed the first ever proof for mtFabH that large scale dynamic motion is important for its catalytic functioning. Further, we proposed a likely portal for substrate entry and product exit in mtFabH. This proposed flap formed by a single polypeptide segment (residues 183 – 209, ecFabH numbering) could expose most

of the acyl and CoA channels, thus serving as an entry and exit portal for substrate/product. We plan to investigate the proposed role of this polypeptide flap using a combination of mutational and other biochemical tools. An analysis of a series of mtFabH mutations at the hinge residues of this proposed flap -- for example, mutating the conserved glycine residues to more restrictive and bulkier residues like alanine or proline - should help us understand the role of these residues.

5. In a previous study by Besra et al[57], it has been observed that, under the experimental conditions used, the extent of acylation is found to be less than 25 %. Further, the rate of acylation is surprisingly slower than the overall condensation rate of mtfabH. These results indicated a possible in-equivalency between the two monomers of the mtFabH dimer. In this study, we have shown for the first time that both mtFabH monomers can be fully acylated or alkylated by a mixture of acyl-CoA or alkyl-CoA disulfide. Surprisingly, ESI-MS studies showed that only dodecanoyl-CoA reacted with mtFabH from a mix of C_6-C_{20} -CoAs. This observation is in concordance with a previous one[57] where longer substrates are processed more efficiently when cognate ACPM was utilized. These observations suggest a possible role of ACPM in priming of substrates and/or off-loading of products from mtFabH. We propose to investigate this particular aspect of mtFabH functioning using a variety of biochemical techniques including mutagenesis and mass spectrometry.

6. The assay developed in this study (chapter 2) was used to test a series of naphthalene based compounds which were identified in a library screening effort by Walter Reed Research Institute (chapter 6). This assay was also used to test a series of compounds which were found effective against ecFabH.[104] The commercial availability of all the components of our assay and its simplicity makes it much more efficient to screen numerous potential inhibitors at one time without prior preparation of substrates and with minimal expenditure. We plan to further utilize our assay to speed the discovery and development of novel inhibitors of mtFabH as potential anti-tubercular agents.

References

(1) Tuberculosis Factsheets; World Health Organization, 2006.

(2) Sniderm D.E.; Raviglione, M. a. K., A. *Tuberculosis: Pathogenesis, Protection and Control*; American Society for Microbiology: Washington, D.C., 1994; 3-11.

(3) Dye, C.; Scheele, S.; Dolin, P.; Pathania, V.; Raviglione, M. C. Consensus statement. Global burden of tuberculosis: estimated incidence, prevalence, and mortality by country. WHO Global Surveillance and Monitoring Project. *Jama* **1999**, *282*, 677-686.

(4) McKinney, J. D. J., W. R.Jr. and Bloom, B.R. *Emerging Infections*; Academic Press: New York, 1998; 51-146.

(5) Basso, L. A.; Blanchard, J. S. Resistance to antitubercular drugs. *Adv Exp Med Biol* **1998**, *456*, 115-144.

(6) Blanchard, J. S. Molecular mechanisms of drug resistance in Mycobacterium tuberculosis. *Annu Rev Biochem* **1996**, *65*, 215-239.

(7) Rattan, A.; Kalia, A.; Ahmad, N. Multidrug-resistant Mycobacterium tuberculosis: molecular perspectives. *Emerg Infect Dis* **1998**, *4*, 195-209.

(8) Barry, C. E., 3rd; Mdluli, K. Drug sensitivity and environmental adaptation of mycobacterial cell wall components. *Trends Microbiol* **1996**, *4*, 275-281.

(9) Brennan, P. J.; Nikaido, H. The envelope of mycobacteria. *Annu Rev Biochem* **1995**, *64*, 29-63.

(10) Trias, J.; Benz, R. Permeability of the cell wall of Mycobacterium smegmatis. *Mol Microbiol* **1994**, *14*, 283-290.

(11) Chatterjee, D. The mycobacterial cell wall: structure, biosynthesis and sites of drug action. *Curr Opin Chem Biol* **1997**, *1*, 579-588.

(12) Barry, C. E., 3rd; Lee, R. E.; Mdluli, K.; Sampson, A. E.; Schroeder, B. G. et al. Mycolic acids: structure, biosynthesis and physiological functions. *Prog Lipid Res* **1998**, *37*, 143-179.

(13) Liu, J.; Barry, C. E., 3rd; Besra, G. S.; Nikaido, H. Mycolic acid structure determines the fluidity of the mycobacterial cell wall. *J Biol Chem* **1996**, *271*, 29545-29551.

(14) Draper, P. *The Biology of the Mycobacteria*; Academic Press: London, 1982; pp 9-52.

(15) Armstrong, J. A.; Hart, P. D. Response of cultured macrophages to Mycobacterium tuberculosis, with observations on fusion of lysosomes with phagosomes. *J Exp Med* **1971**, *134*, 713-740.

(16) Clemens, D. L. Mycobacterium tuberculosis: bringing down the wall. *Trends Microbiol* **1997**, *5*, 383-385.

(17) Nikaido, H. Prevention of drug access to bacterial targets: permeability barriers and active efflux. *Science* **1994**, *264*, 382-388.

(18) Glickman, M. S.; Cox, J. S.; Jacobs, W. R., Jr. A novel mycolic acid cyclopropane synthetase is required for cording, persistence, and virulence of Mycobacterium tuberculosis. *Mol Cell* **2000**, *5*, 717-727.

(19) Minnikin, D. E. *The Biology of Mycobacteria*; Academic Press: London, 1982; 95-184.

(20) Chirala, S. S.; Wakil, S. J. Structure and function of animal fatty acid synthase. *Lipids* **2004**, *39*, 1045-1053.

(21) White, S. W.; Zheng, J.; Zhang, Y. M.; Rock The structural biology of type II fatty acid biosynthesis. *Annu Rev Biochem* **2005**, *74*, 791-831.

(22) Payne, D. J.; Warren, P. V.; Holmes, D. J.; Ji, Y.; Lonsdale, J. T. Bacterial fatty-acid biosynthesis: a genomics-driven target for antibacterial drug discovery. *Drug Discov Today* **2001**, *6*, 537-544.

(23) Zhang, Y. M.; White, S. W.; Rock, C. O. Inhibiting bacterial fatty acid synthesis. *J Biol Chem* **2006**, *281*, 17541-17544.

(24) Bloch, K. Control mechanisms for fatty acid synthesis in Mycobacterium smegmatis. *Adv Enzymol Relat Areas Mol Biol* **1977**, *45*, 1-84.

(25) Cole, S. T.; Brosch, R.; Parkhill, J.; Garnier, T.; Churcher, C. et al. Deciphering the biology of Mycobacterium tuberculosis from the complete genome sequence. *Nature* **1998**, *393*, 537-544.

(26) Choi, K. H.; Kremer, L.; Besra, G. S.; Rock, C. O. Identification and substrate specificity of beta -ketoacyl (acyl carrier protein) synthase III (mtFabH) from Mycobacterium tuberculosis. *J Biol Chem* **2000**, *275*, 28201-28207.

(27) Scarsdale, J. N.; Kazanina, G.; He, X.; Reynolds, K. A.; Wright, H. T. Crystal structure of the Mycobacterium tuberculosis beta-ketoacyl-acyl carrier protein synthase III. *J Biol Chem* **2001**, *276*, 20516-20522.

(28) Takayama, K.; Wang, C.; Besra, G. S. Pathway to synthesis and processing of mycolic acids in Mycobacterium tuberculosis. *Clin Microbiol Rev* **2005**, *18*, 81-101.

(29) Schroeder, E. K.; de Souza, N.; Santos, D. S.; Blanchard, J. S.; Basso, L. A. Drugs that inhibit mycolic acid biosynthesis in Mycobacterium tuberculosis. *Curr Pharm Biotechnol* **2002**, *3*, 197-225.

(30) Takayama, K.; Schnoes, H. K.; Armstrong, E. L.; Boyle, R. W. Site of inhibitory action of isoniazid in the synthesis of mycolic acids in Mycobacterium tuberculosis. *J Lipid Res* **1975**, *16*, 308-317.

(31) Takayama, K.; Wang, L.; David, H. L. Effect of isoniazid on the in vivo mycolic acid synthesis, cell growth, and viability of Mycobacterium tuberculosis. *Antimicrob Agents Chemother* **1972**, *2*, 29-35.

(32) Wang, L.; Takayama, K. Relationship between the uptake of isoniazid and its action on in vivo mycolic acid synthesis in Mycobacterium tuberculosis. *Antimicrob Agents Chemother* **1972**, *2*, 438-441.

(33) Winder, F. G.; Collins, P. B. Inhibition by isoniazid of synthesis of mycolic acids in Mycobacterium tuberculosis. *J Gen Microbiol* **1970**, *63*, 41-48.

(34) Banerjee, A.; Dubnau, E.; Quemard, A.; Balasubramanian, V.; Um, K. S. et al. inhA, a gene encoding a target for isoniazid and ethionamide in Mycobacterium tuberculosis. *Science* **1994**, *263*, 227-230.

(35) Mdluli, K.; Slayden, R. A.; Zhu, Y.; Ramaswamy, S.; Pan, X. et al. Inhibition of a Mycobacterium tuberculosis beta-ketoacyl ACP synthase by isoniazid. *Science* **1998**, *280*, 1607-1610.

(36) Argyrou, A.; Vetting, M. W.; Aladegbami, B.; Blanchard, J. S. Mycobacterium tuberculosis dihydrofolate reductase is a target for isoniazid. *Nat Struct Mol Biol* **2006**, *13*, 408-413.

(37) Rozwarski, D. A.; Grant, G. A.; Barton, D. H.; Jacobs, W. R., Jr.; Sacchettini, J. C. Modification of the NADH of the isoniazid target (InhA) from Mycobacterium tuberculosis. *Science* **1998**, *279*, 98-102.

(38) Musser, J. M.; Kapur, V.; Williams, D. L.; Kreiswirth, B. N.; van Soolingen, D. et al. Characterization of the catalase-peroxidase gene (katG) and inhA locus in isoniazid-resistant and -susceptible strains of Mycobacterium tuberculosis by automated DNA sequencing: restricted array of mutations associated with drug resistance. *J Infect Dis* **1996**, *173*, 196-202.

(39) Heifets, L. B. Antimycobacterial drugs. *Semin Respir Infect* **1994**, *9*, 84-103.

(40) Butler, W. R.; Kilburn, J. O. Susceptibility of Mycobacterium tuberculosis to pyrazinamide and its relationship to pyrazinamidase activity. *Antimicrob Agents Chemother* **1983**, *24*, 600-601.

(41) Miller, M. A.; Thibert, L.; Desjardins, F.; Siddiqi, S. H.; Dascal, A. Testing of susceptibility of Mycobacterium tuberculosis to pyrazinamide: comparison of Bactec method with pyrazinamidase assay. *J Clin Microbiol* **1995**, *33*, 2468-2470.

(42) Konno, K.; Feldmann, F. M.; McDermott, W. Pyrazinamide susceptibility and amidase activity of tubercle bacilli. *Am Rev Respir Dis* **1967**, *95*, 461-469.

(43) Noto, T.; Miyakawa, S.; Oishi, H.; Endo, H.; Okazaki, H. Thiolactomycin, a new antibiotic. III. In vitro antibacterial activity. *J Antibiot (Tokyo)* **1982**, *35*, 401-410.

(44) Stover, C. K.; Warrener, P.; VanDevanter, D. R.; Sherman, D. R.; Arain, T. M. et al. A small-molecule nitroimidazopyran drug candidate for the treatment of tuberculosis. *Nature* **2000**, *405*, 962-966.

(45) Manjunatha, U. H.; Boshoff, H.; Dowd, C. S.; Zhang, L.; Albert, T. J. et al. Identification of a nitroimidazo-oxazine-specific protein involved in PA-824 resistance in Mycobacterium tuberculosis. *Proc Natl Acad Sci U S A* **2006**, *103*, 431-436.

(46) Hayashi, T.; Yamamoto, O.; Sasaki, H.; Okazaki, H.; Kawaguchi, A. Inhibition of fatty acid synthesis by the antibiotic thiolactomycin. *J Antibiot (Tokyo)* **1984**, *37*, 1456-1461.

(47) Miyakawa, S.; Suzuki, K.; Noto, T.; Harada, Y.; Okazaki, H. Thiolactomycin, a new antibiotic. IV. Biological properties and chemotherapeutic activity in mice. *J Antibiot (Tokyo)* **1982**, *35*, 411-419.

(48) Sasaki, H.; Oishi, H.; Hayashi, T.; Matsuura, I.; Ando, K. et al. Thiolactomycin, a new antibiotic. II. Structure elucidation. *J Antibiot (Tokyo)* **1982**, *35*, 396-400.

(49) Slayden, R. A.; Lee, R. E.; Armour, J. W.; Cooper, A. M.; Orme, I. M. et al. Antimycobacterial action of thiolactomycin: an inhibitor of fatty acid and mycolic acid synthesis. *Antimicrob Agents Chemother* **1996**, *40*, 2813-2819.

(50) Kremer, L.; Douglas, J. D.; Baulard, A. R.; Morehouse, C.; Guy, M. R. et al. Thiolactomycin and related analogues as novel anti-mycobacterial agents targeting KasA and KasB condensing enzymes in Mycobacterium tuberculosis. *J Biol Chem* **2000**, *275*, 16857-16864.

(51) Douglas, J. D.; Senior, S. J.; Morehouse, C.; Phetsukiri, B.; Campbell, I. B. et al. Analogues of thiolactomycin: potential drugs with enhanced anti-mycobacterial activity. *Microbiology* **2002**, *148*, 3101-3109.

(52) Kim, P.; Zhang, Y. M.; Shenoy, G.; Nguyen, Q. A.; Boshoff, H. I. et al. Structure-activity relationships at the 5-position of thiolactomycin: an intact (5R)-isoprene unit is required for activity against the condensing enzymes from Mycobacterium tuberculosis and Escherichia coli. *J Med Chem* **2006**, *49*, 159-171.

(53) Senior, S. J.; Illarionov, P. A.; Gurcha, S. S.; Campbell, I. B.; Schaeffer, M. L. et al. Biphenyl-based analogues of thiolactomycin, active against Mycobacterium tuberculosis mtFabH fatty acid condensing enzyme. *Bioorg Med Chem Lett* **2003**, *13*, 3685-3688.

(54) Senior, S. J.; Illarionov, P. A.; Gurcha, S. S.; Campbell, I. B.; Schaeffer, M. L. et al. Acetylene-based analogues of thiolactomycin, active against Mycobacterium tuberculosis mtFabH fatty acid condensing enzyme. *Bioorg Med Chem Lett* **2004**, *14*, 373-376.

(55) Han, L.; Lobo, S.; Reynolds, K. A. Characterization of beta-ketoacyl-acyl carrier protein synthase III from Streptomyces glaucescens and its role in initiation of fatty acid biosynthesis. *J Bacteriol* **1998**, *180*, 4481-4486.

(56) Jackowski, S.; Rock, C. O. Acetoacetyl-acyl carrier protein synthase, a potential regulator of fatty acid biosynthesis in bacteria. *J Biol Chem* **1987**, *262*, 7927-7931.

(57) Brown, A. K.; Sridharan, S.; Kremer, L.; Lindenberg, S.; Dover, L. G. et al. Probing the mechanism of the Mycobacterium tuberculosis beta-ketoacyl-acyl carrier protein synthase III mtFabH: factors influencing catalysis and substrate specificity. *J Biol Chem* **2005**, *280*, 32539-32547.

(58) Nie, Z.; Perretta, C.; Lu, J.; Su, Y.; Margosiak, S. et al. Structure-based design, synthesis, and study of potent inhibitors of beta-ketoacyl-acyl carrier protein synthase III as potential antimicrobial agents. *J Med Chem* **2005**, *48*, 1596-1609.

(59) Tsay, J. T.; Oh, W.; Larson, T. J.; Jackowski, S.; Rock, C. O. Isolation and characterization of the beta-ketoacyl-acyl carrier protein synthase III gene (fabH) from Escherichia coli K-12. *J Biol Chem* **1992**, *267*, 6807-6814.

(60) Barron, E. J., and Mooney, L.A. Determination of Acyl-Thiolesters by Gas-Liquid Chromatography of Their Sodium Borohydride Reduction Products. *Anal. Chem.* **1968**, *40*, 1742--1744.

(61) Garwin, J. L.; Klages, A. L.; Cronan, J. E., Jr. Structural, enzymatic, and genetic studies of beta-ketoacyl-acyl carrier protein synthases I and II of Escherichia coli. *J Biol Chem* **1980**, *255*, 11949-11956.

(62) Davies, C.; Heath, R. J.; White, S. W.; Rock, C. O. The 1.8 A crystal structure and active-site architecture of beta-ketoacyl-acyl carrier protein synthase III (FabH) from escherichia coli. *Structure* **2000**, *8*, 185-195.

(63) Qiu, X.; Janson, C. A.; Smith, W. W.; Head, M.; Lonsdale, J. et al. Refined structures of beta-ketoacyl-acyl carrier protein synthase III. *J Mol Biol* **2001**, *307*, 341-356.

(64) Mathieu, M.; Zeelen, J. P.; Pauptit, R. A.; Erdmann, R.; Kunau, W. H. et al. The 2.8 A crystal structure of peroxisomal 3-ketoacyl-CoA thiolase of Saccharomyces cerevisiae: a five-layered alpha beta alpha beta alpha structure constructed from two core domains of identical topology. *Structure* **1994**, *2*, 797-808.

(65) Olsen, J. G.; Kadziola, A.; von Wettstein-Knowles, P.; Siggaard-Andersen, M.; Larsen, S. Structures of beta-ketoacyl-acyl carrier protein synthase I complexed with fatty acids elucidate its catalytic machinery. *Structure* **2001**, *9*, 233-243.

(66) Huang, W.; Jia, J.; Edwards, P.; Dehesh, K.; Schneider, G. et al. Crystal structure of beta-ketoacyl-acyl carrier protein synthase II from E.coli reveals the molecular architecture of condensing enzymes. *Embo J* **1998**, *17*, 1183-1191.

(67) Moche, M.; Dehesh, K.; Edwards, P.; Lindqvist, Y. The crystal structure of beta-ketoacyl-acyl carrier protein synthase II from Synechocystis sp. at 1.54 A resolution and its relationship to other condensing enzymes. *J Mol Biol* **2001**, *305*, 491-503.

(68) Ferrer, J. L.; Jez, J. M.; Bowman, M. E.; Dixon, R. A.; Noel, J. P. Structure of chalcone synthase and the molecular basis of plant polyketide biosynthesis. *Nat Struct Biol* **1999**, *6*, 775-784.

(69) Jez, J. M.; Austin, M. B.; Ferrer, J.; Bowman, M. E.; Schroder, J. et al. Structural control of polyketide formation in plant-specific polyketide synthases. *Chem Biol* **2000**, *7*, 919-930.

(70) Pan, H.; Tsai, S.; Meadows, E. S.; Miercke, L. J.; Keatinge-Clay, A. T. et al. Crystal structure of the priming beta-ketosynthase from the R1128 polyketide biosynthetic pathway. *Structure* **2002**, *10*, 1559-1568.

(71) Brunger, A. T.; Adams, P. D.; Clore, G. M.; DeLano, W. L.; Gros, P. et al. Crystallography & NMR system: A new software suite for macromolecular structure determination. *Acta Crystallogr D Biol Crystallogr* **1998**, *54*, 905-921.

(72) Murshudov, G. N.; Vagin, A. A.; Dodson, E. J. Refinement of macromolecular structures by the maximum-likelihood method. *Acta Crystallogr D Biol Crystallogr* **1997**, *53*, 240-255.

(73) Jones, T. A.; Zou, J. Y.; Cowan, S. W.; Kjeldgaard, M. Improved methods for building protein models in electron density maps and the location of errors in these models. *Acta Crystallogr A* **1991**, *47 (Pt 2)*, 110-119.

(74) McRee, D. E. XtalView/Xfit--A versatile program for manipulating atomic coordinates and electron density. *J Struct Biol* **1999**, *125*, 156-165.

(75) Hooft, R. W.; Vriend, G.; Sander, C.; Abola, E. E. Errors in protein structures. *Nature* **1996**, *381*, 272.

(76) Kleywegt, G. J.; Jones, T. A. Efficient rebuilding of protein structures. *Acta Crystallogr D Biol Crystallogr* **1996**, *52*, 829-832.

(77) Word, J. M.; Lovell, S. C.; LaBean, T. H.; Taylor, H. C.; Zalis, M. E. et al. Visualizing and quantifying molecular goodness-of-fit: small-probe contact dots with explicit hydrogen atoms. *J Mol Biol* **1999**, *285*, 1711-1733.

(78) Vaguine, A. A.; Richelle, J.; Wodak, S. J. SFCHECK: a unified set of procedures for evaluating the quality of macromolecular structure-factor data and their agreement with the atomic model. *Acta Crystallogr D Biol Crystallogr* **1999**, *55*, 191-205.

(79) Price, A. C.; Rock, C. O.; White, S. W. The 1.3-Angstrom-resolution crystal structure of beta-ketoacyl-acyl carrier protein synthase II from Streptococcus pneumoniae. *J Bacteriol* **2003**, *185*, 4136-4143.

(80) Kellogg, G. E.; Semus, S. F.; Abraham, D. J. HINT: a new method of empirical hydrophobic field calculation for CoMFA. *J Comput Aided Mol Des* **1991**, *5*, 545-552.

(81) He, X.; Reynolds, K. A. Purification, characterization, and identification of novel inhibitors of the beta-ketoacyl-acyl carrier protein synthase III (FabH) from Staphylococcus aureus. *Antimicrob Agents Chemother* **2002**, *46*, 1310-1318.

(82) Qiu, X.; Janson, C. A.; Konstantinidis, A. K.; Nwagwu, S.; Silverman, C. et al. Crystal structure of beta-ketoacyl-acyl carrier protein synthase III. A key condensing enzyme in bacterial fatty acid biosynthesis. *J Biol Chem* **1999**, *274*, 36465-36471.

(83) Alhamadsheh, M. M.; Musayev, F.; Komissarov, A. A.; Sachdeva, S.; Wright, H. T. et al. Alkyl-CoA disulfides as inhibitors and mechanistic probes for FabH enzymes. *Chem Biol* **2007**, *14*, 513-524.

(84) Emsley, P.; Cowtan, K. Coot: model-building tools for molecular graphics. *Acta Crystallogr D Biol Crystallogr* **2004**, *60*, 2126-2132.

(85) Murshudov, G. N.; Vagin, A. A.; Lebedev, A.; Wilson, K. S.; Dodson, E. J. Efficient anisotropic refinement of macromolecular structures using FFT. *Acta Crystallogr D Biol Crystallogr* **1999**, *55*, 247-255.

(86) Schuttelkopf, A. W.; van Aalten, D. M. PRODRG: a tool for high-throughput crystallography of protein-ligand complexes. *Acta Crystallogr D Biol Crystallogr* **2004**, *60*, 1355-1363.

(87) Lu, Y. J.; Zhang, Y. M.; Rock, C. O. Product diversity and regulation of type II fatty acid synthases. *Biochem Cell Biol* **2004**, *82*, 145-155.

(88) Choi, K. H.; Heath, R. J.; Rock, C. O. beta-ketoacyl-acyl carrier protein synthase III (FabH) is a determining factor in branched-chain fatty acid biosynthesis. *J Bacteriol* **2000**, *182*, 365-370.

(89) Cohen-Gonsaud, M.; Ducasse, S.; Hoh, F.; Zerbib, D.; Labesse, G. et al. Crystal structure of MabA from Mycobacterium tuberculosis, a reductase involved in long-chain fatty acid biosynthesis. *J Mol Biol* **2002**, *320*, 249-261.

(90) Cohen-Gonsaud, M.; Ducasse-Cabanot, S.; Quemard, A.; Labesse, G. Ligand-induced fit in mycobacterial MabA: the sequence-specific C-terminus locks the conformational change. *Proteins* **2005**, *60*, 392-400.

(91) Sridharan, S.; Wang, L.; Brown, A. K.; Dover, L. G.; Kremer, L. et al. X-ray crystal structure of Mycobacterium tuberculosis beta-ketoacyl acyl carrier protein synthase II (mtKasB). *J Mol Biol* **2007**, *366*, 469-480.

(92) Wong, H. C.; Liu, G.; Zhang, Y. M.; Rock, C. O.; Zheng, J. The solution structure of acyl carrier protein from Mycobacterium tuberculosis. *J Biol Chem* **2002**, *277*, 15874-15880.

(93) Rozwarski, D. A.; Vilcheze, C.; Sugantino, M.; Bittman, R.; Sacchettini, J. C. Crystal structure of the Mycobacterium tuberculosis enoyl-ACP reductase, InhA, in complex with NAD+ and a C16 fatty acyl substrate. *J Biol Chem* **1999**, *274*, 15582-15589.

(94) Veyron-Churlet, R.; Bigot, S.; Guerrini, O.; Verdoux, S.; Malaga, W. et al. The biosynthesis of mycolic acids in Mycobacterium tuberculosis relies on multiple specialized elongation complexes interconnected by specific protein-protein interactions. *J Mol Biol* **2005**, *353*, 847-858.

(95) Veyron-Churlet, R.; Guerrini, O.; Mourey, L.; Daffe, M.; Zerbib, D. Protein-protein interactions within the Fatty Acid Synthase-II system of Mycobacterium tuberculosis are essential for mycobacterial viability. *Mol Microbiol* **2004**, *54*, 1161-1172.

(96) Jenni, S.; Leibundgut, M.; Boehringer, D.; Frick, C.; Mikolasek, B. et al. Structure of fungal fatty acid synthase and implications for iterative substrate shuttling. *Science* **2007**, *316*, 254-261.

(97) Leibundgut, M.; Jenni, S.; Frick, C.; Ban, N. Structural basis for substrate delivery by acyl carrier protein in the yeast fatty acid synthase. *Science* **2007**, *316*, 288-290.

(98) Lomakin, I. B.; Xiong, Y.; Steitz, T. A. The crystal structure of yeast fatty acid synthase, a cellular machine with eight active sites working together. *Cell* **2007**, *129*, 319-332.

(99) Roujeinikova, A.; Baldock, C.; Simon, W. J.; Gilroy, J.; Baker, P. J. et al. X-ray crystallographic studies on butyryl-ACP reveal flexibility of the structure around a putative acyl chain binding site. *Structure* **2002**, *10*, 825-835.

(100) Musayev, F.; Sachdeva, S.; Scarsdale, J. N.; Reynolds, K. A.; Wright, H. T. Crystal structure of a substrate complex of Mycobacterium tuberculosis beta-ketoacyl-acyl carrier protein synthase III (FabH) with lauroyl-coenzyme A. *J Mol Biol* **2005**, *346*, 1313-1321.

(101) Khandekar, S. S.; Gentry, D. R.; Van Aller, G. S.; Warren, P.; Xiang, H. et al. Identification, substrate specificity, and inhibition of the Streptococcus pneumoniae beta-ketoacyl-acyl carrier protein synthase III (FabH). *J Biol Chem* **2001**, *276*, 30024-30030.

(102) Daines, R. A.; Pendrak, I.; Sham, K.; Van Aller, G. S.; Konstantinidis, A. K. et al. First X-ray cocrystal structure of a bacterial FabH condensing enzyme and a small molecule inhibitor achieved using rational design and homology modeling. *J Med Chem* **2003**, *46*, 5-8.

(103) He, X.; Reeve, A. M.; Desai, U. R.; Kellogg, G. E.; Reynolds, K. A. 1,2-dithiole-3-ones as potent inhibitors of the bacterial 3-ketoacyl acyl carrier protein synthase III (FabH). *Antimicrob Agents Chemother* **2004**, *48*, 3093-3102.

(104) Alhamadsheh, M. M.; Waters, N. C.; Huddler, D. P.; Kreishman-Deitrick, M.; Florova, G. et al. Synthesis and biological evaluation of thiazolidine-2-one 1,1-dioxide as inhibitors of Escherichia coli beta-ketoacyl-ACP-synthase III (FabH). *Bioorg Med Chem Lett* **2007**, *17*, 879-883.

Appendix 1

A.1 Results

A.1.1 Characterization of the E-I complex:

A.1.1.1 Probing the nature of association between mtFabH and Inhibitors 1-3:

We utilized a simple reversibility test to investigate the nature of association (covalent vs. non-covalent) between mtFabH and the inhibitors **1-3** (Figure X1). The enzyme was pre-incubated with excess of inhibitor at 37 ˚C for 60 minutes and the activity of this inhibited enzyme is checked using the standard assay to confirm the formation of E-I complex (> 95% inhibition; Figure X1 - "E~I complex" column). The control experiment is set up with untreated mtFabH under similar conditions. The

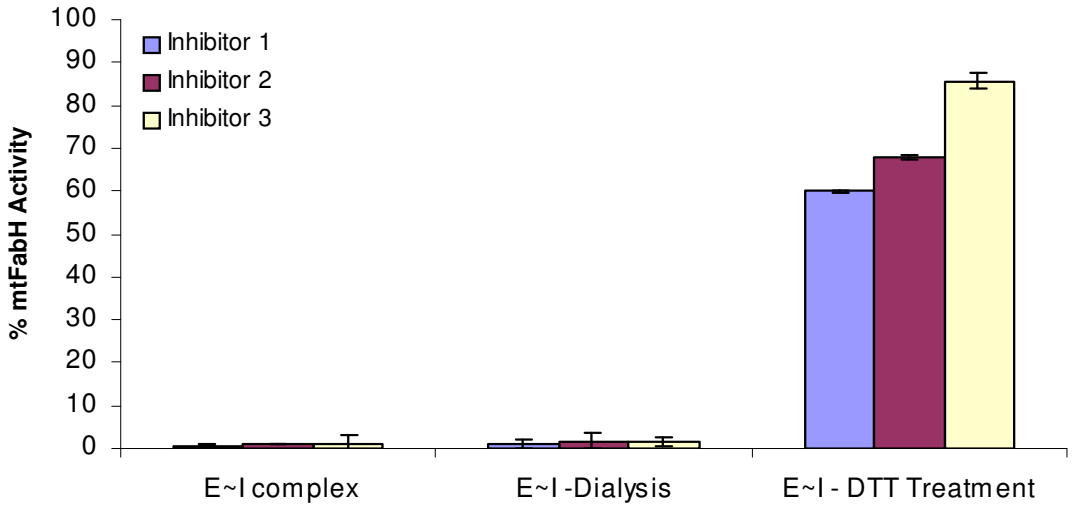

Figure X1: Probing the nature of association between mtFabH and I - The effect of dialysis and DTT treatment on condensation activity of mtFabH treated with inhibitor 1 (blue bars), 2 (maroon bars) or 3 (beige bars).

complex is then subjected to multiple dilution-concentration steps (a 1000 fold dilution factor is achieved as described in methods) to remove any excess or readily dissociable inhibitor from the enzyme and the residual enzymatic activity is indicative of reversibility of E-I complex. A non-covalent reversible E-I complex under these conditions would dissociate easily and the resultant freed enzyme would show restoration of activity while on the other hand, a covalently bound mtFabH in E~I complex would still show inhibited enzymatic activity. The experimental data showed that inhibitor treated mtFabH on dilution shows 1-2 % enzymatic activity (compared to Control; Figure above – "E~I – Dialysis" column) with all three inhibitors and thus suggested a non-reversible complex formation. This complex when treated with excess DTT (and subsequently dialyzed) resulted in restoration of 60-90% of activity compared to mtFabH control (Figure above - "E~I - DTT treatment" column; DTT treatment of mtFabH~Inhibitor **1, 2** and **3** showed 59.9 %, 67.95 % and 85.65 % restoration of activity respectively) suggesting the formation of a disulfide linkage between mtFabH and the inhibitor series. Mass spectrometry and X-ray crystallographic studies as discussed in chapter 5 confirmed the formation of this disulfide linkage between the mtFabH cysteines and the inhibitor and also showed the exact nature of the complex formed.

A.1.1.2 Identification of the site of modification:

To investigate the precise site of modification, we performed limited proteolysis of mtFabH - Inhibitor complex by trypsin followed by Reverse Phase-HPLC (RP-HPLC) fractionation of the resultant peptides to look for any modified peptide peaks. The control experiment consisted of untreated mtFabH digested in parallel under identical set of conditions. The modification of mtFabH peptide with the inhibitor would most likely alter its hydrophobicity and thus an appearance of new peptide peak or movement of existing one on the C_{18} matrix could implicate the modified peptide fragment. This peptide fragment could then be characterized to conclusively identify the nature and site of the modification.

A.1.1.2.1 Standardization of Digestion conditions:

We first started with the optimization of various digestion and HPLC conditions to ensure sensitivity and reproducibility in each run. The UV traces of undigested WT mtFabH and inhibitors (Control reactions) are shown in Figure X2. It was evident from the HPLC traces that the inhibitors bound tenaciously to the C_{18} column matrix and eluted at 100 % acetonitrile concentration (Figure X2b and X2c). The maximum concentration of acetonitrile required to elute all peptide fragments was found to be ~ 60% and thus after a few HPLC runs 100 % acetonitrile was used to wash the column to ensure reproducibility. Other variables such as the amount of trypsin, time of digestion and the digestion conditions were also optimized and the results are shown in Figures X3,

X4 and X5. Based on the peptide profiles (HPLC traces), the digestion reaction was set to run under native conditions with 1:20 w/w of mtFabH / trypsin for 11 hrs as described in materials and methods. The digestion reaction was not run for extended period of time to preserve any labile association between mtFabH and inhibitors. Also, Dehydroascorbic acid was added to maintain the oxidizing conditions to maintain disulfide bonds.

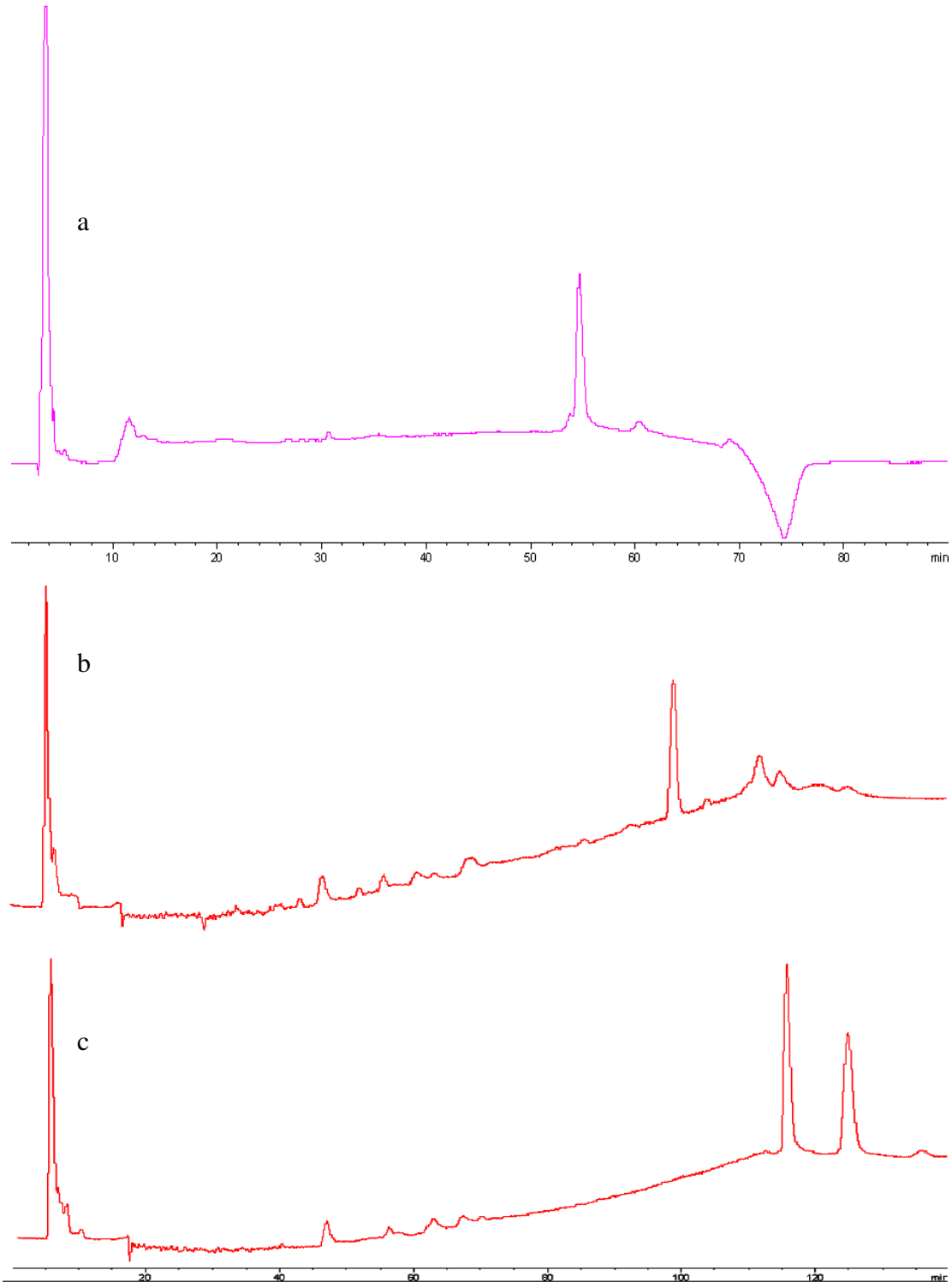

Figure X2: Standardization of digestion conditions – Control reactions- RP-HPLC traces of a) undigested WT mtFabH, b) WT mtFabH + Inhibitor **1** and c) WT mtFabH + Inhibitor **2**. The conditions used are described in the methods section. The UV detection wavelength is set at 204 nm.

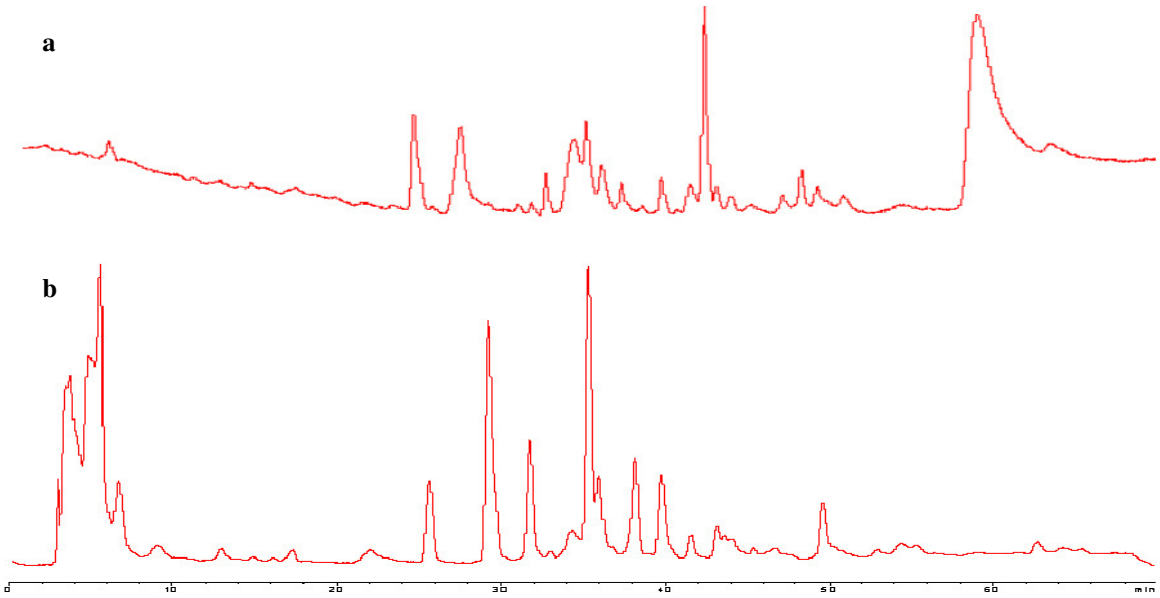

Figure X3: Standardization of digestion conditions- trypsin / mtFabH ratio: RP-HPLC analysis of the peptide mixture obtained from trypsinolysis of WT mtFabH performed at a) 1 : 60 trypsin / mtFabH ratio and b) 1 : 20 trypsin / mtFabH ratio.

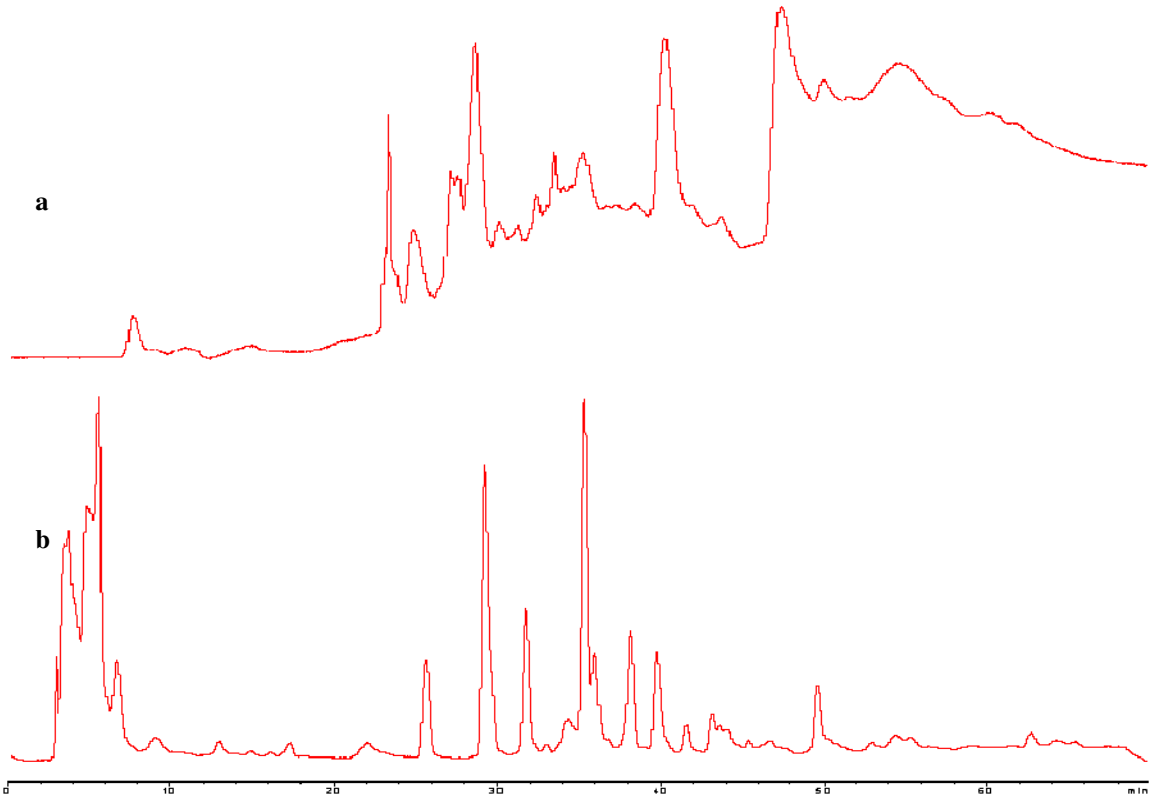

Figure X4: Standardization of digestion conditions- Native vs Denatured: RP-HPLC analysis of peptide mixture obtained from trypsinolysis of WT mtFabH performed under a) Denaturing conditions with guanidium chloride and b) native conditions.

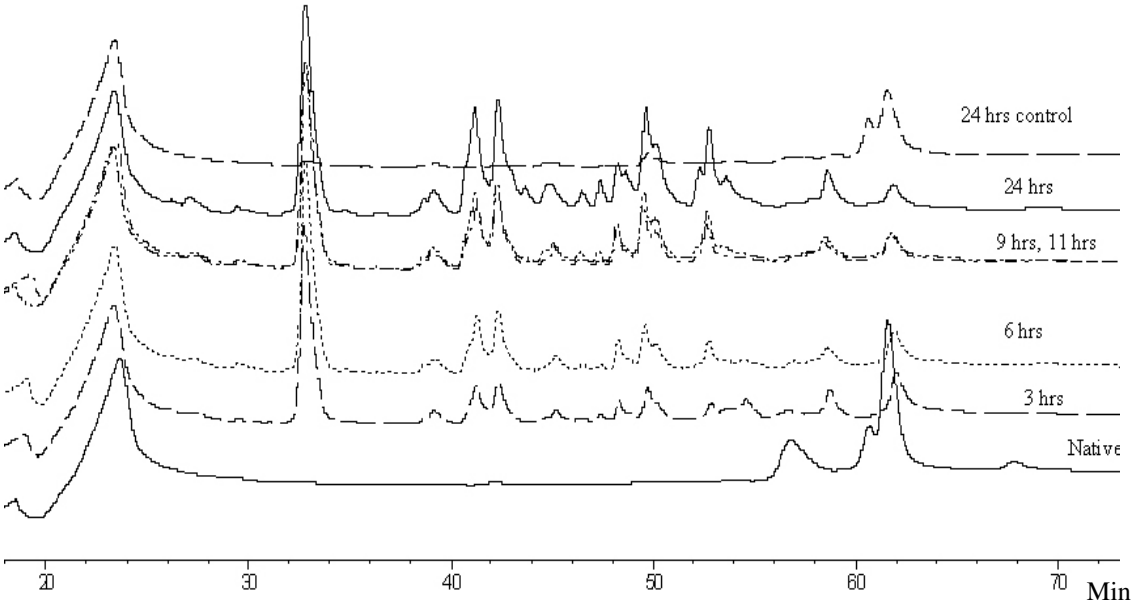

Figure X5: Standardization of digestion conditions -time of digestion: RP-HPLC analysis of peptide mixture obtained from trypsinolysis of WT mtFabH for various digestion times.

A.1.1.2.2 Tryptic digest analysis of the mtFabH- 1 complex:

The comparison of the HPLC profile of trypsin digested mtFabH- **1** complex (test) and untreated mtFabH (control) showed the appearance of two distinct new peaks at 34 and 41 minutes at 257 nm (Figure X6). To probe the reducibility of these new peaks (as suggested by the initial reversibility study - Figure X1) we incubated the control (untreated mtFabH – trypsin digested) and test (mtFabH-**1** complex – trypsin digested) with DTT for 30 minutes and performed HPLC analysis on the resultant reduced peptide mixture. As evident from Figure X7, the peptide peak at 34 minutes disappeared on treatment with DTT suggesting the presence of a reducible disulfide bond while the second peak at 41 minutes stayed unchanged.

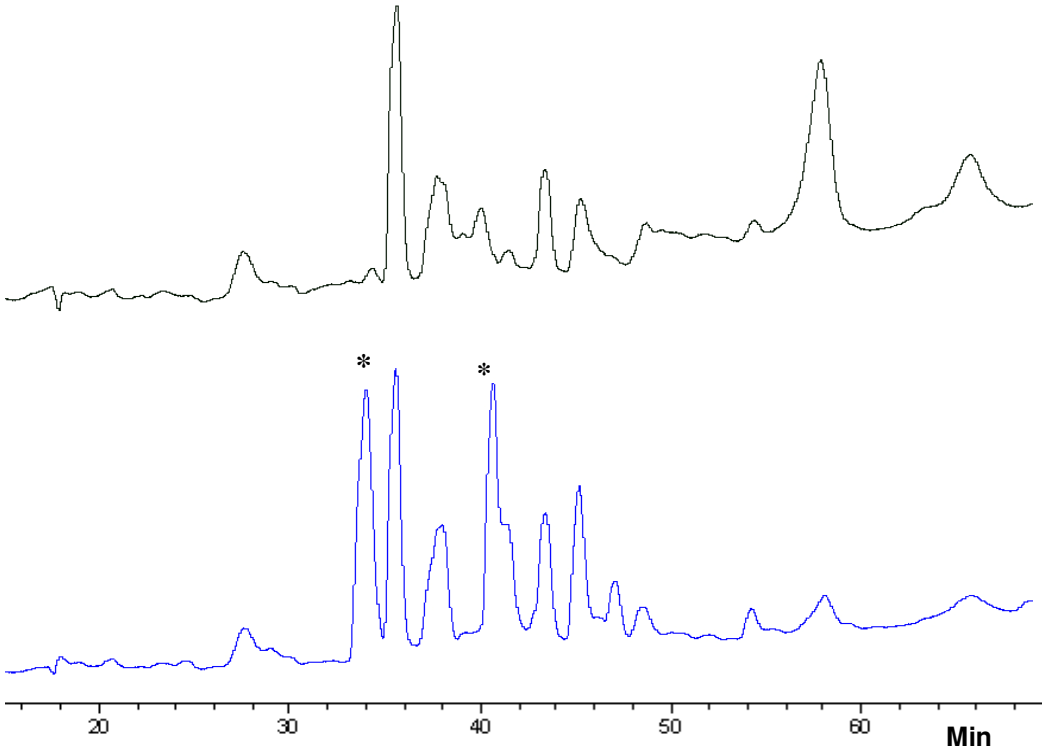

Figure X6: HPLC analysis of tryptic peptides of mtFabH-Inhibitor 1 complex - The extended HPLC traces of peptide mixture obtained from trypsinolysis of - a) unmodified mtFabH - λ 204 nm b) mtFabH-inhibitor **1** complex - λ 204 nm c) unmodified mtFabH - λ 257 nm d) mtFabH-Inhibitor **1** complex - λ 257 nm. The new peaks are indicated by asterisks.

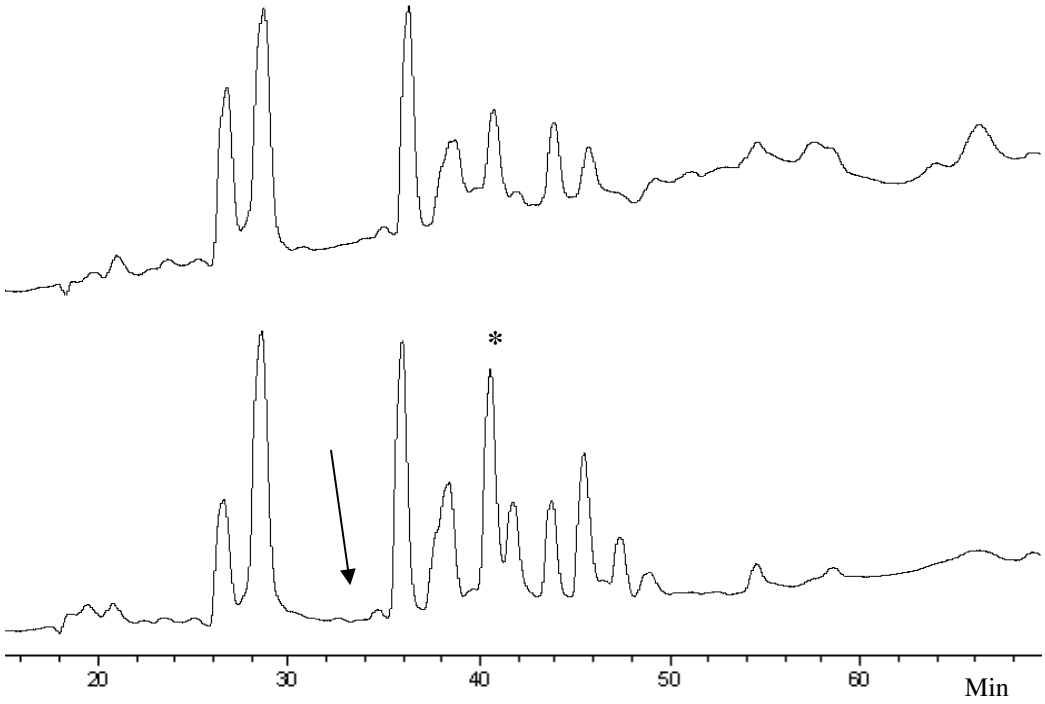

Figure X7: A Test of reducibility of new peaks from mtFabH-1 complex – Untreated and Inhibitor **1** treated mtFabH peptides were incubated with DTT and subsequently analyzed by HPLC at 257 nm. Figure a) DTT reduced - untreated mtFabH tryptic peptides and b) DTT reduced – inhibitor **1** treated mtFabH tryptic peptides. The reducible peak is marked by an arrow and the non-reducible peak is marked by an *.

A.1.1.2.2.1 Primary sequence of the modified peptide and the residue of attachment:

To further investigate the identity of these new peaks, we purified them on C_{18} matrix and subjected them to Mass Spectrometric analysis in the Matrix Assisted Laser Desorption Ionization –Time of Flight (MALDI-TOF) mode. The masses (m/z) of the two peaks were determined to be 2599 and 1147 Da (34 and 41 minutes respectively) as shown in Figures X8b and X8c. The unique mass of the first peak (m/z 2599 Da) at 34 minutes corresponded very well with the mtFabH peptide Val16-Arg36 of mass 2523 Da (envisioned by in-silico tryptic digestion of mtFabH) modified by fragment A (mass 77 Da) of inhibitor **1**. To test this hypothesis, we utilized the technique of "product ion analysis" in MALDI/TOF/TOF mode to analyze the two peptides. Only identical peptides give exactly the same "fingerprint ions" in this technique in mass spectrometric analyses. In this technique, the peptide in question is allowed to collide with neutral gas molecules (often Helium, nitrogen or argon) or air, which result in fragmentation of the peptide into smaller ions. The key sequence-specific fragment ions seen frequently are the "y-type" (formed when the charge is retained at C-terminus of fragment ion) and "b-type" ions (when charge is retained at N –terminus) which can be compared to any peptide to confirm their identity. Moreover, a modification at any particular residue will alter the sequence specific pattern of key ions thus potentially revealing vital information about the modification.

In order to obtain the proposed (unmodified) peptide fragment Val16-Arg36 of theoretical mass 2523 Da, we digested the untreated mtFabH with trypsin and performed direct MALDI/TOF analysis on the entire peptide mixture to search for the parent mass (Figure X9). The m/z of 2523 Da is selected and subjected to product ion analysis in MALDI/TOF/TOF mode (Figure X10a). In parallel, the new peak of 2599 Da mass at 34 minutes was subjected to MALDI/TOF/TOF analysis (Figure X10b) and the fragmentation pattern of both peptides was compared. Comparing Figures X10a and X10b, the masses of "y" series ions were found to be exactly the same until ion y13 thus proving that the two peptides at hand were identical. An exact mass differential of 77 Da on ions "y15" (compared to theoretical fragmentation pattern shown in Figure X10) and "y16" (MALDI/TOF/TOF spectral data on both peptides) proved that Cys23 is modified with a 77 Da species. This data clearly identified the peak at 34 minutes in trypsin digested mtFabH- **1** complex is the "V^{16} V T N D E I C^{23} Q H I D S S D E W I Y T R^{36} " peptide modified with fragment A of inhibitor 1 linked with Cys23. Additionally, the reducibility of this peak (as discussed above) also relates well to the proposed disulfide bond formation between the thiolate of Cys23 and fragment A of inhibitor **1**.

The second mass of 1147 Da (peak 2 at 41 minutes in Figure X6) did not correlate with any of the expected masses of the theoretical digested mtFabH peptides. This could be a result of aberrant (star) digestion or auto digestion (by trypsin) and thus was not explored further.

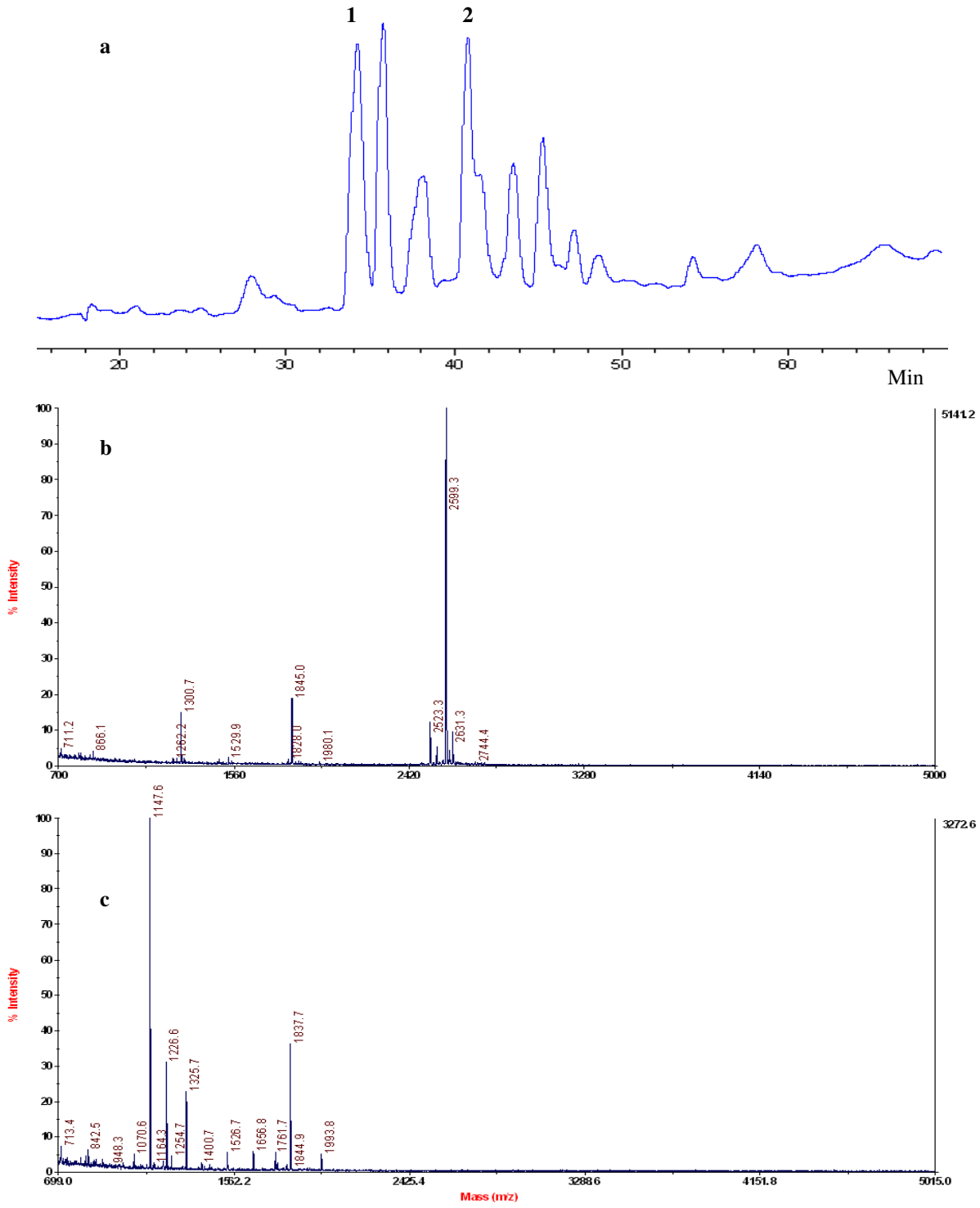

Figure X8: Identification of new peptides observed on trypsinolysis of Inhibitor 1 treated mtFabH. The extended HPLC trace (wavelength 257 nm) of peptide mixture obtained from trypsinolysis of mtFabH -Inhibitor **1** complex (a). The peptides are numbered and the MALDI-MS spectra of peak 1 (b) and peak 2 (c) are shown.

a

T1 G S S H H H H H H S S G L V P R T2 G S H M T E I A T T S G
T3 A R S V G L L S V G A Y R P E R T4 V V T N D E I C Q H I D S
T5 S D E W I Y T R T6 G I K T R R F A A D D E S A A S M A T
T7 E A C R R A L S N A G L S A A D I D G V I V T T N T H F L
T8 Q T P P A A P M V A A S L G A K G I L G F D L S A G C A
T9 G F G Y A L G A A A D M I R G G G A A T M L V V G T E K
T10 L S P T I D M Y D R T11 G N C F I F A D G A A A V V V G E T P
T12 F Q G I G P T V A G S D G E Q A D A I R Q D I D W I T F A
T13 Q N P S G P R P F V R T13 L E G P A V F R T14 W A A F K M G D V
T15 G R R A M D A A G V R P D Q I D V F V P H Q A N S R T16 I N
T17 E L L V K N L Q L R P D A V V A N D I E H T G N T S A A S
I P L A M A E L L T T G A A K P G D L A L L I G Y G A G L
T18 S Y A A Q V V R M P K G *

b

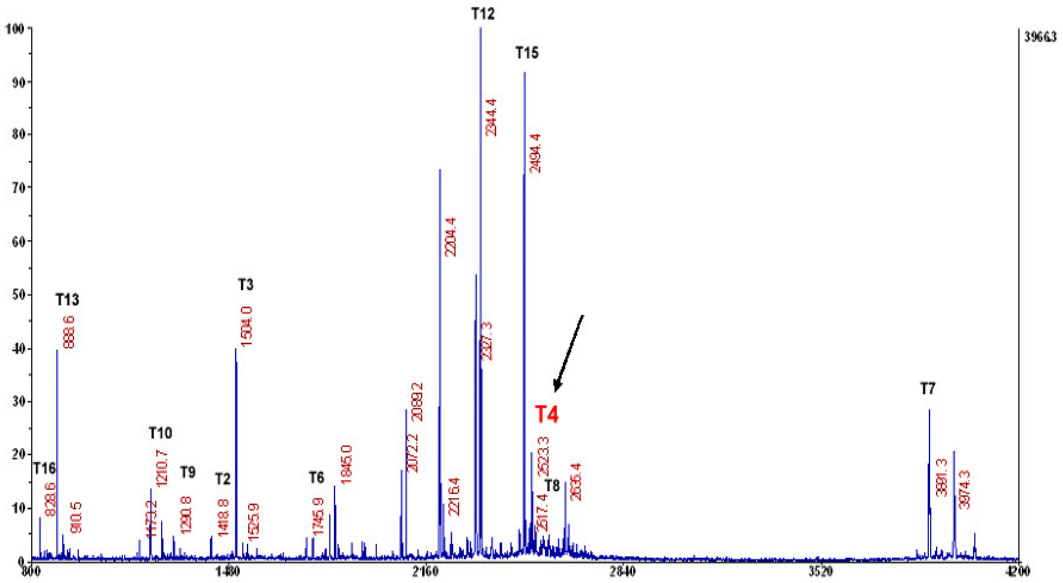

Figure X9: Search for proposed parent peptide Val16-Arg36 containing Cys23 (m/z 2523 Da).

a) Theoretical mtFabH peptides on in-silico digestion with trypsin. The proposed parent peak of m/z 2523 (peptideT4) is underlined in red.

b) Experimental MALDI/TOF mass spectrum of peptide mixture obtained on trypsinolysis of untreated mtFabH. The arrow indicates the proposed parent peptide T4 of correct mass m/z 2523 Da.

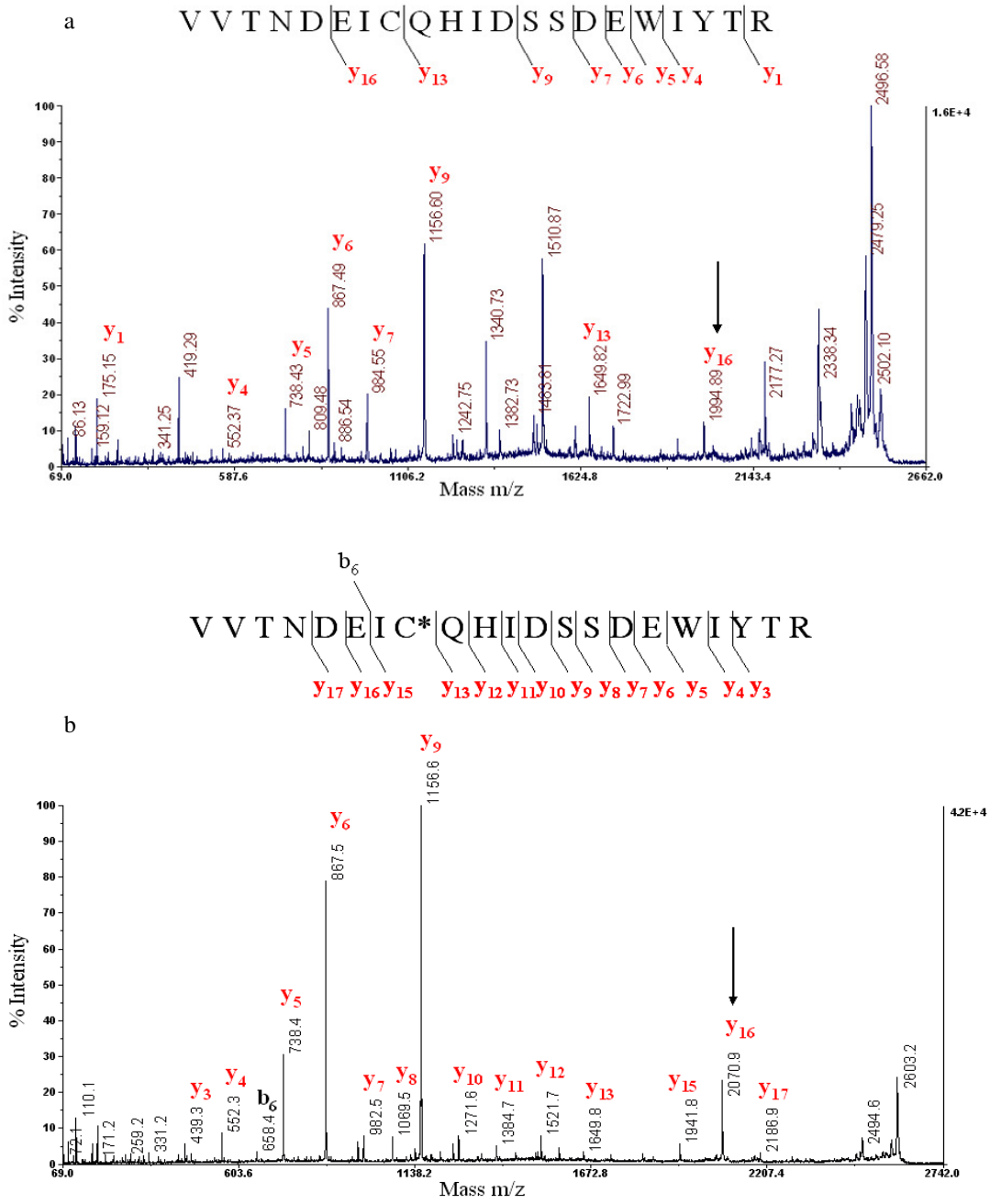

Figure X10: Relationship between peptide T4 of untreated mtFabH and HPLC peak 1 of mtFabH-1 digest: Tandem mass analysis of (a) proposed parent peptide T4 m/z - 2523 and (b) new peptide "1" m/z – 2599 (new peak at 34 minutes in figure 6). The series of y ions as labeled demonstrate that the sequence of the modified peptide is V^{16} V T N D E I C* Q H I D S S D E W I Y T R^{36}) where asterisk denotes the residue modified. The ions y16 show a mass difference of 76.01 Da (2070.9 Da versus 1994.89 Da) corresponding well with addition of fragment A of inhibitor 1.

A.1.1.2.3 Tryptic digest analysis of the mtFabH- 2 complex:

A comparison of HPLC traces of trypsin digested mtFabH- **2** complex with Control (untreated mtFabH) showed the appearance of a new peak at 49 minutes (Figure X11). As outlined above, we probed the reducibility of this new peak by incubating it with DTT for 30 minutes followed by HPLC analysis of the reduced mixture (Figure X12). The disappearance of this "new" peak was consistent with a reducible bond, most likely a disulfide one between a mtFabH peptide and **2**.

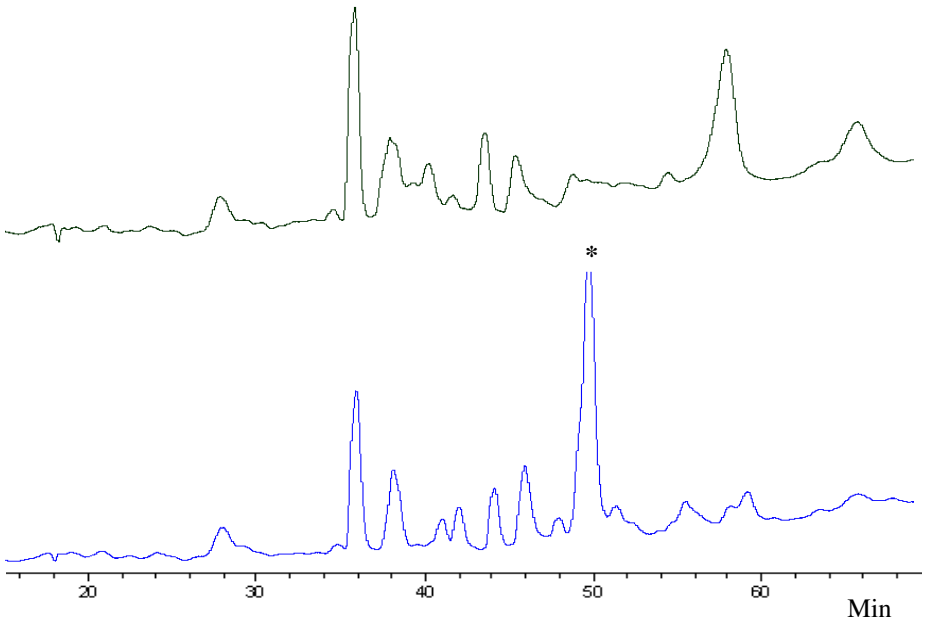

Figure X11: HPLC analysis of mtFabH-Inhibitor 2 tryptic peptides -HPLC fractionation (257 nm wavelength) of the peptide mixture obtained from trypsinolysis of a) untreated mtFabH and b) mtFabH treated with excess of inhibitor **2**. The new peptide is indicated by an asterisk.

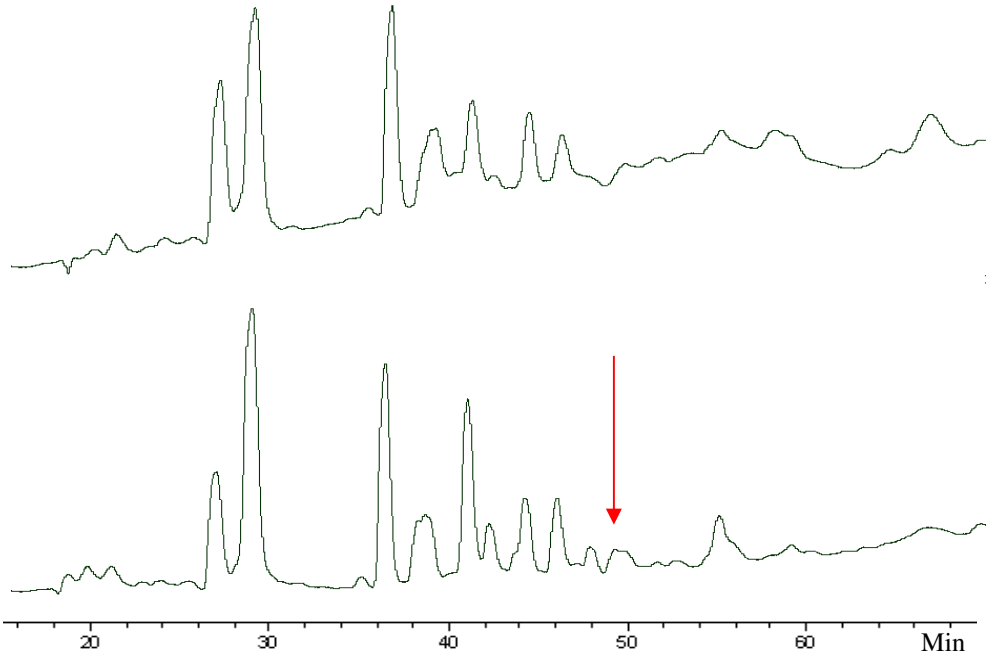

Figure X12: A Test of reducibility of new peaks from mtFabH-2 complex – Untreated and inhibitor **2** treated mtFabH peptides were incubated with DTT and subsequently analyzed by HPLC at 257 nm. Figure a) DTT reduced - untreated mtFabH tryptic peptides and b) DTT reduced – inhibitor 2 treated mtFabH tryptic peptides. The new peak is reducible as marked by an arrow.

To unambiguously identify this new peptide, we purified it and the mass was determined to be 2739.4 Da by MALDI/TOF (Figure X13b). The mass value of 2739 Da corresponded very well with modification of Cys23 containing peptide of mass 2523 Da with fragment A' (theoretical mass 217 Da) of 2 (refer to chapter 5, Figure 30 for fragment A'). Finally, the "product ion analysis technique" on "new" peak of m/z 2739 and proposed parent mass of m/z 2523 revealed the identity of both peptides to be "V^{16} V T N D E I C^{23} Q H I D S S D E W I Y T R^{36}" with fragment A' of 2 covalently linked at Cys23 (Figures X14 a and b).

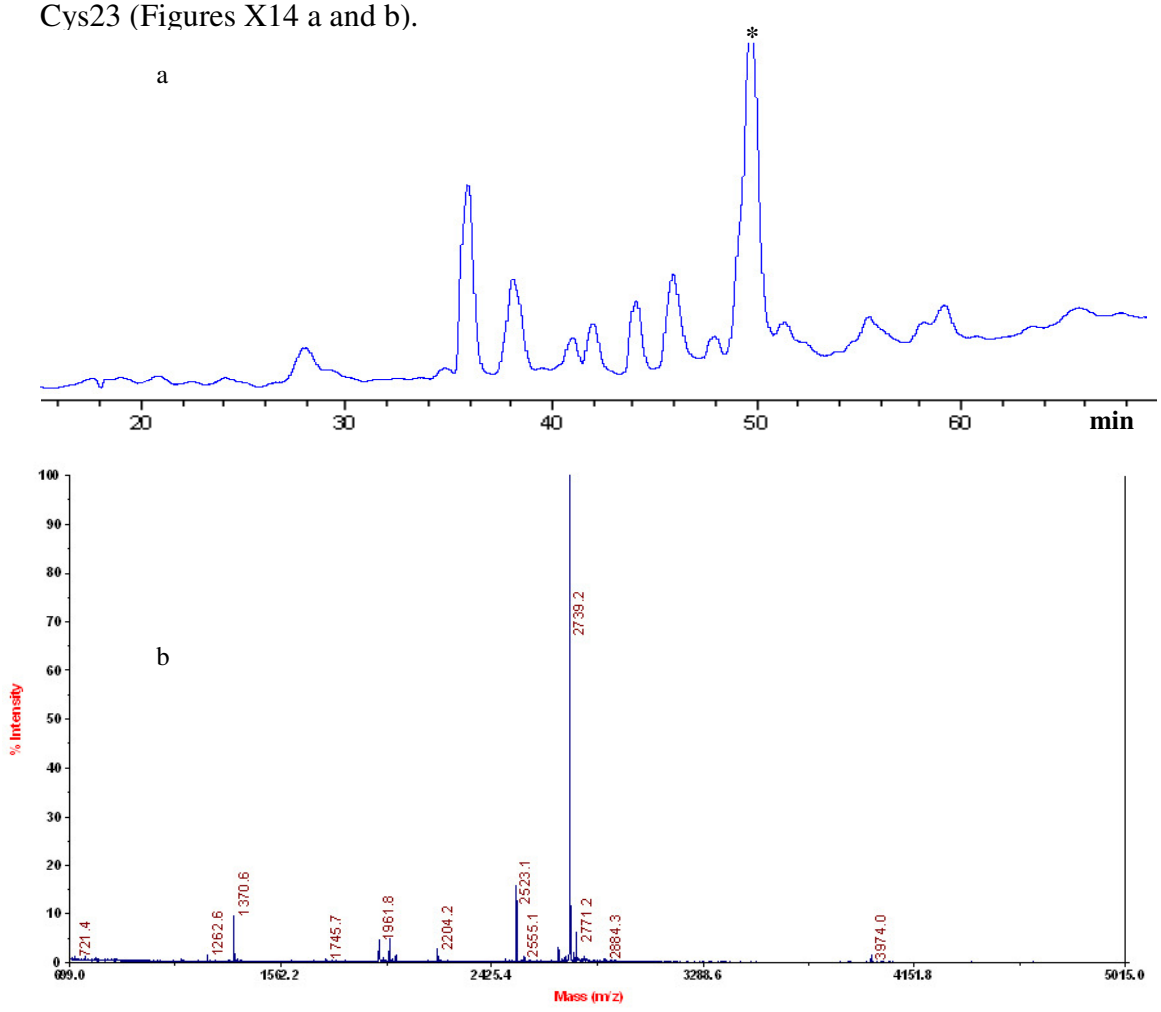

Figure X13: Identification of the new peptide peak observed on trypsinolysis of Inhibitor 2 treated mtFabH. The HPLC traces (wavelength 257 nm) of peptide mixture obtained from trypsinolysis of mtFabH treated with Inhibitor **2** (a). The peaks are assigned by an asterisk and its MALDI-MS spectrum is shown in (b).

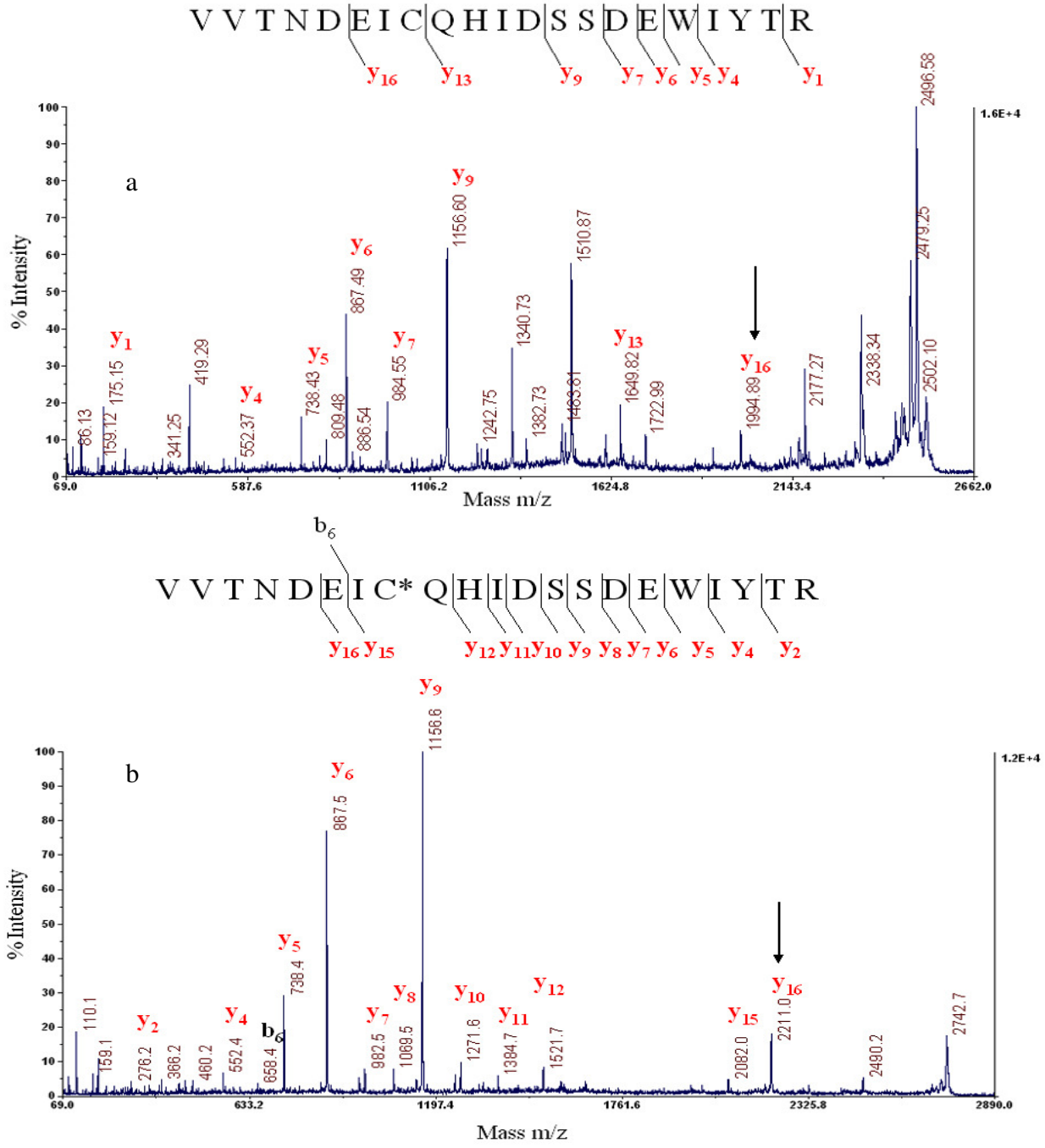

Figure X14: Relationship between peptide T4 of untreated mtFabH and new peak of mtFabH-2 digest: Tandem mass analysis of (a) proposed parent peptide T4 and (b) new peptide peak in figure . The series of y ions as labeled demonstrate that the sequence of the modified peptide is V^{16} V T N D E I C* Q H I D S S D E W I Y T R^{36}) where asterisk denote the residue modified. The ions y16 show a mass difference of 216 Da (2211.0 Da versus 1994.89 Da) corresponding well with addition of fragment A" of inhibitor **2**.

A.2 Method:

A.2.1 Reversibility studies:

Reversibility studies were performed by the standard microcon dilution method. A solution of the mtFabH (100 µL of 2.6-5.2 µM solution in 50 mM sodium phosphate buffer, pH 7) was pre-incubated with inhibitor **1** (1.2 µL of 34 mM solution in MeOH; final inhibitor conc. 400 µM), inhibitor **2** or **3** (2.17 µL of 23 mM solution in MeOH; final inhibitor conc. 500 µM) for 60 min at 37˚ Celsius. Control experiments containing mtFabH enzyme were treated with 2.5 µl of MeOH (no inhibitor) in same manner. Two aliquots from each solution (1 µl each) were withdrawn and the mtFabH activity was determined under standard assay conditions. The remaining enzyme solutions were diluted to 500 µl with sodium phosphate buffer, pH 7.0 and concentrated to 50 µl using 50 kDa molecular weight cutoff Microcon concentrator at 8000 rpm on a benchtop centrifuge. Another aliqout of 450 µl buffer was added and the Microcon step repeated 3 times to obtain the final dilution factor of about 10,000 and enzyme activity was determined. The enzyme solutions were then treated with DTT (20 mM final concentration) for 30 min at room temperature, desalted against buffer solution to remove the excess DTT and the enzyme activity was determined. The enzyme concentration was determined by Bio-Rad protein assay in all aliquots and equal amounts of enzyme were used for all assays.

A.2.2 HPLC analysis of E-I complex:

A solution of 100 µg native WT mtFabH in 50 µl sodium phosphate buffer 50 mM, pH 7.0 was injected onto wide pore 250 X 10 mm C_{18} RP column, pore size 300 A˚, particle size 10 µM and the HPLC gradient was run by increasing the acetonitrile conc. from 0-60 % in 60 minutes at 2 ml/min. For controls, 1 mM solutions of inhibitors **1** or **2** (1.6 µl of 34 mM inhibitor **1** or 2.3 µl of 23 mM inhibitor **2** were added to a final volume of 50 µl sodium phosphate buffer 50 mM, pH 7.0) were injected onto the C_{18} RP-HPLC column and the gradient increase of 1 % acetonitrile per minute was maintained until 100 % acetonitrile (HPLC Buffer B) was achieved and then kept at buffer B for 40 minutes. For the selection of best conditions for further analyses, various digestion variables (e.g. native vs. denatured conditions, amount of trypsin to be used and time of digestion) were also standardized. A 0.74 mg/ml solution of WT mtFabH was treated with guanidium hydrochloride (final conc. 6 M) in Tris-HCl pH 8.5 and then desalted with sodium phosphate pH 7.0 using Hitrap desalting column. The protein was concentrated using 50 kDa cutoff Microcon concentrator and then digested with trypsin for 6-8 hrs at 37 ˚C at 200 rpm shaking(ratio 1 : 30 of trypsin : mtFabH) in parallel to native WT mtFabH. About 100 µg digested peptide mixture was injected onto the C_{18} column and analyzed as described above. The amount of trypsin to be used for digestion was determined by monitoring the extent of digestion at mtFabH : trypsin ratios of 60:1 and 20:1 w/w for 24 hrs. To estimate an appropriate time for digestion, mtFabH was digested with trypsin (20:1 ratio w/w) at 37 ˚C and 200 rpm shaking and aliquots of 100 µg peptide mixture

were collected and analyzed at 3, 6, 9, 11 and 24 hours. The peptide traces were compared with 0 hrs and 24-hrs control (No trypsin added).

A typical standardized trypsin reaction was performed as described below. A solution of mtFabH (~10uM) in sodium phosphate buffer 50 mM, pH 7.0, 2 mM dehydroascorbic acid was incubated with ~ 100 µM inhibitor (in methanol) for 1 hr and then desalted using either Pierce Desalting spin columns or Hitrap desalting columns. The concentration of methanol in final mixture was kept at or below 1%. Trypsin in 1 mM HCl, pH 3.0 was added to bring the ratio of mtFabH: trypsin to be 20:1 w/w and the digestion mixture was kept at 37 ˚C for 9-11 hrs with shaking at ~ 200 rpm. A solution of above digested mixture was treated with 10 mM DTT (final conc.) at 37 ˚C for 1 hr and then analyzed by RP-HPLC as described below. An amount of 100 µg (typically) of total peptides was loaded onto widepore 250 X 10 mm C_{18} column, pore size 300 A˚, particle size 10 µM and the HPLC analysis was performed at a flow rate of 1 ml/min. The mobile phases used for HPLC analyses were: buffer A: 97 % water, 3 % acetonitrile, 0.01 % formic acid; buffer B: 97 % acetonitrile, 3 % water, 0.01 % formic acid. The gradient was started with 100 % buffer A for 5 minutes and then increased to 60 % B in 60 minutes. The concentration of buffer A was returned to 100 % in next 5 minutes and 20 minutes of 100 % buffer A was allowed for equilibration step. The peptides were detected using dual wavelength UV detector set at 204 and 257 nm.

A.2.3 MALDI-MS and MALDI/MS/MS analysis:

A.2.3.1 Sample preparation:

A solution of 25 µM mtFabH in sodium phosphate buffer 50 mM, pH 7.0, 2 mM dehydroascorbic acid was incubated with 250 µM inhibitor **1** (in methanol) for 1 hr and then desalted using Pierce desalting spin columns. Trypsin in 1 mM HCl, pH 3.0 was added to bring the ratio of mtFabH: trypsin to be 20:1 w/w and the digestion mixture was kept at 37 ˚C for 11 hrs with shaking at ~ 200 rpm. The control reaction consisted of untreated mtFabH. Pierce Pepclean spin columns® (C_{18} resin column) were used to clean up the digested peptide samples for subsequent MALDI analysis. The following solutions were prepared as per manufacturer's guidelines; activation solution: 50% acetonitrile; equilibration solution: 0.5% TFA in 5% acetonitrile; sample buffer: 2% TFA in 20% acetonitrile; wash solution: 0.5% TFA in 5% acetonitrile; elution buffer: 70% acetonitrile. A 15 µl aliquot from both trypsin digested control and test was taken out and mixed with 45 µl of sample buffer to bring the final concentrations of acetonitrile and TFA to be 5 % and 0.5 % respectively. The C_{18} resin was activated with 2 changes of 200 µl activation solution and then equilibrated with 3 changes of 200 µl equilibration solution. The column was then loaded with 30 µg of peptide mixture and washed with 3-4 changes of wash solution. Then 2 volumes of 10-µl elution solution were used to elute the peptide mixture, which was stored in - 20 ˚C until the analyses.

A.2.3.2 MALDI analysis conditions:

The parent and product ion mass spectra of the tryptic peptides were acquired on a MALDI-TOF/TOF mass spectrometer equipped with a Nd:YAG laser (355 nm) operating at 200 Hz (4700 Proteomics Analyzer; Applied Biosystems, Foster City, CA). A minimum of 1500 shots was averaged for each spectrum. The instrument was externally calibrated in the positive ion reflector mode with a standard peptide mixture (4700 Proteomics Analyzer calibration mixture; Applied Biosystems) by following the manufacturer's instructions. The matrix solution was prepared by dissolving 2 mg of alpha-cyano-4-hydroxycinnamic acid (CHCA) in 1 mL of 50% acetonitrile/0.1% trifluoroacetic acid. An aliquot of the tryptic digest was mixed with the matrix solution at volume ratios of 1:3 to 1:10, depending on sample concentration. A 0.5 µl aliquot of the sample/matrix mixture was deposited onto a 192-well stainless steel MALDI target plate and allowed to air-dry. Before sample analysis by mass spectrometry, 2 microliters of cold water was applied on the deposits and removed within 1 min to remove water-soluble salts and other impurities. Mass spectra were recorded in the positive ion reflector mode over an *m*/*z* range of 800-4000. The ions of interest were selected and subjected to CID (collision-induced dissociation) using filtered air as the collision gas and a collision energy set of 1 keV.

Vita

Sarbjot Singh Sachdeva was born on August 15th, 1979 in New Delhi, India. He received his Bachelor of Pharmacy degree from Faculty of Pharmacy, Jamia Hamdard, New Delhi, India in 2001. He was admitted into the VCU Department of Medicinal Chemistry, School of Pharmacy in 2001 for his graduate studies.